DEVELOPMENT AND NUMERICAL MODELING OF COMPOSITE STRUCTURES

By

Hamid Gerami

A Thesis

Submitted to the Faculty of Graduate Studies

In Partial Fulfillment of the Requirement for the Degree of

Master of Science

Department of Civil Engineering

University of Manitoba

Winnipeg, Manitoba

June 2016

Dedication

This thesis is dedicated to my wife, my daughter, my parents, and brothers. I acknowledge this journey would not have been possible without their encouragement and support.

I also need to express my gratitude to my friends Adrien Sparling, Mohamed Alnouri, Monika Niemczyk, Rafi Mahabbat and Babak Salimifard. Thanks for all the warm memories you guys made for me in E1-268.

Abstract

This thesis deals with the development and numerical modeling of Fiber Reinforced Polymer (FRP) wind turbine towers and luminaires. More specifically, this project is designed to capitalize on the technologies developed at the University of Manitoba to design FRP composite structures for use in remote communities where the costs of transportation and erection make the use of steel towers prohibitive. The work presented includes the analysis of a 50 m tall 750 kW wind turbine tower according to International Electrotechnical Commission (IEC) and Canadian Standard Association (CSA) standards using Glass Fiber Reinforced Polymer (GFRP), Carbon Fiber Reinforced Polymer (CFRP) and conventional steel. Standard luminaires, 6 m and 12 m, were also designed according to American Association of State Highway and Transportation Officials (AASHTO) standards for highway luminaires. The results showed that FRP can be effectively used as an alternative material for wind turbine towers and luminaires. Fiber Reinforced Polymer (FRP) composite wind turbine towers and luminaires studied in this project are lighter than similar structures fabricated using steel. Furthermore, these structures also meet the structural performance requirements set by AASHTO, IEC and CSA standards.

Table of Contents

List of figures:

List of tables:

Acknowledgements

The author wishes to acknowledge the contributions of the following individuals and groups without whom this project would not have been a success.

- Dr. Dimos Polyzois, P.Eng., supervisor of this project for his patience, encouragement and guidance throughout this study.
- Members of committee, Dr. Svecova, P.Eng., and Dr. Jayaraman, P.Eng., for their comments and helpful suggestions.
- NSERC CREATE-SERA program and University of Manitoba for the financial support provided.
- Dr. Klowak, P.Eng., W.R.McQuade Heavy Structure Laboratory Manager, and Mr. Pachal, for their technical assistance in this project.

Chapter 1: Introduction

1.1 General

Composite materials are formed through the combination of two or more discrete materials whose properties are superior to those of the individual materials. In recent years, a new type of composite material has been promoted for use in supporting structures for wind turbines, light standards, and utility poles. This material is referred to as Fiber-Reinforced Polymer (FRP). To produce this material, high-strength fibers such as carbon, aramid or glass are saturated with lightweight thermoset resin, which acts as a binder material of the composite and holds together the load-carrying fibers. These fibers provide the main reinforcement of the matrix and are distinguished by their high length-to-diameter ratios (Metiche, 2012).

One of the first applications of high-specific-strength (strength/density) and high-specific-stiffness (stiffness/density) FRP composites was in the military aircraft industry, where weight is an essential factor in maneuverability and overall performance of aircraft. Fiber-reinforced polymer technology was established during World War II, where it was employed in the development of the B-17 bomber program (OTA, 1986). In modern industry, FRP composite materials are utilized in numerous applications, such as architectural structures and sports equipment, as well as in the aerospace, automotive and marine industries (Metiche, 2012).

After discovering the exceptional potential of FRP composites with high specific strength and high specific stiffness, extensive research was conducted to study their potential applications in civil engineering. One of the major attributes that has made FRP an attractive alternative to traditional materials in a variety of civil engineering applications is their high strength-to-weight

ratio (Labossière & Turkkan, 1992). Therefore, numerous structures and bridges constructed in North America, Japan, and Europe have adopted FRP as a tensile element in pre-stressed concrete (Mufti, Erki, & Jaeger, 1991). Fiber Reinforced Polymer (FRP) is used in the oil and gas industry in diverse operations, ranging from simple roof trusses to pipes and very sophisticated structures such as offshore oil drilling platforms (Fibergrate Composite Structures, 2015).

The lightweight characteristics of FRP make handling and installation easier, resulting in lower labor and transportation expenses. These materials are also appropriate for rehabilitation projects. Chimneys, columns, slabs, and girders have been reinforced using FRP to strengthen them against overloads from earthquakes (Mufti, Erki, & Jaeger, 1991). Repair materials are most often unidirectional fiber tapes or fiber-wound strands and fabrics. Flexural and shear strengthening are also possible using these products. Ehsani (1994) has demonstrated that FRP overwraps or jackets can be utilized to retrofit columns in highway bridges, enhancing column resistance against lateral seismic loads.

1.2 Need for investigation

The high cost of transporting steel structures, in addition to performance issues such as corrosion, have led to innovative solutions using lightweight FRP composite materials in structural applications. The corrosion is a common problem in steel structures, which can lead to a reduction in cross-sectional structural properties, loss of strength and degradation of appearance (Bull, 2015).

Considering the severe weather conditions in remote areas of Canada, the major advantages of FRP composites as an alternative material to conventional steel in the fabrication of light

standards and wind turbine towers are their high corrosion resistance and high strength-to-weight ratio.

A technical knowledge gap exists in the use of filament-winding technology to fabricate light standards, as well as in the design and analysis of FRP composite wind turbine towers under severe loading conditions according to new CSA and IEC standards. Due to recent changes in international (IEC, AASHTO) and national (CSA) standards, there are not sufficient structural performance data available to be able to design such structures as wind turbine towers and luminaires using composite materials. Therefore, this research project is aimed at filling the current research gap and provides renewable-energy authorities with additional performance data to allow these systems to be implemented in future projects.

This research study is unique in a number of ways: (a) focuses on the use of FRP composite materials for light standards and wind turbine towers; (b) involves the analysis of FRP composite structures; (c) addresses the application of current performance based standards to design wind turbine towers; and (d) includes the development of a comprehensive finite element analysis of FRP composite structures to evaluate different modes of failure, such as material failure criteria and local buckling. To complete the numerical analysis, different fiber orientations and cross-section dimensions were studied under different static and dynamic load combinations to find the optimal designs which are presented in Chapters 4 and 5. Wherever possible, the finite element models developed were verified using existing experimental data.

1.3 Objectives

The goal of this research study is to examine the applications of FRP composites as lightweight alternative materials for wind turbine towers and light standards. More specifically the objectives of the study are:

a) To determine wind load requirements for the targeted structures using AASHTO Standard Specifications for light standards; CAN/CSA-C61400-1:14 (Wind turbines-Part 1: Design requirements); CAN/CSA-C61400-2:08 (Wind turbines-Part 2: Design requirements for small wind turbines); ISO 4354:2009 (Wind actions on structures); and NBCC (2005) for wind turbine towers.
b) To develop numerical models for analyzing hollow tubular FRP composite structures;
c) To verify the numerical models using published experimental data;
d) To design FRP composite poles for typical light-utility applications (6 m and 12 m);
e) To determine an optimal design for an FRP composite tapered tower to support a 750 kW wind turbine; and,
f) To compare the structural performance of an FRP composite wind turbine tower to a steel tower.

1.4 Methodology

The research program is presented in three phases. The first phase involves the verification of finite element models using published experimental results. The ANSYS Mechanical APDL software was employed to create the finite-element models using shell element 281. Results from a static analysis, taking into consideration large deflections and cross-section distortions, are compared to experimental data from previous published works. Verification involves deflection

profiles, strains, and modes of failure. The results show that ANSYS finite-element software can be used as a highly effective tool to design and analyze FRP composite structures. The verified numerical models are used in Phases 2 and 3 to design the FRP composite structures.

In Phases 2 and 3, 6 m and 12 m composite poles for supporting light standards, and 50 m tall wind turbine towers to support a 750 KW turbine are analyzed. Three sets of parametric studies are carried out to determine the optimal number of longitudinal layers, longitudinal fiber orientation and cross-section dimensions for these structures. The optimal designs are presented in Chapter 4 (light standards) and Chapter 5 (wind turbine towers).

1.5 Chapters

This report has six chapters. The introduction and objectives are presented in this chapter. Chapter 2 covers a comprehensive literature review. It consists of a brief history of wind as a sustainable and renewable source of energy as well as a brief history of FRP materials and different composite manufacturing methods. Furthermore, existing design specifications and standards, as well as a review of previous experimental and theoretical studies, are discussed.

The verification of finite-element analyses is presented in Chapter 3. The development of the finite-element modeling, loading calculations, and parametric study of FRP composite poles are covered in Chapters 4 and 5. The parametric study examines the effect of longitudinal layers, the effect of longitudinal fiber orientation, and the effect of cross-section dimensions on the strength of composite poles.

Chapter 6 summarizes the results of this study and provides recommendations for future research on composite structures.

Chapter 2: Literature review

2.1 Brief history of wind energy

Exploiting wind as a source of energy has its roots in ancient Egypt, where it was used to propel boats and sail from shore to shore on the Nile river. Babylon civilization was the first to invent windmills as a machine that generates circular motion using vanes attached to an axis. By the 10th century A.D., the Persians had invented horizontal windmills that had sails rotating in a horizontal plane around a vertical axis. They used this technology to grind grain for centuries (Ungkurapinan, 2005).

In Europe, energy potential of wind was discovered much later. Primitive working windmills date from 12th century in the small village in Yorkshire, UK. Hundreds of years later, they were revised to be able to pump water and take back much of Netherlands from the sea (Ungkurapinan, 2005). In 1854, Daniel Halladay designed the first water windmill in North America that could pump water. He began fabricating his invention in Ellington, Connecticut. Settlers in the west coast of United States also took advantage of this invention to pump water and raise livestock (U.S Department of Energy, 2015).

In the 1980s, concerns about the environmental impact and decreasing availability of fossil fuels inspired engineers to design efficient windmills to generate electricity. These new turbines were first installed in Altamont Pass Wind Farm, California, as well as in Denmark (California Wind Energy Association, 2015). Since those early days, wind turbines have been highly developed, and wind energy has proven itself as a reliable and environmentally friendly type of energy.

Modern megawatt-class wind turbines can produce utility-grade electricity that can compete with traditional methods of energy production. These turbines can provide enough energy to power 300 to 600 houses, meaning their capacity is about 30 times more than the first wind turbines from 30 years ago. Therefore, for an equal level of power production, much fewer turbines are required in comparison to the 1980s (Ungkurapinan, 2005). Aesthetically, these turbines have been upgraded as well. They consist of rotor blades that rotate softly and slowly atop a tall, brightly colored tower, enabling them to harmonize with surrounding area.

2.2 Types of wind turbine tower

The main task of the tower in a wind turbine is to support different components of the system, such as blades, the nacelle, gear box, and generator. Towers must be designed to be strong enough to be able to resist any applied loads. The three most common types of wind turbines are:

- Tubular towers (steel or concrete)
- Lattice towers
- Guyed towers

To construct large wind turbines, tubular towers are suitable options, since they can be fabricated in multiple sections, with flanges at both ends, and then assembled on site. To save material and increase the strength at critical sections, these multiple sections are usually tapered, with their diameter decreasing toward the top. Furthermore, compared to other types of wind turbines, tubular towers integrate with landscapes better aesthetically, and in cold-temperature climates, they can protect personnel from the wind, as service work is conducted inside them.

To manufacture lattice towers, steel sections are welded together; this type of tower is lighter compared to tubular towers with comparable stiffness. As a result, the cost savings is the

principal advantage of lattice towers. The major disadvantages of lattice towers are their visual display and the fact that in cold temperatures maintenance work on them is almost impossible. For these reasons, lattice towers are not an attractive option for large-scale wind turbine operations.

A guyed tower is a tower structure which is supported by guy wires which provide stability against lateral displacement. Guyed towers are most suitable for smaller wind turbines, though a few larger prototypes were manufactured in the 1980s. This type of tower is lightweight and thus more economical; but they require a large footprint. In addition, because of the nature of this type of structure, it is more susceptible to vandalism, which can endanger its long-term safety.

2.3 FRP materials

Fiber Reinforced Polymers (FRP) are generally categorized as advanced composite materials. In comparison to conventional materials, where available products are limited to what industry can provide, the entire FRP manufacturing process can be closely engineered to fabricate a custom product for different operations. In the process of designing FRP structures, engineers can select different types of fibers, matrix materials, and geometrical properties, so that final product is optimized both structurally and economically. A brief description of the components of FRP materials is given in the following sections.

2.3.1 Fibers

The structural properties of FRPs are predominantly determined by the fibers used in the product. These are usually glass, carbon, aramid or basalt. Carbon fibers have about 6-10

micrometer radius (Chung, 2012), have a high stiffness and high tensile strength, as well as low weight, high temperature tolerance, and high chemical resistance. These properties have made carbon fibers an attractive material for aerospace, motorsports, military, and civil engineering applications.

Aramid fibers are characterized by their superior toughness, high tensile strength and low density. Aramid fibers are less expensive than carbon fibers, but as a result of their poor compressive strength and difficulties in cutting and machining, their use is restricted (Chung, 2012). These fibers are available in different formats, the most popular of which are roving and mating.

Glass fibers are the most common fiber used for fabricating FRP composites. They are not as strong as the other two fibers but they still have high electrical insulating properties, a high strength-to-weight ratio and a low susceptibility to moisture. Glass fibers are less brittle and, from an economic point of view, are much less expensive, which leads to less expensive final product.

Various types of glass fibers are available: A-glass (Alkali-lime glass), E-CR-glass (Electrical/Chemical Resistance), D-glass (low Dielectric constant), R-glass (high mechanical properties), and S-glass (Alumino silicate glass with a high tensile strength) (Chung, 2012). The most common glass fibers used are E-Glass, because of their relatively lower costs. For more demanding applications, S-Glass fibers are used because of their high tensile strength.

The type of glass fiber used for manufacturing the experimental poles and coupons fabricated at University of Manitoba are E-Glass, with a designation of 1100 TEX, which refers to the specific weight of the glass roving used (Philopulos, 2002). The properties of the various types of glass fibers are listed in Table 2.1.

Table 2.1: Properties for a variety of high-performance fibers (Frederick T. Wallenberger, Paul A. Bingham, 2009)

Property	**Unit**	**Carbon**	**Aramid**	**E-Glass**	**S-Glass**
Density	g/cm^3	1.8	1.45	2.58	2.46
Tensile strength	MPa	4900	3000	3445	4890
Tensile modulus	GPa	230	112.4	72.3	86.9
Compressive strength	MPa	1570	200	1080	1600
Strain to failure	%	1.5	2.4s	4.8	5.7

2.3.2 Matrix materials

Matrix and fibers are two basic components of fiber-reinforced Polymers. The primary role of the matrix is to envelop and support load-carrying fibers. To choose a proper matrix, specific requirements should be considered. For example, the matrix should properly impregnate and bond with the fibers (chemically adaptive) in a reasonable curing period of time.

In FRP manufacturing, the matrix material is usually selected from a wide range of resins. Based on effect of heat on the resin's properties, they can be classified under “thermoplastic” or “thermosetting.” Thermoplastics soften when heated and harden when cooled. This process of softening or hardening can be repeated without any major effect on material properties. But

when thermosetting resins are cured, they will not become liquid again, although their material properties will change considerably if they reach certain temperatures. For filament winding applications, thermosetting resins such as epoxies, polyesters, and vinyl-esters are usually selected (Chung, 2012). The properties of these three thermosetting resins are discussed below.

2.3.2.1 Epoxies

Epoxy resins also known as polyepoxides are produced by combining an epoxide (such as epichlorohydrin) and a polyamine (like triethylenetetramine). The final product is an epoxy with high viscosity (Molded fiberglass companies, 2015).

The advantages of epoxies include high resistance to alkali and other solvents, great adhesion, easy application on a wide variety of surfaces, little shrinkage, high fatigue, and excellent electrical insulating properties (Reichhold, 2009).

However, epoxy resins have relatively low resistance in acidic environments with pH less than 3. Furthermore, they become yellow when they are exposed to weathering and they have a rather slow curing process compared to other resins (Reichhold, 2009).

2.3.2.2 Polyesters

Polyesters are another type of polymer that can be used as the supporting matrix material for load-bearing fibers in FRP products. Polyesters are usually used in combination with glass fibers, resulting in excellent structural performance, as well as a high thermal resistance and other physical properties (Reichhold, 2009). In comparison to epoxies, Polyesters have higher resistance against both alkali and acid environments, which makes them a suitable option for protecting steel products in harsh conditions.

2.3.2.3 Vinyl Esters

Vinyl esters can be considered as an alternative option for polyesters and epoxies. Their mechanical properties such as strength and toughness are half way between polyesters and epoxies. It has a low viscosity of about 200 centipoise, which is less than both polyesters and epoxies (Chung, 2012). Vinyl esters have shorter curing process compared to epoxies, and they provide better control over hardness development rate. Vinyl esters and polyesters share a similar molecular structure, but vinyl esters are more flexible and can tolerate repeated flexing without cracking. They are also highly resistant to alkali agents and water penetration, but they are less resistant to acids in comparison to polyesters (Molded fiberglass companies, 2015).

2.4 Manufacturing process of composite parts

2.4.1 Hand Lay-up

Hand lay-up is a popular basic method to fabricate large FRP composite products in low volumes. In this method, the size of the part is not a limit. Hand lay-up has been used to produce radomes, concrete forms or wind turbine sections. Wooden, metal or composite molds can be used in this process. To prepare an appropriate surface, a pigmented gel coat is sprayed on the mold surface. When the mold is ready, each FRP composite laminate or mat is impregnated with resin and placed manually on the mandrel until the desired thickness is achieved. Brushes or spreaders are then used to eliminate entrapped air and completely wet composite fibers with resin.

2.4.2 Filament winding

The University of Manitoba's R&D facilities have dedicated a great amount of time and effort to studying and experimenting with FRP composite materials. Burachynsky (2002) started an extensive study on developing filament-winding procedures specifically for fabricating FRP composite poles. He argued that with current state of the art technology, filament winding can trim costs and optimize material usage to enhance long-term efficiency (Burachynsky, 2002).

Filament winding is an attractive process for a number of reasons, such as low production cost, flexibility of design, controlled fiber orientation, and high fiber volume. This process involves winding resin-saturated filaments of FRP through a wind eye under an exact tension on a rotating mandrel. Winding always follows a prescribed geometric pattern. For axisymmetric components, the pattern must be repeated to provide complete coverage of the mandrel (Munro, 1988).

Filament winding was first introduced by the M.W. Kellog Co. in 1947, when they fabricated the earliest known filament-winding machine (Munro, 1988). The first main product of filament winding technology dates back to 1940s with the fabrication of a nozzle for the X248 rocket motor. In the process of fabricating that nozzle, E-glass fibers were impregnated with epoxy resin to be able to resist high temperatures (Munro, 1988).

The first commercial application of filament winding emerged from the Manhattan Project, which employed this technology to produce lightweight composite hoops in 1954. It then became the groundwork for Naval Ordnance Laboratory rings utilized in shear and tension tests (Munro, 1988). In the 1960s, McClean Anderson designed and fabricated the first commercial filament winding devices and in 1965 the U.S. Army Aviation Systems Command received their first six-

axis machine designed and produced by Goldworthy Engineering (Munro, 1988). Gar Wood Industries fabricated the first known GFRP poles in 1950s (Derrick, 1996), at a time when fiberglass technology had attracted extensive attention.

Filament winding is now being used in a variety of industrial and structural applications. Rocket booster casings and MX missiles utilize helically wound tube-type components composed of either fiberglass or graphite fibers in their production (Metiche, 2012).

Pressure vessels of elongated or spherical filament-wound fiber composites are utilized in other applications, such as storage tanks for compressed natural gas (CNG) (Munro, 1988). Other sophisticated structures involve symmetrical square and rectangular box sections, ellipsoid shapes, and tapered poles for various industrial applications. Non-axisymmetric structures include pipe tees, elbows, bumper frames, leaf springs, and T-shaped air ducts. Aircraft fuselages, helicopter blades, windmill blades, and boom sections are other non-axisymmetric products used for mechanical engineering applications (Munro, 1988). This research project concentrates on using filament winding technology to fabricate support structures for wind turbines and light standards.

2.5 Pole design specifications and standards

In this thesis, two structural applications of GFRP composites are theoretically investigated. It covers the numerical analysis of wind turbine towers and light standards, as well as evaluating advantages and disadvantages of GFRP structures compared to conventional materials.

In conducting the research presented in this thesis, two design standards are used: IEC 61400-1 and CSA C61400-1-14. There are 27 IEC standards covering different aspects of the design of wind turbines, such as structural design, power performance, and acoustic noise measurements. In 2008, the Canadian Standards Association adopted IEC 61400-1 and included some amendments in its CSA C61400-1 Standard. These two Standards are discussed in detail in the following sections.

Glass Fiber Reinforced Polymer light standards were designed using AASHTO Standard Specifications for structural supports for highway signs, luminaires, and traffic signals. This Standard provides referenced information for the design, material, fabrication, and construction of sign, luminaire, and traffic signal support structures.

2.5.1 Wind turbine tower design standards

2.5.1.1 IEC 61400-1 International Standard

Prior to 2008, the design, analysis and certification of wind turbines were based on the Gemanischer Lloyd's Rules and Regulations, Part 1: Wind Energy, and the IEC 61400-1 International Standard. These Standards provided instructions for manufacturing procedures, material, and load combinations under different climatic conditions. A broad range of wind speeds, including turbulence and extreme wind conditions, are considered to calculate external loads on the tower.

The IEC 61400-1 Standard classifies wind turbines, based on wind speed, into four different classes: Class I,II,III and S. Each class represents a range of robustness determined by average wind speed and turbulence intensity on the structure. Class I, II, and III wind turbines are designed to have a lifespan of at least 20 years. When special wind pressures or external

conditions are applied to the structure, or special safety features are needed, towers are designed conforming to Class S requirements. Design parameters for this category are determined by the designer, and specified in the project documentations. These parameters should be at least as extreme as the environmental conditions where the wind turbine will be constructed and used. Table 2.2 provides the basic parameters for wind turbines according to IEC 61400-1 Standard.

Table 2.2: Basic parameters for wind turbine classification (IEC 61400-1, 2005)

Reference wind speed*	**Wind turbine class**			
	I	**II**	**III**	**S**
$V_{ref\ (m/s)}$	50	42.5	17.5	Values specified by the designer

*V_{ref} : Reference wind speed average (at hub height) over 10 min

2.5.1.2 CAN/CSA-C61400-2-08 Standard

The CAN/CSA-C61400-1 Standard is an adaptation of the International Electrotechnical Commission (IEC) Standard 61400-1. Two amendments were made to the IEC Standard in 2008 and 2010 to include Canadian deviations. The CSA's adoption of the IEC Standard has fundamental differences for environmental, electrical, and structural safety requirements to comply with distinct Canadian conditions and ensure the engineering integrity of wind turbines during the planned lifespan of the structure. The CSA C61400-1 Standard provides instructions and regulations for all subsystems of wind turbines including internal electrical subassemblies, hydraulic or pneumatic systems, control, and protection mechanisms as well as design guidelines for all supporting structures.

2.5.1.2.1 Design method

Load cases and load combinations specified in the CSA C61400-1 Standard cover all design situations and external conditions a wind turbine might be subjected to during its lifetime. In special cases when a high level of precision is required to calculate design values, the CSA C61400-1 Standard requires full-scale testing of turbines to validate dynamic model results and verify the suitability of the design. If an experimental process is used to evaluate calculations, loads applied to the test structure and external conditions should be set to reflect the loads and external conditions applied to a similar structure in an actual wind farm.

2.5.1.2.2 Safety classes

The CSA C61400-1 Standard defines two safety classes for wind turbine systems: Normal safety class and special safety class. The normal safety class is advised when failure can lead to casualties or might cause social or economical damages. The special safety class is used when customer requests for special safety measures or local instructions be considered. To design Class S wind turbines, both CSA and IEC use similar wind turbine classifications. The partial safety factors defined by the CSA C61400-1 Standard can be found in Subsection 7.6 of the CSA Standard.

2.5.1.2.3 Design methodology

The CSA C61400-1 Standard employs Limit State Design (LSD) for wind turbine supporting structures. To design structures based on this method, two basic criteria must be satisfied: the Ultimate Limit State (ULS) and Serviceability Limit State (SLS). This code also permits full-scale experiments as an alternative method for validating structural designs.

2.5.1.2.4 Loads

To design wind turbine towers, a wide range of loads needs to be considered. These include static gravitational and inertia loads applied to the structure by gravity; aerodynamic loads that result from airflow and its interaction with the fixed and rotating components of wind turbine; actuation loads originating from the operation and control of the wind turbine; and other loads such as ice loads and wake loads.

2.5.1.2.5 Load cases

The combination of different factors, such as design conditions, operational methods and external conditions, determine the load cases for wind turbine design. To evaluate the structural integrity of wind turbines, all applicable load cases with a substantial possibility of occurrence should be taken into account. The CSA C61400-1 Standard combines the following design situations to design and analyze wind-turbine systems: normal design situations in combination with normal or extreme external conditions; fault design situations, as well as external conditions; and installation and maintenance design situations, in addition to external conditions. In case severe external conditions happen in combination with a fault situation, a reasonable combination of the two should be used to determine the proper load case. Furthermore, according to the CSA C61400-1 Standard, the design should be based on wind speeds that cause the worst design conditions.

2.5.2 Luminaire design standards

2.5.2.1 AASHTO Standard Specifications for structural supports for highway signs, luminaires and traffic signals

The design of the light standards investigated in this study is based on the AASHTO Standard Specifications. This Standard is the outcome of a collaborative study carried out by the Highway Research Program (NCHRP) Project 17-10 and NCHRP Report 411 (AASHTO, 2013). It provides instructions for designing, fabricating, and erecting support structures for signs, luminaires, and traffic signals.

Modern light standards involve the use of common tubular structures 6 m (20 ft) to 12 m (40 ft) high and supporting one or two luminaires. High-level luminaires are employed to light up larger areas: they are 17 m (55 ft) to 46 m (150 ft) high and support four to twelve luminaires. Various types of luminaire structural supports are presented in Figure 2.1.

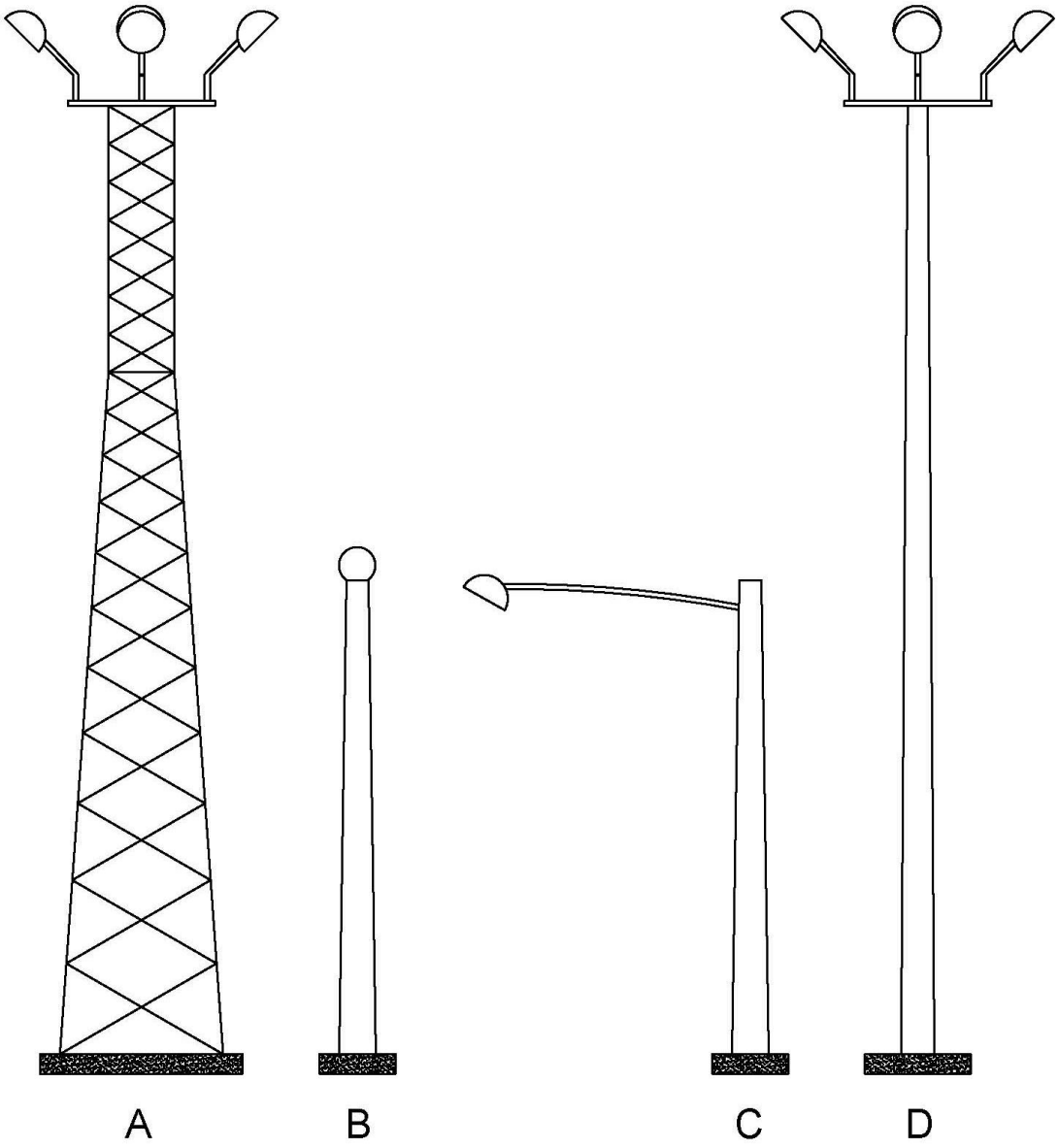

A) High level Luminaire support-Truss type
B) Typical pole with luminaire
C) Typical pole with luminaire arm
D) High level luminaire support-Pole type

Figure 2.1: Luminaire structural support (AASHTO, 2013)

2.5.2.1.1 Fiber-reinforced composite design

Composite materials are normally directionally dependent (anisotropic) by nature, and FRPs are not an exception. Material properties such as ultimate tensile and compressive strength, shear strength, elastic modulus and Poisson's ratio depend on fiber content, the orientation of fibers, and type of fiber and matrix material used for the experiment.

Even though FRP composites are classified as viscoelastic materials, which means their mechanical properties are time- and temperature-dependent, for design purposes AASHTO Standard Specifications categorize them as linearly elastic, obeying Hooke's law. Since a composite's structural behavior is relatively linear up to the point of failure, these Standard Specifications also assume that bending plane sections remain planar and shear deformations are not accounted for in the analysis.

2.5.2.1.2 Loads

AASHTO provides the following instructions to calculate design loads:

- Dead load (DL): To calculate dead load, all permanently attached components, as well as assembling accessories and other servicing components, should be considered.
- Ice load (Ice): An ice load of 145 Pa is required for vertical and horizontal components of structural supports, luminaires, and traffic signals.
- Wind load (W): Luminaire structural support should be designed for the effects of wind load from any direction. For this purpose AASHTO suggests two cases of normal and transverse wind loads be considered and applied to the structure simultaneously (AASHTO, 2013, sub-clause 3.9.3).

2.5.2.1.3 Group load combinations

To ensure an appropriate margin of safety for luminaires, AASHTO requires the following load combinations (Table 2.3):

Table 2.3: Group load combinations (AASHTO, 2013)

Group load	Load Combination
I	DL
II	DL+W
III	DL+Ice+1/2(W)
IV	Fatigue

2.5.2.1.4 Fatigue design

Different wind conditions such as natural or truck-induced gusts, vortex shedding, and galloping can cause large-amplitude vibrations as well as fatigue damages to the luminaire supporting structure.

To prevent fatigue cracks and large-amplitude vibrations, AASHTO requires the structure to be analyzed for equivalent static wind loads applied to the structure separately (AASHTO, 2013, Sections 11.6 and 11.9). This Standard also accepts a dynamic analysis of the structure using proper dynamic load functions as an alternative method for equivalent static loads.

2.5.2.1.5 Serviceability requirements

The AASHTO Standard Specifications set deflection limits for vertical and horizontal components of structural supports. These limits are used to ensure an aesthetically appropriate

structure under dead loads, as well as allowable serviceability deflections under applied loads. Conventional elastic methods are acceptable by this Standard to determine deflections.

The deflection limits for luminaire structural support according to AASHTO (2013) are: (a) A tip deflection under group I load combination (DL only) limited to 2.5% of structure height, and (b) a tip deflection under group II and III load combinations (DL + W) limited to 15% of structure height.

In the following Chapters, AASHTO Standard Specifications (2013) and CSA-C61400-1 Standard are used to examine the structural performance of 6 m and 12 m luminaires as well as a 50 m tall wind turbine tower using finite element software ANSYS.

Chapter 3 focuses on the verification of the finite element analysis using data from previously published works (Philopulos, 2002). Verification involves deflection profiles, strains, and modes of failure.

Chapter 3: Verification of the Finite Element Analysis

3.1 Introduction

Finite element analysis is a powerful numerical method for solving sophisticated problems in engineering. It is most commonly used in cases where analytical methods cannot offer a precise close formed solution. The basic concept of the finite element technique is to use a finite number of defined elements whose displacement behaviour is described by a fixed number of degrees of freedom to predict the structural behaviour of structures.

Generally, stress and strain analyses of structures are carried out using considerable simplifications and idealizations. Mass is assumed to be concentrated at center of gravity or vertical elements are considered to be a line segment (same cross section). Using the finite element method, however, we can analyze more complex real world structures with much higher accuracy.

3.2 Finite element modeling

This study proposes the use of GFRP towers as an alternative structure for remote areas where the cost of transportation and erection prohibits the use of tubular steel towers. For this reason, understanding the structural performance of GFRP towers is essential.

Since it is impractical and financially impossible to test all different cross sections and materials under different loading conditions, a critical part of this study is to develop an analytical tool for the design of these structures. Fortunately, in studying filament wound GFRP poles, the finite element method can be applied to laminated shell theory as well. Navaratna et al. (1968)

employed the finite element method to study the stability of shell structures, and almost a decade later Gould and Basu (1977) used the same approach to investigate linear buckling and incremental deformation of shells.

In 1974, Noor and Mathers investigated the nonlinear performance of laminated shells using the finite element method. In their study they used eight nodded and twelve nodded shear flexible quadrilateral shell elements. Reddy (1981) used different shell theories to study large deflection of layered anisotropic shells. He later extended his research to laminated composite shells and to analyze them he adopted a three-dimensional finite element method (Reddy & Chao, 1983). The work of Reddy and Chao (1983) made it possible to analyze a broad range of thin and moderately thick laminated shells. To analyze laminated anisotropic composite thin shells that have imperfections, Saigal et al. (1986) offered computational procedures that enable the finite element method to be used in the analysis.

In 1988, Jun and Hong utilized the finite element method to investigate nonlinear buckling behaviour of laminated composite cylindrical shells. They expanded their project to include a parametric study of thee effect of fiber angle on the structural performance of composite shells (Jun & Hong, 1988). Jeusette and Laschet (1990) used the finite element analysis to investigate the pre- and post-buckling behaviour of curved composite shells. They did this by applying a three-dimensional multi-layered finite element method to their analysis.

In the present research investigation, the ANSYS finite element software is employed to generate numerical models that can simulate the structural performance of FRP composite towers and poles. Large deflections and cross-section distortion were taken into account in the analysis and

proper failure criteria are used to determine the ultimate load. The core model for the GFRP poles is verified through comparison with the experimental results obtained from previous research studies at University of Manitoba (Philopulos, 2002).

3.2.1 Element selection

In the finite element analysis presented here, shell element 281 is used to develop the analytical model. This element has 8 nodes with 6 degrees of freedom at each node. This element is selected due to its ability to model a laminate with unlimited number of layers with constant or variable thickness. In addition, it takes into consideration large deflections and the analysis of the structure is based on multiple failure criteria. Membrane stresses and strains are also included in the analysis. The shell element 281 is also appropriate because the material properties for the element are defined in terms of the principal axes of the element. Using a single lamina for reference, the element coordinate system identifies X-axis to be parallel to the fibers direction, Y-axis to be perpendicular to the fiber direction, and the Z-axis to pass through the thickness of the element.

3.2.2 Stress-strain relationship

To calculate stress and strains in an orthotropic composite, the software uses the following stress-strain relationship:

$$\{\sigma\} = [D]\{\varepsilon_{el}\} \qquad 3.1$$

Where $\{\sigma\}$ is the stress vector, [D] is stress-strain matrix and $\{\varepsilon_{el}\}$ is the elastic strain vector. The stress-strain equation can also be written as:

$$\{\varepsilon_{el}\} = [D]^{-1}\{\sigma\} \quad 3.2$$

Where $[D]^{-1}$ can be computed using the following matrix (ANSYS , 2015):

$$[D]^{-1} = \begin{bmatrix} 1/E_x & -\nu_{xy}/E_x & -\nu_{xz}/E_x & 0 & 0 & 0 \\ -\nu_{yx}/E_y & 1/E_y & -\nu_{yz}/E_y & 0 & 0 & 0 \\ -\nu_{zx}/E_z & -\nu_{zy}/E_z & 1/E_z & 0 & 0 & 0 \\ 0 & 0 & 0 & 1/G_{xy} & 0 & 0 \\ 0 & 0 & 0 & 0 & 1/G_{yz} & 0 \\ 0 & 0 & 0 & 0 & 0 & 1/G_{xz} \end{bmatrix} \quad 3.3$$

3.2.3 Geometric nonlinearity

When strains created in a structure after applying load are more than a few percent, geometric nonlinearities need to be considered. That is, if large deflections happen in a structure, its changing shape can generate nonlinear reactions in the structure known as geometric nonlinearities.

Geometric nonlinearities mean that the stiffness of the structure [k] changes when considerable deformations occur. In this study, nonlinearities in area and thickness are accounted for in the ANSYS finite element models. Static or transient analyses are used to take geometric nonlinearities into consideration and are referred to as large strain or finite strain analysis. In large strain analysis theory the structural shape changes progressively and the geometry continuously changes. In this case the stresses need to be calculated using an appropriate algorithm such as the lagrangian method (incremental analysis) in order to account for geometric nonlinearities and finite deflections.

The following relationship is used by the incremental method to calculate nonlinear deformations:

$$[k_i]\Delta u_i = \{F_i\} \quad 3.4$$

Where $[k_i]$ is the stiffness matrix and is defined as:

$$[k_i] = \int [B_i]^T [D_i][B_i] d(vol) \quad 3.5$$

Where, [Bi] is the strain-displacement matrix in terms of the current geometry; [Di] is the current stress-strain matrix; and F_i is the Newton-Raphson restoring force and has the following form:

$$[F_i] = \int [B_i]^T [\delta_i] d(vol) \quad 3.6$$

This force is calculated using an incremental procedure in which a series of linear iterations converge to the actual final solution.

3.2.4 Failure criteria

Failure takes place when loads exceed the limit defined by the chosen failure criterion. Fiber Reinforced Polymers (FRP) are categorized as orthotropic materials and, contrary to isotropic materials, their strength depends on the direction of the fibers and direction of loading. Shear stress theory and Von Mises criteria are commonly used failure criteria for isotropic materials. In case of orthotropic materials, several researchers attempted to develop semi-experimental and mathematical models to explain orthotropic materials behaviour under combined stresses (Gibson, 1995). In 1857, William Rankine developed the Rankine theory, now referred to as the Maximum Stress Theory, for brittle materials. According to this theory, failure happens when the maximum principal stress at any point surpasses material ultimate resistance. In 1920, Jenkins presented an extension to this theory making it applicable to orthotropic materials as well.

The Maximum strain criterion and maximum stress criterion share similar concepts except that according to the maximum strain theory, failure happens when the principal strains exceed the uniaxial strains at failure. Waddoups (1967) extended this theory to composite materials.

The Von Mises failure criterion is suitable for describing plastic deformation of ductile materials such as steel. Failure is assumed to have taken place in the material when the Von Mises critical value is reached (known as yield stress). Hill (1948) extended Von Mises theory to include polymers and in particular composites. He assumed the behaviour of these materials is initially isotropic and that anisotropic behaviour initiates when large deformations take place. He modified his theory by adding exponential factors to the calculation. The degree of anisotropy of the material determines these exponential factors.

In 1965, Tsai and Azzi proposed the failure criteria known as the Tsai-Hill criteria which are an extension to Hill's failure criteria and are suitable for analyzing orthotropic and transversely isotropic laminas. The Tsai-Hill criteria assume strengths in tension and compression are the same. Therefore, the failure surface would be a symmetrical ellipse. To study anisotropic composite materials with different properties in compression and tension, Tsai and Wu (1971) suggested a phenomenological failure criterion. Tsai and Wu criteria use linear and quadratic terms in the calculations, linear terms to make a distinction between tension and compression strength properties and quadratic terms that generate ellipsoid failure surface in stress space.

Hashin (1980) also presented failure criteria for unidirectional fiber composites. His three-dimensional failure criteria accounts for more than one stress component to assess different failure modes. These criteria were developed for unidirectional fiber composites. Therefore, if they are applied to other laminates or non-polymeric composites the results will be approximate.

To evaluate the ultimate capacity of the FRP composite structures, the Tsai-Wu failure criterion, also known as the interactive polynomial theory or quadratic polynomial failure theory, is employed in this study. This failure criterion can take into account interactions that might happen between stress components (ANSYS , 2015).

3.3 Verifying Finite element models using experimental results

Two applications of GFRP structures are investigated in this thesis: wind turbine towers and light standards. To study the behaviour of these structures under different load combinations, the finite element software ANSYS is employed and results are presented in Chapters 4 and 5.

The first step in a comprehensive numerical study of FRP composite structures is to validate the numerical modeling. To verify the three-dimensional finite-element (FE) models developed in this research study, the experimental results obtained by Philopulos (2002) are used. These FE models are validated in three ways: (a) verifying deflection values; (b) verifying strain results; and (c) verifying modes of failure. The tested poles are modeled in Mechanical ANSYS V.16 using graphical user interface. Shell element 281 is selected and the pole geometry is created using key points. Material properties obtained by Philopulos (2002) using coupon tests are used in this modeling (Table 3.1).

Table 3.1: Properties of E-glass/Polyester Resin Filament Wound Coupons (Philopulos, 2002)

Properties of E-glass/Polyester Resin Filament Wound Coupons	
Fiber-to-weight volume	58.1%
Longitudinal modulus (E_1)	19.03 GPa
Transverse modulus (E_2)	6.14 GPa
In-plane shear modulus (G_{12})	3.58 GPa
Major Poisson's ratio (ν)	0.35
Longitudinal tensile strength (F_{1t})	620.55 MPa
Longitudinal compressive strength (F_{1c})	-551.60 MPa
Transverse tensile strength (F_{2t})	33.61 MPa
Transverse compressive strength (F_{2c})	-108.94 MPa
In-plane shear strength ($\tau_{u)}$	96.53 MPa

The pole dimensions tested by Philopulos (2002) are presented in Table 3.2 and the ultimate loads are presented in Table 3.3. The loads are applied to the nodes located 305 mm below the tip of the structure (Figure 3.1).

Table 3.2: Pole dimensions (Philopulos, 2002)

Pole	Pole length (mm)	Bottom diameter (mm)	Top diameter (mm)	Joint length (mm)	Average thickness (mm)
A	6000	210	159	305 (with a pole cap)	3
B	6000	210	159	305	3

Static analysis, including geometric nonlinearities due to large deformations, are selected for these tests and stress, strain, deflections, and modes of failure are obtained. Sections 3.3.1 - 3.3.3 provide the evaluation of numerical results compared to data collected through experiments.

Table 3.3: Summary of pole testing (Philopulos, 2002)

Pole	Ultimate load (N)	Mode of failure
A	2441	Local buckling
B	2358	Local buckling

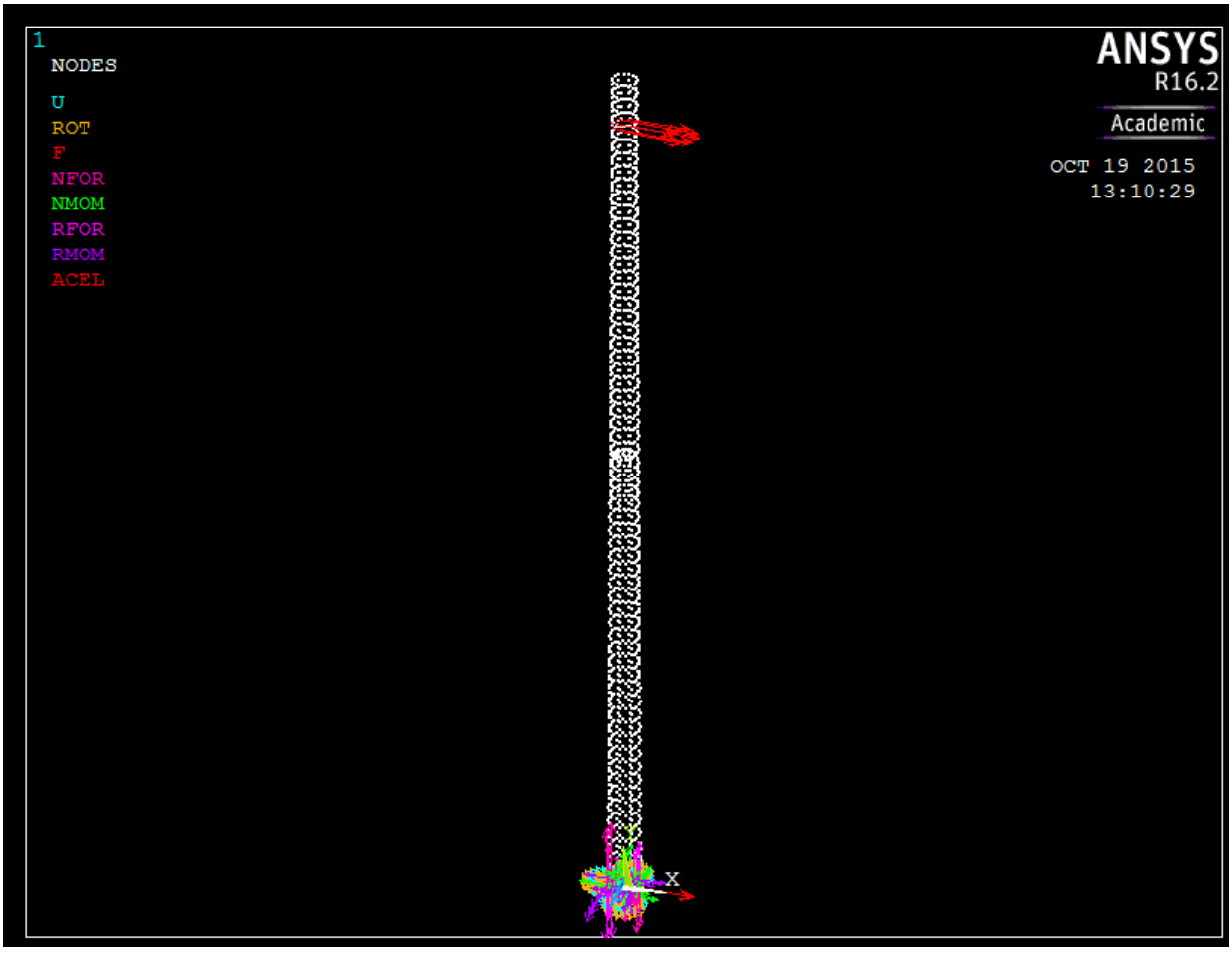

Figure 3.1: Loads applied to the nodes located 305 mm below the tip of the structure

3.3.1 Verifying Deflection Diagrams

3.3.1.1 Introduction

Philopulos (2002) tested four GFRP poles until failure. Poles were tested as cantilevers and a load was applied at 305 mm from the tip of the pole at constant displacement controlled rate of 0.5 mm/min (Figure 3.2). The load-deflection profiles from two of the poles tested, Pole A and Pole B, along with the finite element results are presented in Sections 3.3.1.3.1 and 3.3.1.3.2. The cross sectional properties of the two poles are given in Table 3.2.

Figure 3.2: Pole tested by Philopulos (2002)

3.3.1.2 Modeling Method

The test set-up used in the experiments reported by Philopulos (2002) includes a special FRP composite flange to connect the poles to a steel fixture. This flange, in combination with the steel

fixture, was designed to provide rigid connection for samples under testing. The composite flange however, deformed under loading and the additional deflection caused by this deformation was accounted for by using a moment-deflection diagram of the composite flange (Philopulos, 2002).

3.3.1.3 Modeling of tested GFRP poles

3.3.1.3.1 Deflection of Pole A

Experimental and numerical deflection profiles for Pole A tested by Philopulos (2002) are presented in Figure 3.3. This figure shows that values predicted by finite element modeling correlate highly with experimental results.

A tip maximum deflection of 1148 mm under a load of 2441 N is reported while the calculated FEA value is 1133 mm. The results indicate that models with rigid support at the base have a high accuracy of 98.5% in predicting tip deflection under ultimate load for Pole A. Figure 3.4 demonstrates the experimental and numerical values for tip deflection under different loads applied to the structure. The FEA deflection results shown in the Figure 3.4 are less than 5% lower than the reported experimental results.

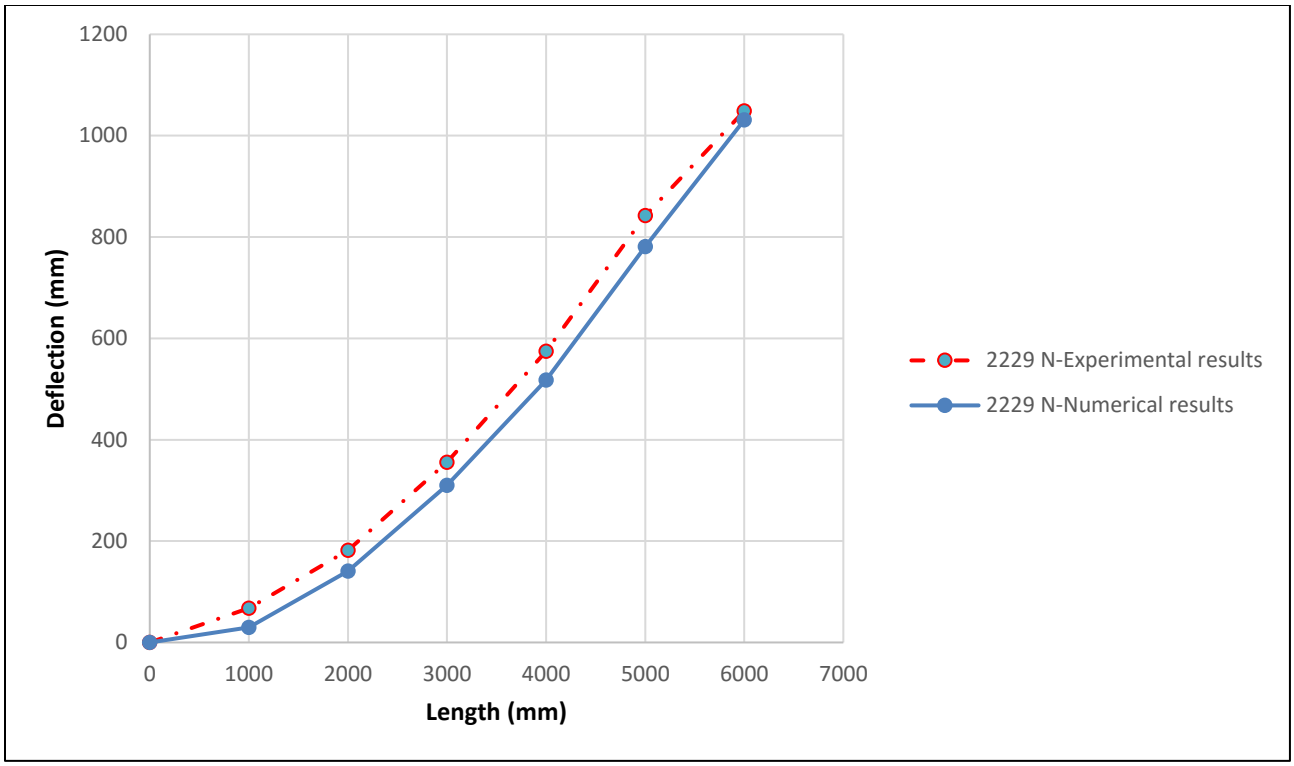

Figure 3.3: Pole A experimental and numerical deflection profiles

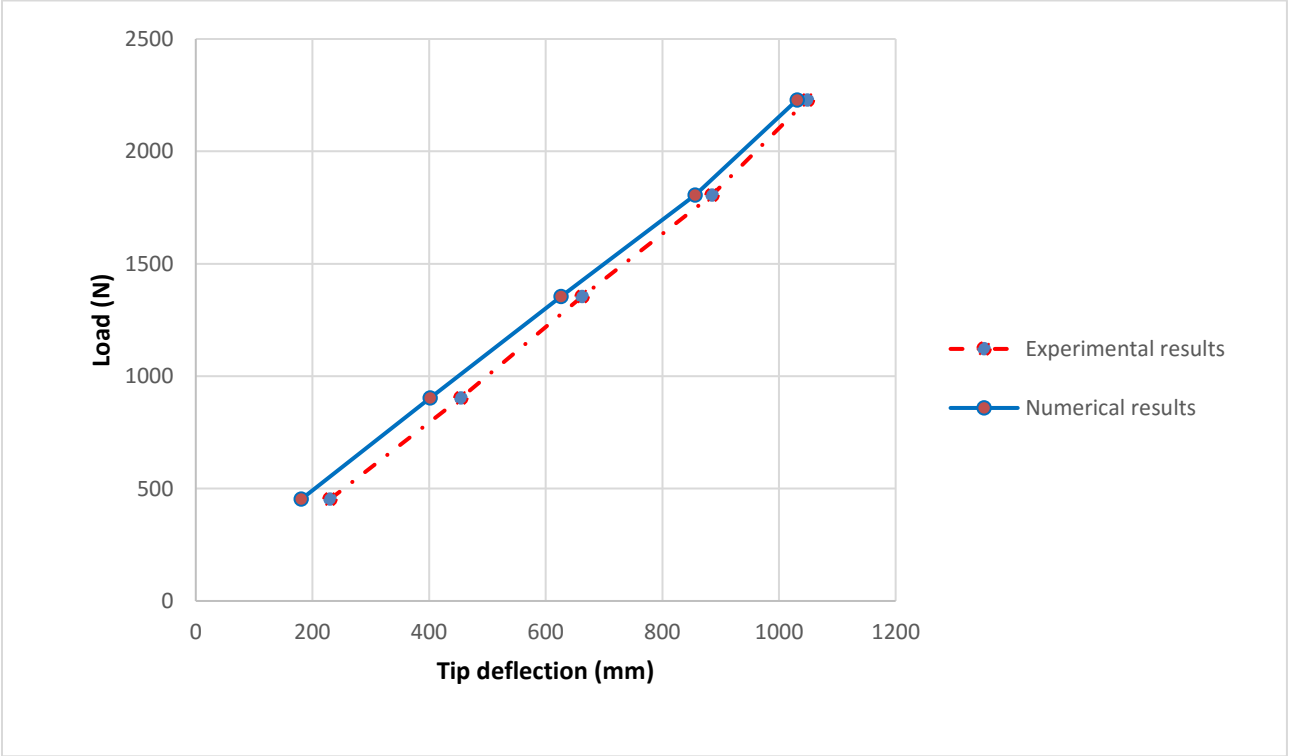

Figure 3.4: Pole A load-tip deflection diagram

3.3.1.3.2 Deflection of Pole B

Deflection profiles for Pole B are presented in Figure 3.5. The tip deflections before failure are 1093 mm and 1070 mm for the experimental program and numerical model, respectively. The FEA model tip deflection prediction is 2.1% less than the experimental result. Figure 3.6 gives Pole B tip deflections under different loads applied to the structure. As in the case of Pole A, numerical results correlate highly with experimental results for Pole B as well. Figure 3.7 shows Pole B deformed shape under the ultimate load obtained by finite element software ANSYS.

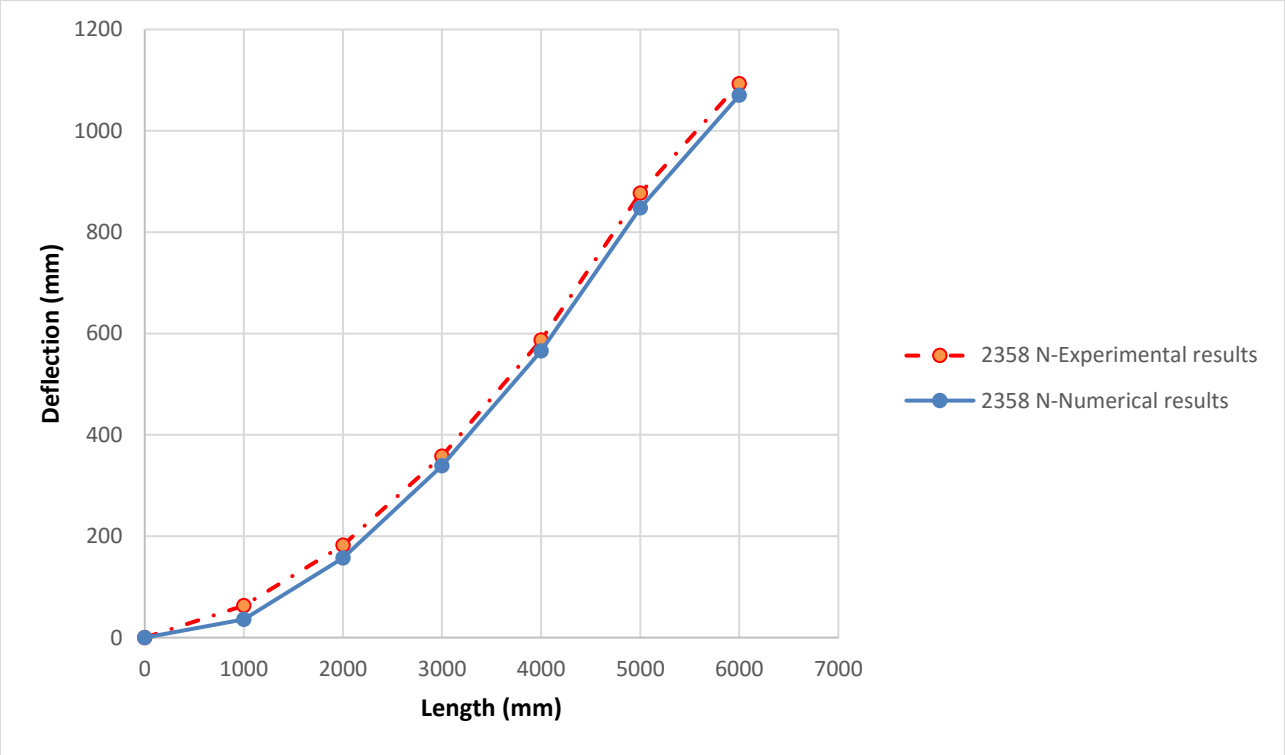

Figure 3.5: Pole B experimental and numerical deflection profiles

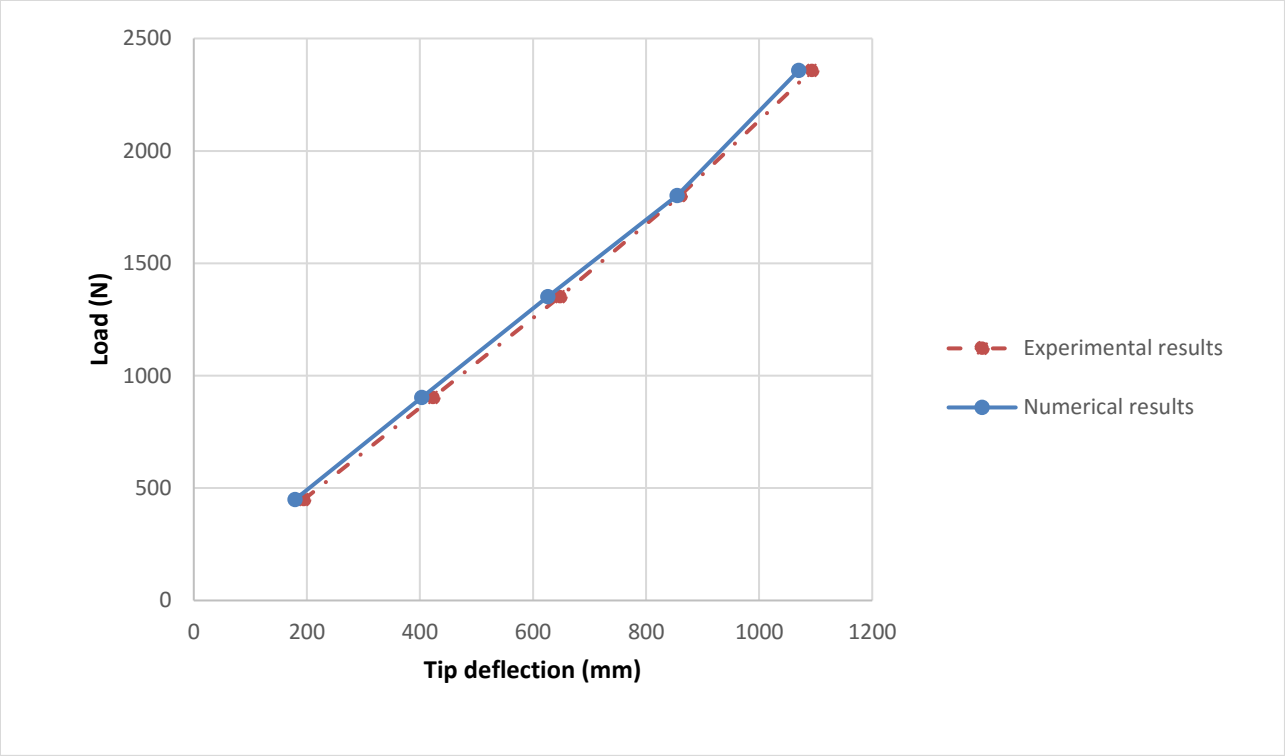

Figure 3.6: Pole B load-tip deflection diagram

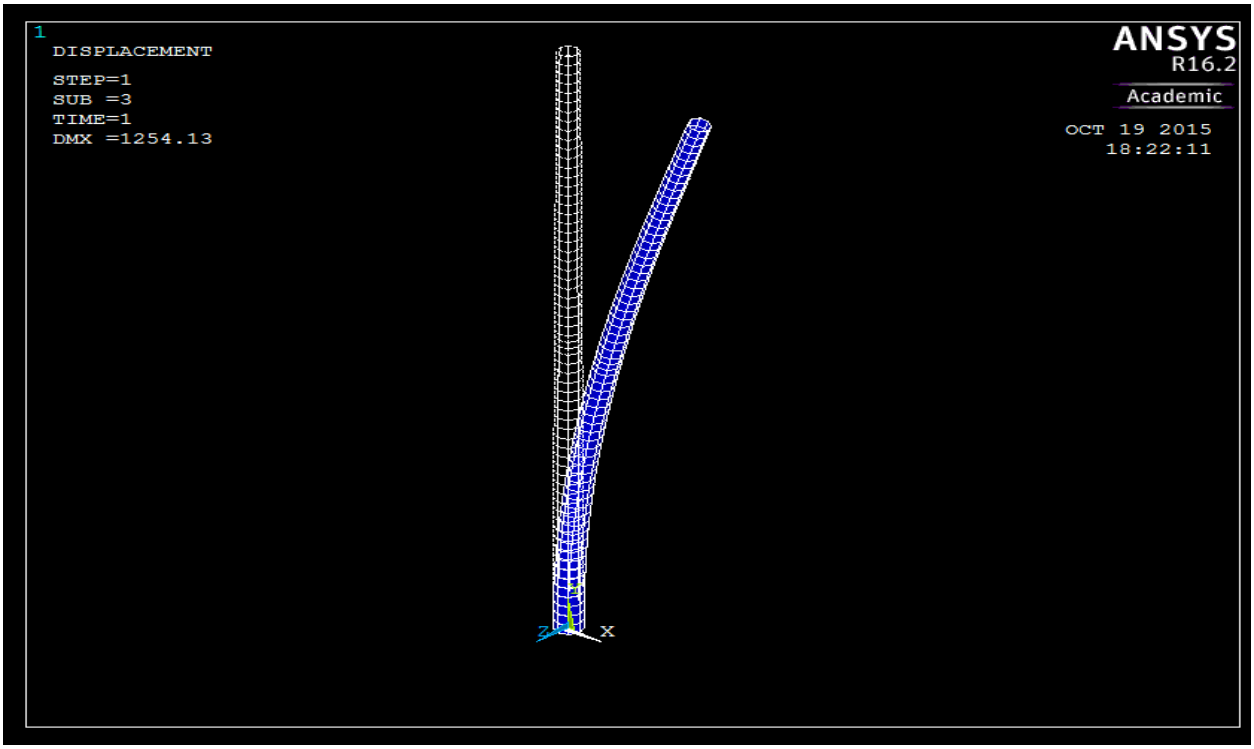

Figure 3.7: Pole B deformed shape under ultimate load

3.3.2 Verifying failure mode

3.3.2.1 Pole A failure mode

Philopulos (2002) tested four tapered GFRP composite poles to failure and Poles A and B failed by local buckling. The numerical models use different failure modes, including the Tsai-Wu, the Maximum stress, the Maximum strain, and local buckling. In this Section it is shown that finite element modeling can also predict modes of failure for these composite poles. To find local buckling easier, deflections were magnified by setting an appropriate user specified scale factor in ANSYS APDL element solution section. Graphical models such as that shown in Figure 3.8 were examined for any evidence of distortion along the pole that may indicate an onset of local buckling. Concentrated dark blue areas in this figure represent locations where local buckling takes place.

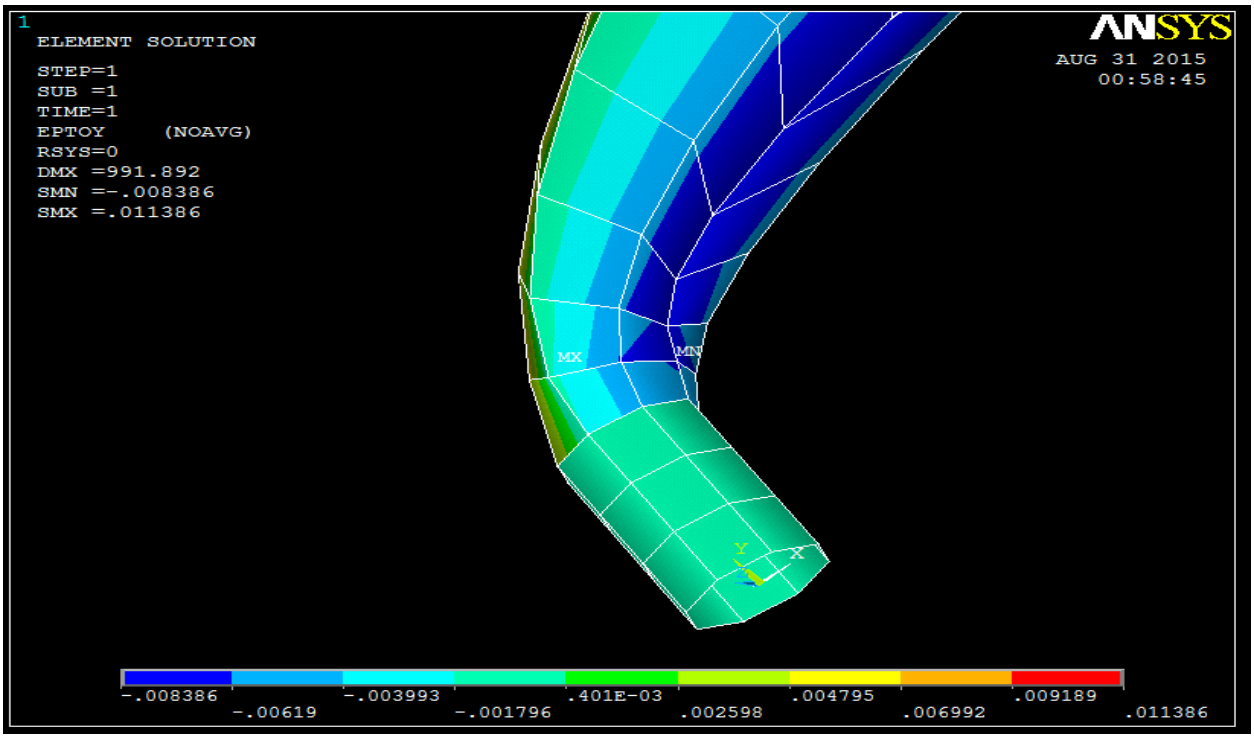

Figure 3.8: Exaggerated deformed shape of Pole A

In the experimental research reported by Philopulos (2002), Pole A is shown to have failed by local buckling close to the base of the structure under an ultimate load of 2441 N applied 305 mm below the tip of the pole. The numerical results, shown in Figure 3.8, confirm the existence of local buckling in Pole A. Concentrated dark blue areas in this figure represent locations where local buckling has taken place.

The Maximum Stress, Tsai-Wu, and Maximum strain failure criteria for Pole A are shown in Figures 3.9, 3.10, and 3.11. The maximum values for Tsai-Wu and Maximum Stress are shown to be present on the tension side of the pole near the support. Maximum strain failure criterion suggests that maximum strains take place at locations where local buckling is observed in the experimental phase (Figure 3.11).

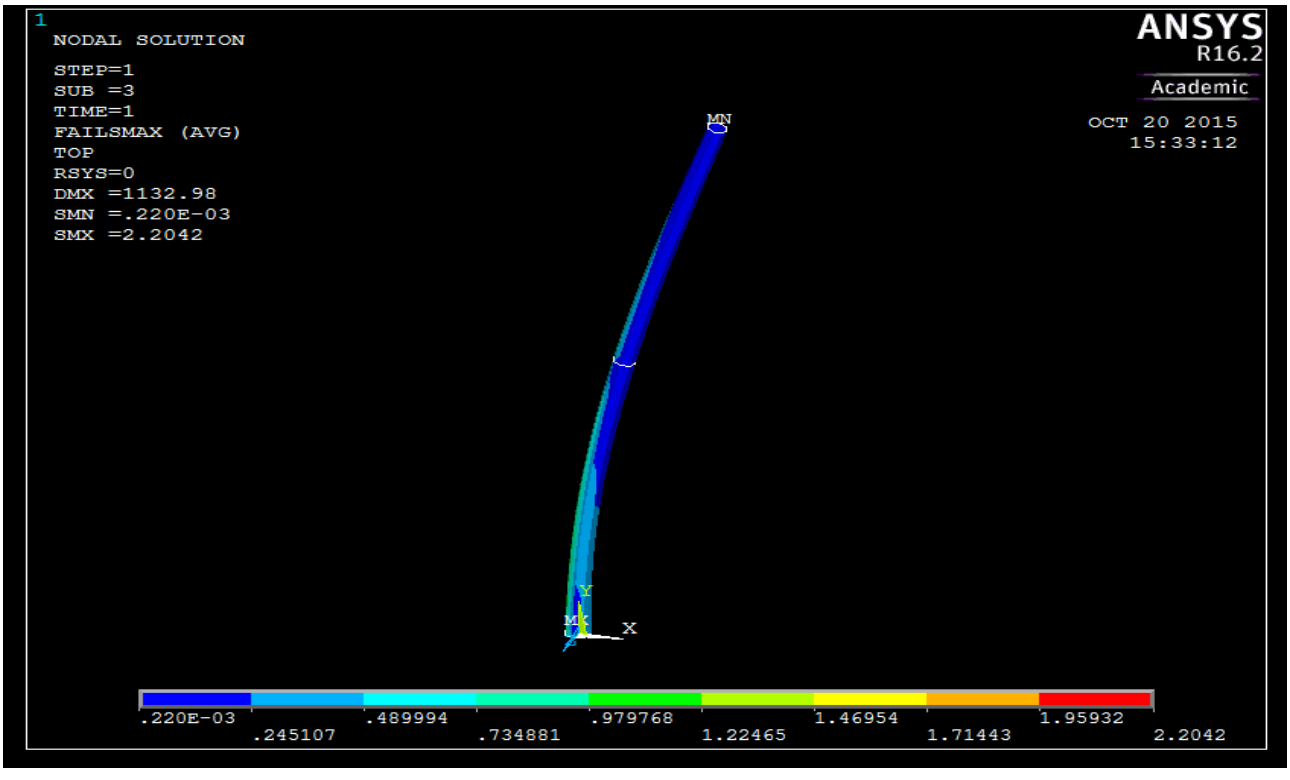

Figure 3.9: Maximum Stress values for Pole A

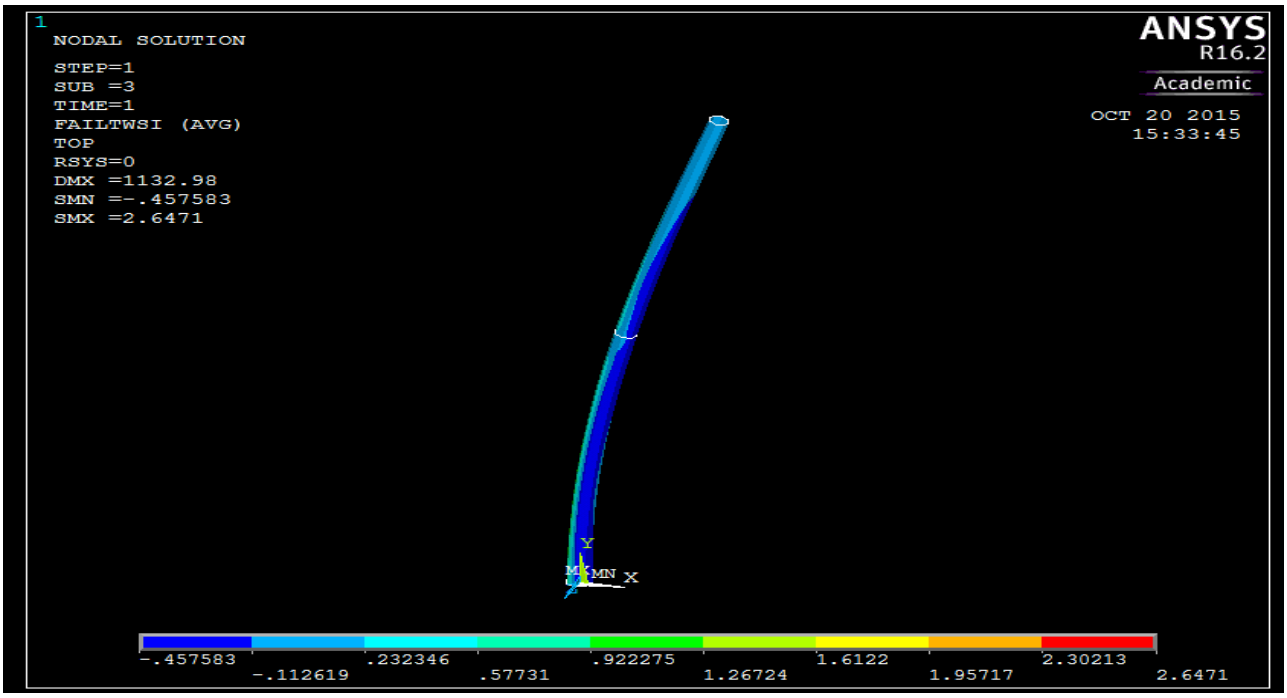

Figure 3.10: Tsai-Wu values for Pole A

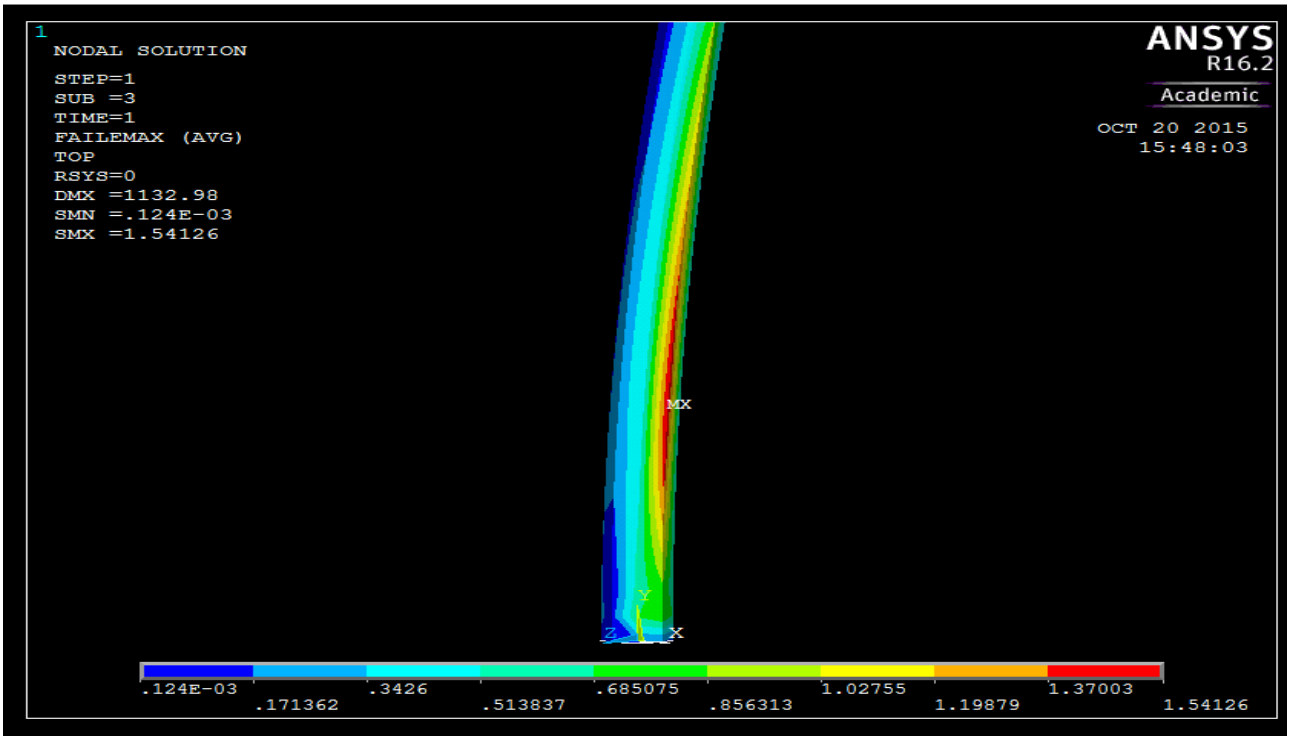

Figure 3.11: Maximum strain values for Pole A

3.3.2.2 Pole B failure mode

As in the case of Pole A, Philopulos (2002) reports that Pole B also failed by local buckling. Maximum Stress and Tsai-Wu values, shown in Figures 3.13 and 3.14 for Pole B, are smaller compared to those of Pole A, which is due to lower ultimate loads applied to Pole B (Table 3.3). Figure 3.12 shows an exaggerated deformed shape of Pole B while the Maximum strain values for Pole B are shown in Figure 3.15.

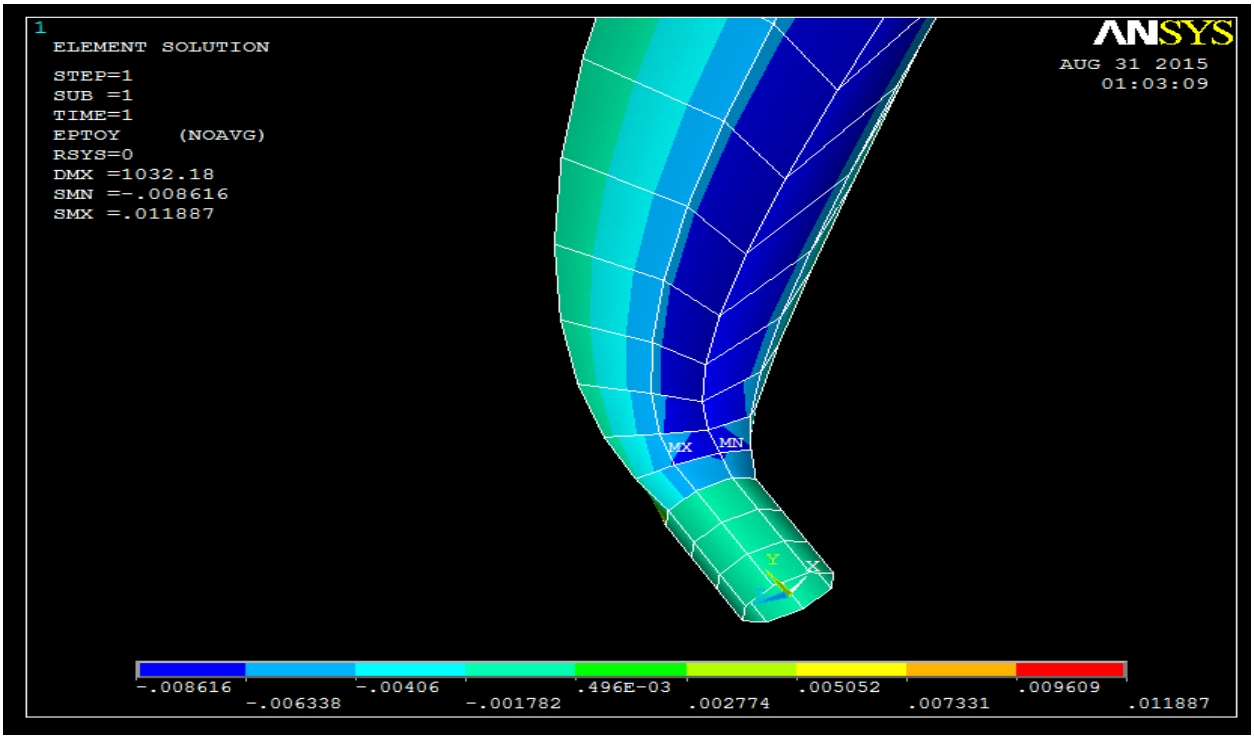

Figure 3.12: Exaggerated deformed shape of Pole B

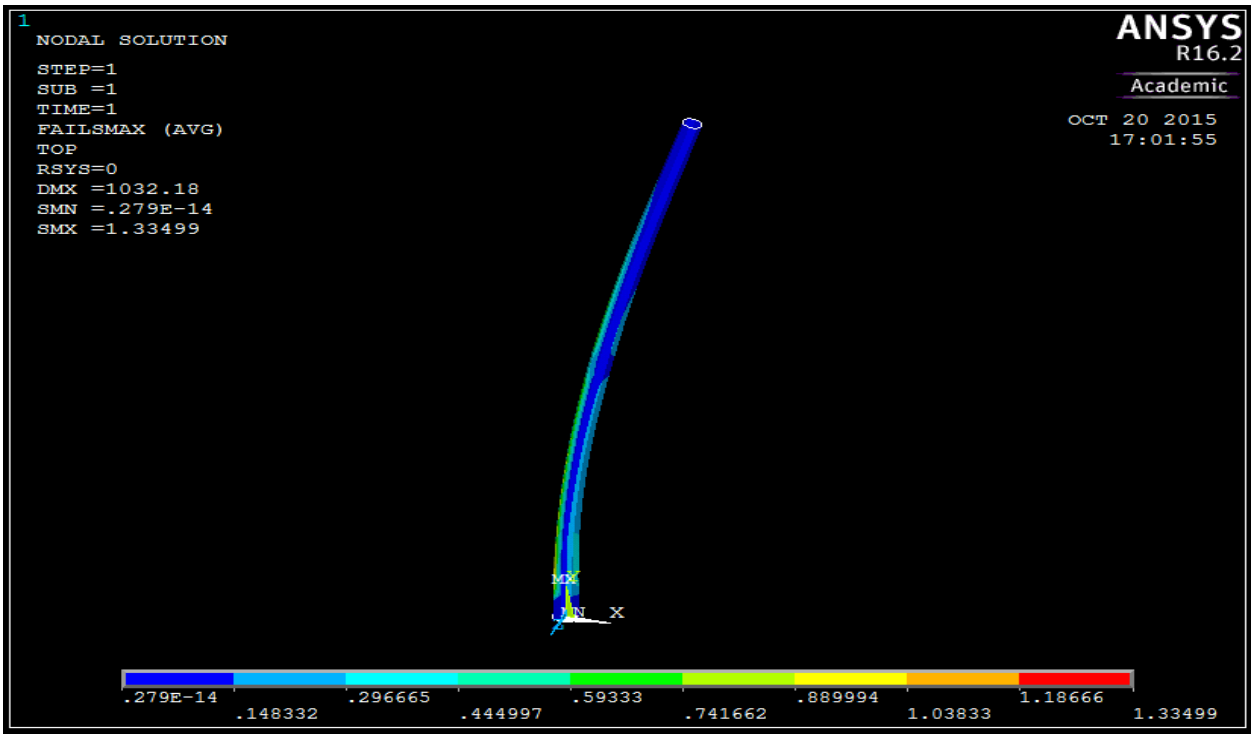

Figure 3.13: Maximum Stress values for Pole B

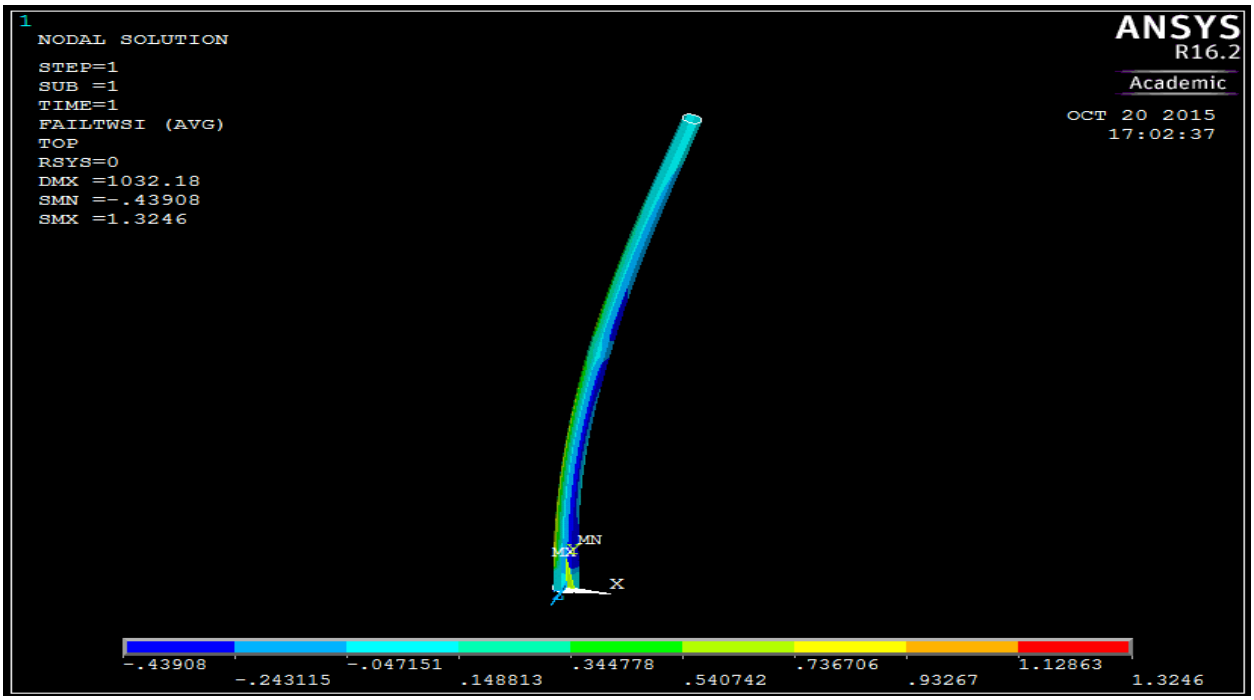

Figure 3.14: Tsai-Wu values for Pole B

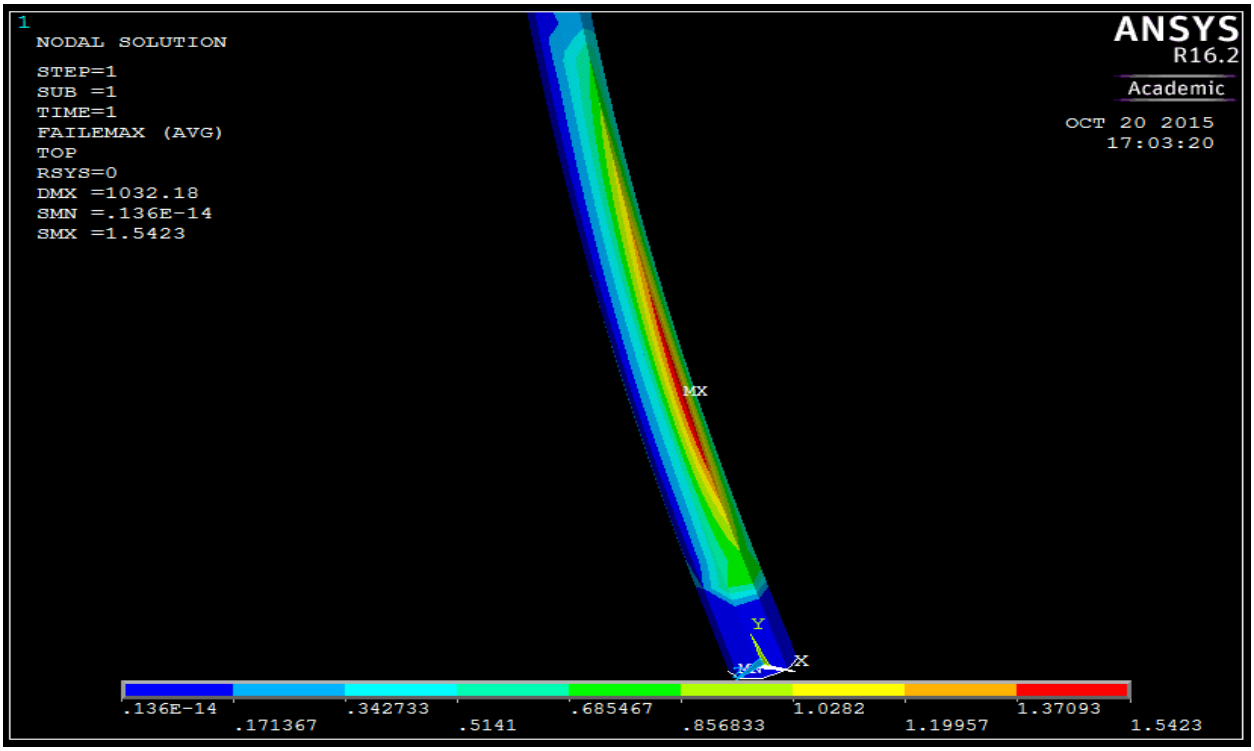

Figure 3.15: Maximum strain values for Pole B

3.3.3 Verifying strains

In the experimental work reported by Philopulos (2002), strain gauges were installed on the compression side of the poles, where failure was anticipated. Therefore, compressive strains are the only experimental data available to verify the numerical modeling for strains.

3.3.3.1 Modeling of tested GFRP poles

Table 3.4 presents the location of strain gauges attached to Poles A and B to record strains occurred during testing (Philopulos, 2002). Data recorded through Data Acquisition System is demonstrated in the following figures in combination with numerical results.

Table 3.4: Location of strain gauges (mm) (Philopulos, 2002)

Strain gauge #	Distance from support (mm)	
	Pole A	Pole B
SG1	0	0
SG2	152	254
SG3	305	508
SG4	457	762
SG5	3048	1016
SG6	3353	1270
SG7	3505	2946
SG8	3658	3048
SG9	-	3150
SG10	-	3302
SG11	-	3454

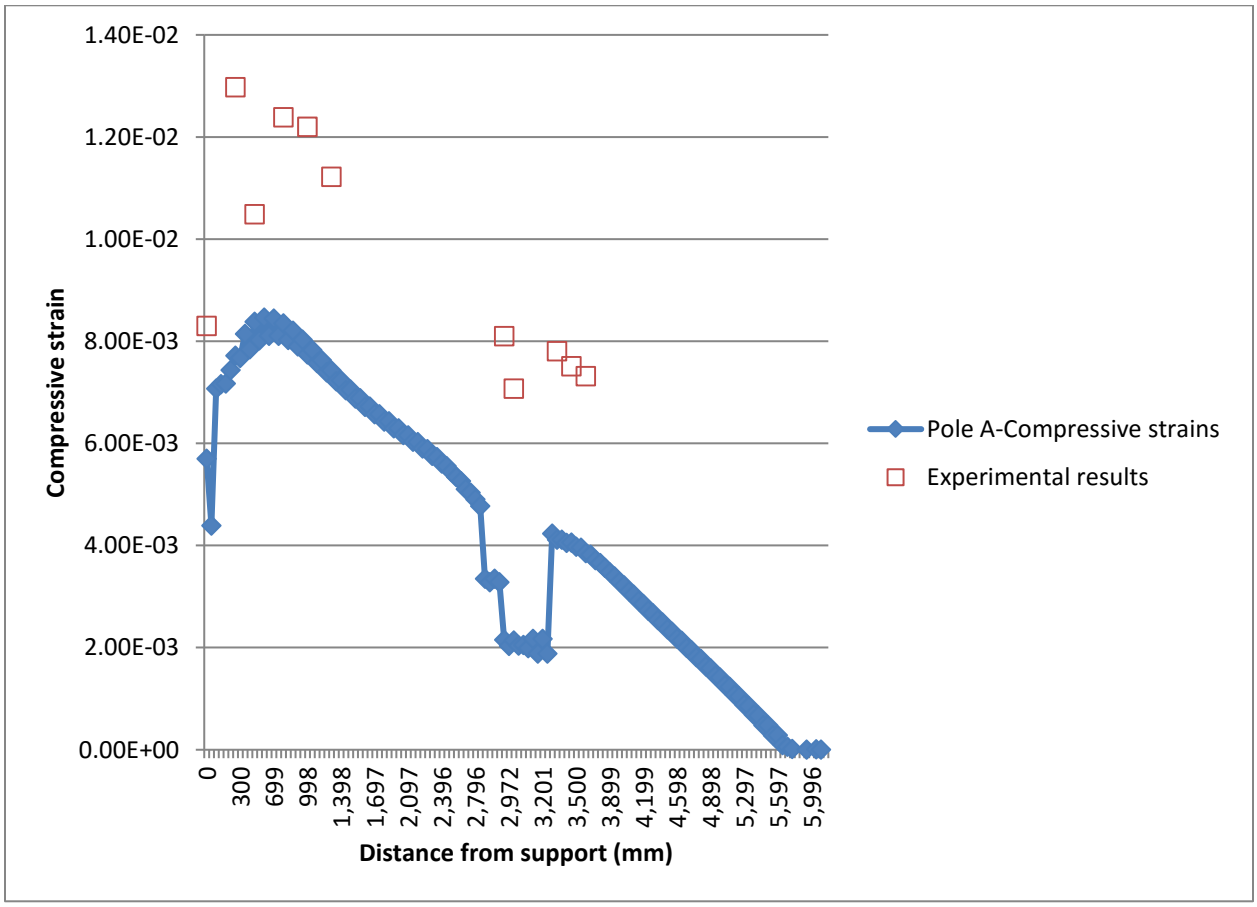

Figure 3.16: Compressive strains along the length of the Pole A

Figure 3.16 shows experimental and FEM results for Pole A. This graph suggests that the numerical method tends to give lower values for compressive strains along the length of the pole in comparison to the experimental results. Tensile strains calculated by the FEM, shown in Figure 3.17, could not be compared with experimental results since no strain gauges were placed on the tensile side of the samples tested.

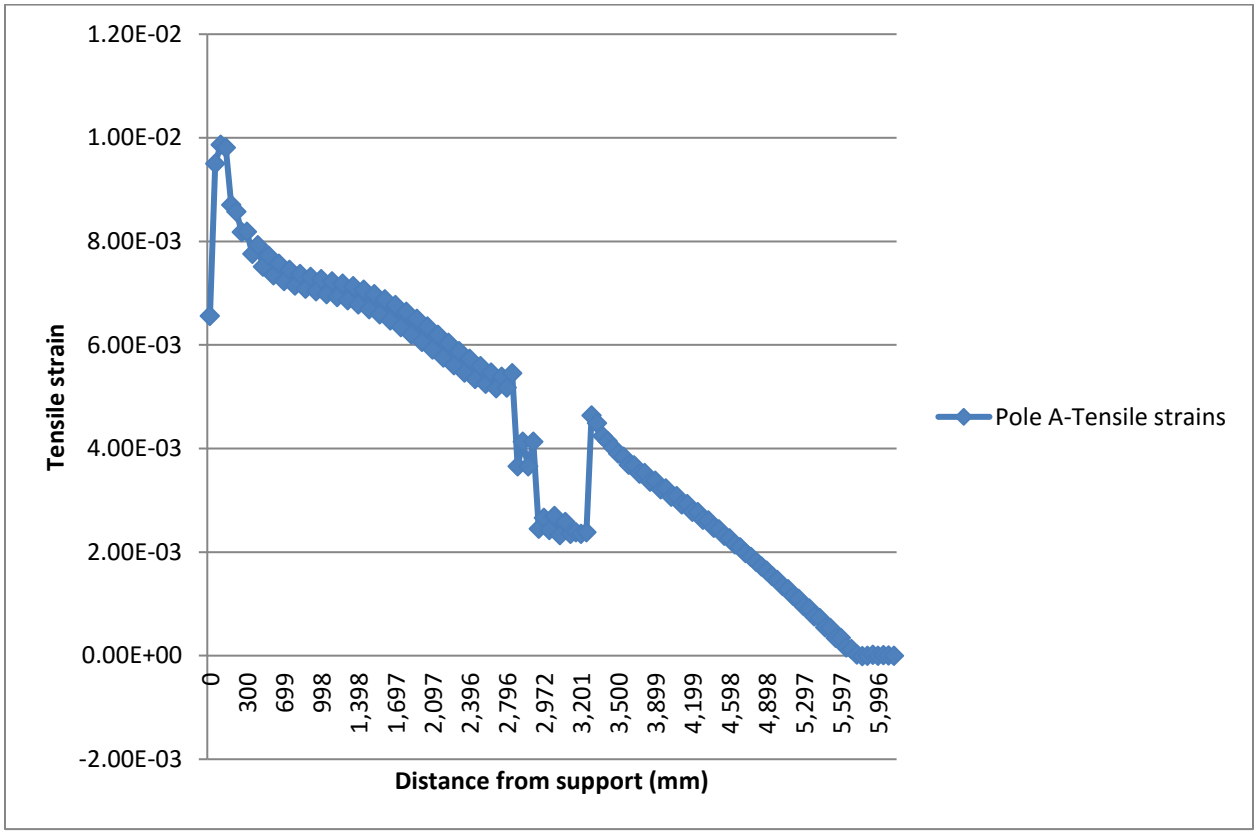

Figure 3.17: Tensile strains along the length of the Pole A

The numerical results for Pole B compare well with the experimental data, as shown in Figure 3.18. The distribution of the tensile strains for Pole B are shown in Figure 3.19.

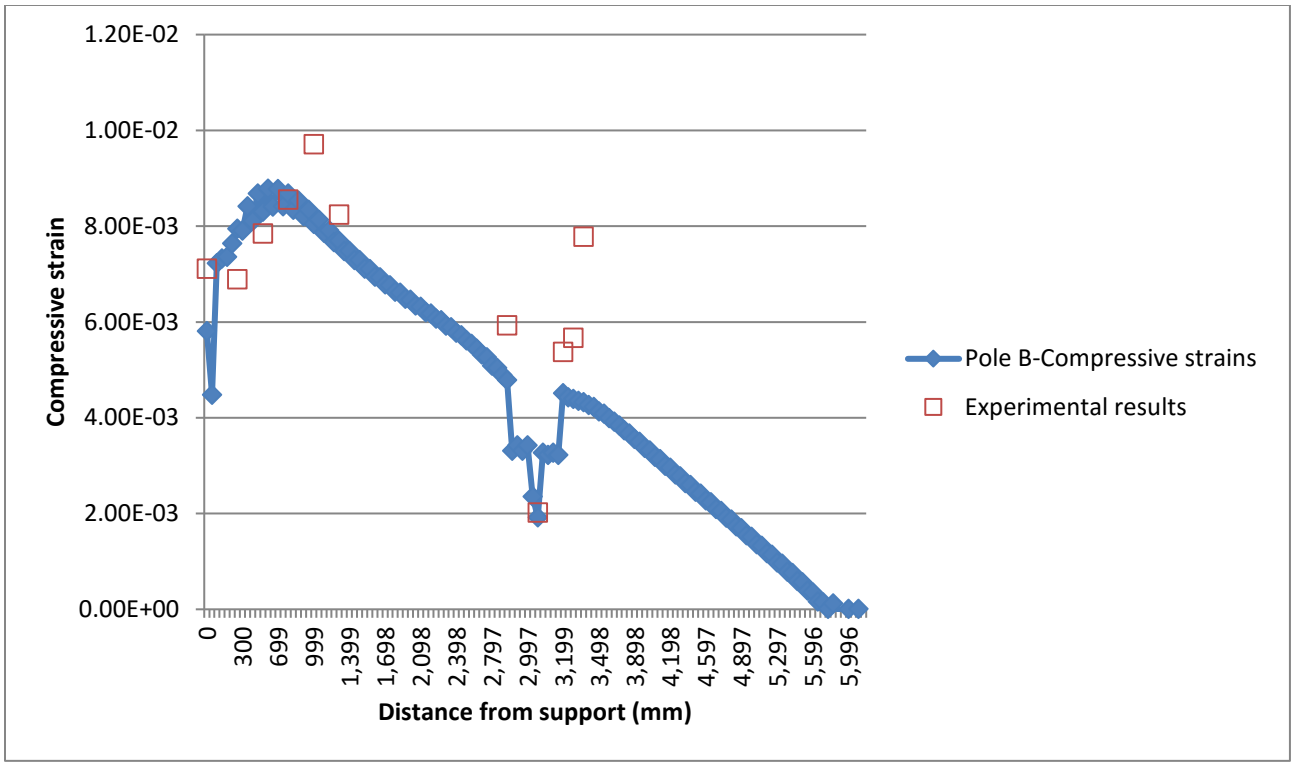

Figure 3.18: Compressive strains along the length of the Pole B

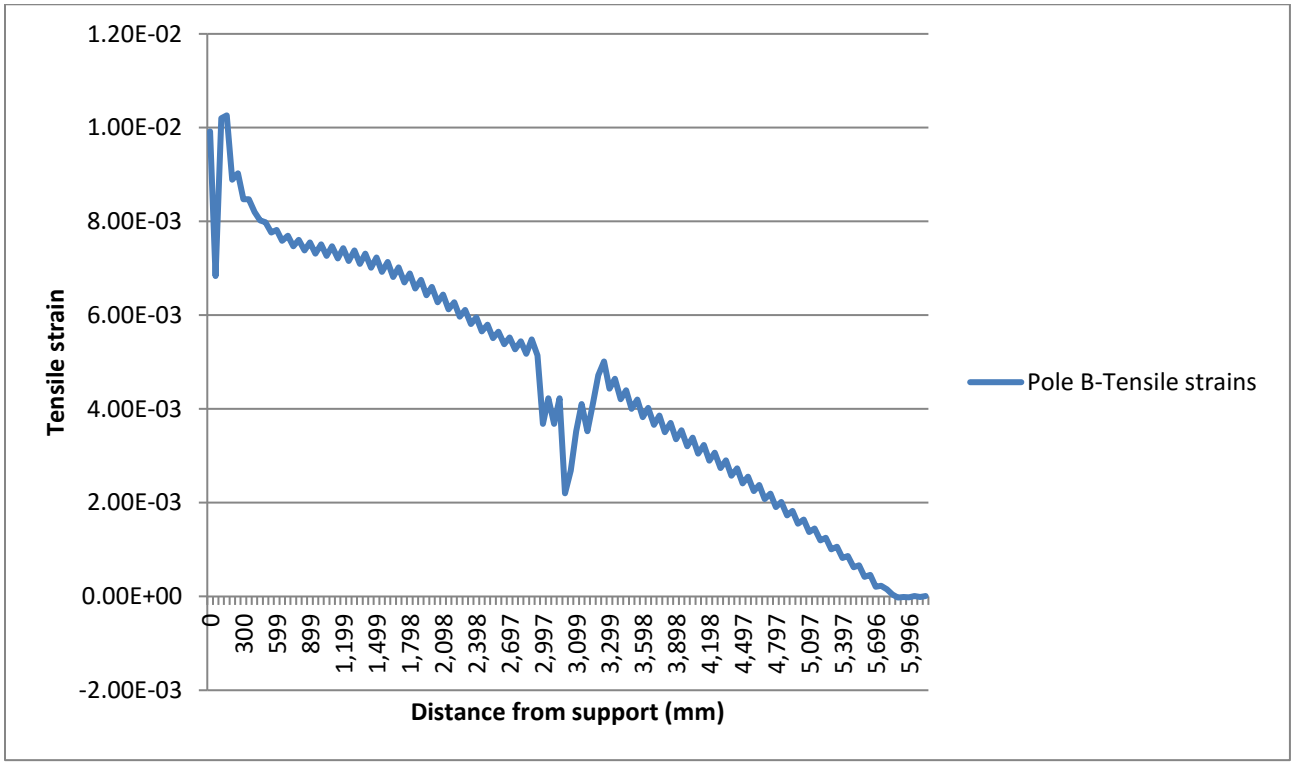

Figure 3.19: Tensile strains along the length of the Pole B

3.4 Verifying the numerical modeling - Conclusions

In Section 3.3.1, deflection profiles for two poles tested by Philopulos (2002) are shown using results from the FEM. Results obtained from finite element models correlated well with experimental results. The failure modes of Poles A and B are discussed in Section 3.3.2. These poles failed by local buckling and numerical models confirm this mode of failure for Poles A and B. In addition to local buckling, the numerical results suggest that material failure could have taken place in these poles near the support.

Tensile and compressive strains of the composite poles tested by Philopulos (2002) are given in Section 3.3.3. Results suggest that numerical values for compressive strains in Pole B are in good agreement with the experimental results. However, numerical and experimental results shown in Figure 3.16 for Pole A do not correlate as well.

In conclusion, the results presented in Sections 3.3.1, 3.3.2 and 3.3.3 provide reliable information to suggest that FEM can be used as a powerful tool for analyzing FRP composite poles.

Chapter 4: Analysis of FRP composite light standards

4.1 Modeling FRP composite poles for light standards

The analysis of FRP composite light standards is presented in this chapter. Light standards are produced in different sizes using a number of different materials including steel, concrete, and wood. In this chapter two sizes of light standards are considered and analyzed according to North American standards: 6 m and 12 m long standards.

The loading calculations, including wind pressure, snow, and icing are discussed in Section 4.2. These load requirements are based on the AASHTO Standard Specifications for structural supports for highway signs, luminaires, and traffic signals (AASHTO, 2013).

The light standards considered in this study consist of tapered tubular FRP sections designed to support a one-arm luminaire, shown in Figure 4.1. To analyze their structural performance, ANSYS software is used and deflection profiles, stress and strain distributions, and different failure modes are investigated. To obtain optimum cross-section dimensions as well as thicknesses and fiber orientations, multiple cases are examined. The results are discussed in Sections 4.4.1 to 4.4.3.

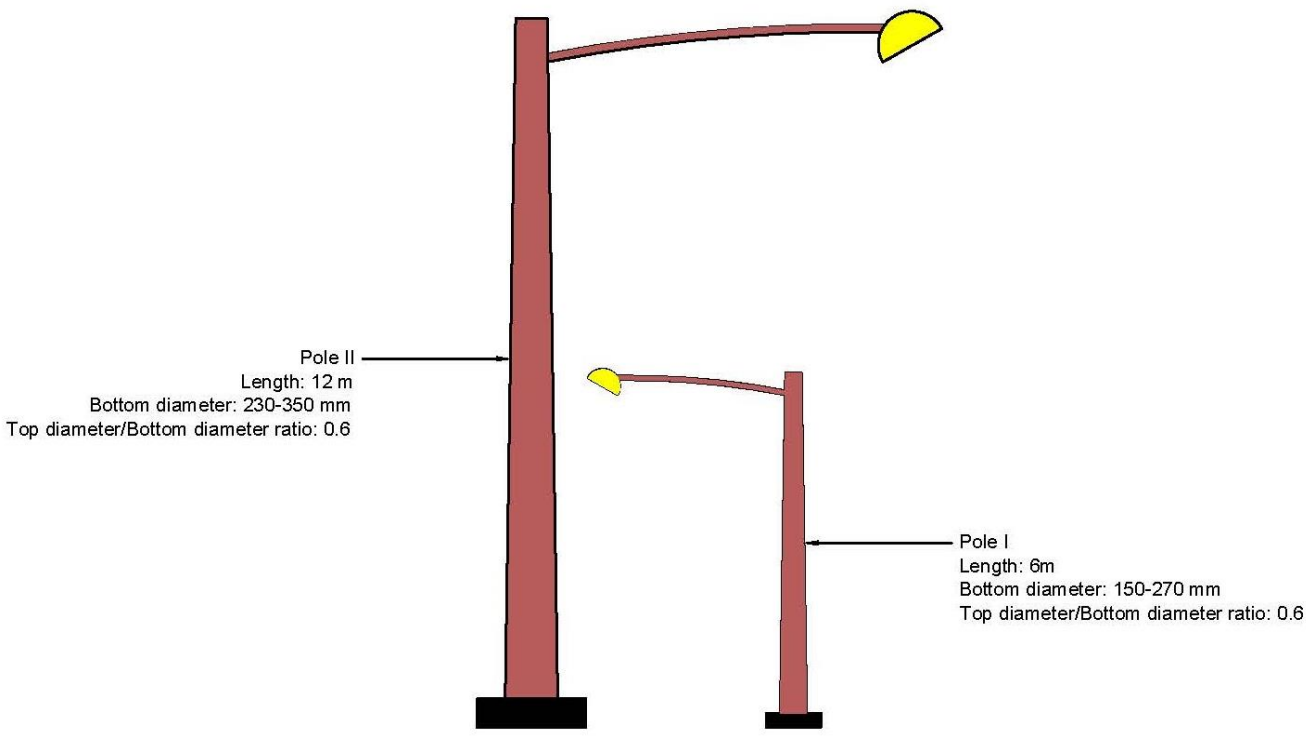

Figure 4.1: Composite poles for light standards

The bottom diameter of the poles being examined range from 150 mm to 270 mm for the 6 m poles and from 230 mm to 350 mm for the 12 m poles. An average wall thickness of 2.4 mm for the 6 m poles and 4 mm for the 12 m poles is used in the analysis. In the modeling process it is assumed that poles are connected rigidly at the support and are free at the top.

4.2 Loading calculations

The AASHTO Standard Specifications, Section 3.1, outline the loading requirements for the design of support structures for luminaires. It includes minimum load cases that should be considered, provides limits of their application and outlines different load combinations for the design of these structures. These requirements are discussed in the following Sections.

4.2.1 Dead load

The dead load for designing luminaires includes the self-weight of the poles, the cantilever arm, the luminaire, and the surge protection device.

To determine the self-weight of the poles, a GFRP density of 1950 kg/m^3 is used (Ungkurapinan, 2005). This self-weight is included in the FEA. The weight of the cantilever arm is assumed to be 10% of the self-weight of the pole. Various data sheets for luminaires and surge protections were consulted in order to obtain an appropriate mass for the surge protection device. Finally a conservative mass of 10 kg for this device, located at the end of cantilevered arm, is used in the FEA. The total mass of the 6 m and 12 m luminaires used in the FEA are 36.4 kg and 87 kg, respectively.

4.2.2 Live load

The AASHTO Standard Specification Section 3.6, also specifies a live load of 2200 N be distributed over 0.6 m in designing members of walkways and service platforms. This load is specified to take into account temporary loads applied during servicing and maintenance of the structure. To service luminaires, usually small- to medium-sized bucket trucks are used. Therefore, this live load was not considered in the FEA of the supporting structures for luminaires.

4.2.3 Ice load

An ice pressure of 145 Pa is used in the design of vertical and horizontal supports (the cantilevered arm) of luminaires. This ice pressure is based on the assumption that a 15 mm radial thickness of ice (AASHTO, 2013) accumulates around the external exposed surfaces of the luminaire. This ice pressure is based on a snow density of 960 kg/m^3 (AASHTO, 2013).

4.2.4 Wind load

The AASHTO Standard Specifications require that a wind pressure be applied horizontally on the luminaires. This wind pressure is based on a basic wind speed with a 50-year mean recurrence interval (AASHTO, 2013). Luminaire design is dominated by wind loads calculated according to Eq. 4.1. A summary of wind pressure calculations and how they are applied to the structure is presented here.

$$P_z = 0.613 K_z G V^2 I_r C_d \qquad 4.1$$

Where, P_z is the wind pressure; K_z is the height and exposure factor; G is the gust effect factor; V is the basic wind speed with a 50-year mean recurrence interval (m/s); I_r is the importance factor based on the r_{th} mean recurrence interval; and C_d is the drag coefficient.

The basic wind speed (V) used in Eq. 4.1 is found in the AASHTO Standard Specifications. A value of 40 m/s is used in the FEA of the 6 m and 12 m poles in this study. This wind speed corresponds to an annual probability of 2% that the wind speed will be met or exceeded in a 50-year mean recurrence interval. According to the same Standard, the minimum design life for luminaire support structures is 50 years. An importance factor of 1 is also assumed in the FEA. Depending on the local ground conditions, the wind speed profile changes in height. This variation is created by the frictional drag caused by various types of terrain. The AASHTO Standard Specifications offer a height and exposure factor of K_z=0.94 and K_z=1.05 for 6 m and 12 m luminaires, respectively.

The gust-effect factor G in Eq. 4.1 accounts for the dynamic interaction of the structure with the gustiness of the wind. AASHTO Standard Specifications require a wind-sensitive design for structures that either have a fundamental frequency equal to or less than 1Hz or their height-to-

least horizontal dimension ratio is greater than 4. This indicates that the luminaires being investigated in this study should follow a wind-sensitive design procedure. For this purpose, the AASHTO Standard Specifications require a minimum value of 1.14 be used for a gust effect factor G.

The drag coefficient C_d is a dimensionless coefficient that represents the resistance of an object in a fluid environment. Drag coefficient of different cross sections are given in the AASHTO Standard Specifications. In general, round sections such as the poles in this study tend to have lower resistance against wind flow around the structure. As a result, lower drag coefficients are suggested for these sections compared to rectangular or triangular sections. A drag coefficient of C_d=0.5 for generally rounded surfaces is specified.

To calculate the applied wind loads, the wind pressure, calculated using Eq. 4.1, is multiplied by the exposed area of the pole, the cantilevered arm, the luminaire, and any other attachments. The probability of maximum wind loads occurring at the same time in both directions is very small, so the AASHTO Standard Specifications suggest the two load cases of normal and transverse wind loads listed in Table 4.1.

Table 4.1: Design wind load cases for vertical supports (AASHTO, 2013)

Load case	**Normal component**	**Transverse component**
1	1.0 (BL)	0.2 (BL)
2	0.6 (BL)	0.3 (BL)

The basic wind load (BL) mentioned in Table 4.1 comprises the effects of the wind load on exposed vertical support, the wind load on luminaire, and the wind load on horizontal support.

To calculate the bending moments, the loads are applied at the centers of their respective pressure areas.

4.2.5 Fatigue

According to AASHTO Standard Specifications, supporting structures for luminaires should follow a wind-sensitive design procedure and damaging vibrations caused by wind load should be taken into account. Clause 10.4.3 in the AASHTO Standard Specifications require appropriate damping or energy-absorption devices be installed to prevent significant wind-induced vibrations in these structures. However, luminaires designed in this study are 6 m and 12 m tall and the AASHTO Standard Specifications, clause 11.7.2, indicate that "Luminaires less than 55 ft tall do not need to be designed for fatigue." Thus, no fatigue considerations are taken into account in this FEA.

4.2.6 Load combinations

The dead load, live load, ice load, and wind load should be combined into appropriate groups to represent rational worst load cases that the structure can experience during its lifetime. The AASHTO Standard Specifications list three group loads, shown in Table 4.2.

Table 4.2: Group load combinations (AASHTO Table 3.4.1)

Group load	Load combination
I	DL
II	DL+W
III	DL+Ice+1/2(W)

*Wind load for group load III are computed using a minimum wind pressure of 1200 Pa (AASHTO, 2013)

The loads used to complete a set of parametric studies in Section 4.4 in order to obtain an optimum size, fiber orientation, and wall thickness for the 6 m and the 12 m tall poles supporting the luminaires are listed in Table 4.3. The AASHTO Standard Specifications also set deflection limits for vertical and horizontal components of structural supports. These limits are used to ensure an aesthetically appropriate structure under dead loads as well as allowable serviceability deflections under applied loads. Conventional elastic methods and equations are acceptable by this Standard to determine deflections.

Table 4.3: Wind load applied to the light standards

6 m luminaires					**12 m luminaires**				
Bottom diameter (mm)	Top diameter (mm)	Height above ground (m)	Wind load (N)		Bottom diameter (mm)	Top diameter (mm)	Height above ground (m)	Wind load (N)	
			Group load II	Group load III				Group load II	Group load III
210	126	1	167	381	300	180	2	534	1091
		2	156	355			4	497	1015
		3	144	328			6	460	940
		4	132	302			8	401	820
		5	121	276			10	386	789
		6	109	249			12	349	714

The deflection limits for the poles, according to the AASHTO Standard Specifications (2013) are:

a) A tip deflection under Group I load combination (DL only) limited to 2.5% of pole height; and,

b) A tip deflection under Group II and III load combinations (DL+W) limited to 15% of pole height.

4.3 Composite pole design

In this Section, various FRP poles for luminaires are investigated using ANSYS. The optimum design for 6 m poles and 12 m poles is detailed in Section 4.5. These two sets of luminaires were designed according to AASHTO Standard Specifications (2013). A nonlinear static analysis was employed for the analysis of these poles and to obtain deflection profiles as well as stress and strain distributions.

To obtain the optimum cross section, the bottom diameters were varried from 150 mm to 270 mm for 6 m poles, and from 230 mm to 350 mm for 12 m poles. Furthermore, different ratios of longitudinal layers to total number of layers and different longitudinal fiber orientations were studied to determine a lay-up process that would result in low internal stresses in the structure, small deflections and a minimum overall weight. The required material properties used in the FEA are based on previously published work by Philopulos (2002) and are discussed in Chapter 3. A fiber volume fraction of 58.1%, obtained in a burn-off test performed by Philopulos (2002), was also used.

4.4 Parametric study

In Chapter 3, numerical results are compared with experimental data in order to validate the finite element models. These finite element models are used to analyze composite poles that support luminaires. Since these GFRP poles are fabricated using the filament-winding method, different parameters that can affect their structural performance need to be studied. In this chapter, three cases are investigated: a) The effect of number of longitudinal layers 2) the effect of longitudinal fiber orientation; and c) the effect of cross-section properties on the performance of the FRP poles. These three cases are examined for two types of FRP poles: 6 m and 12 m long

poles. This parametric study is explained in detail in Sections 4.4.1 to 4.4.3. Optimum designs are provided in Section 4.5.

Different composite pole configurations are analyzed in this chapter using the load combinations presented in Table 4.2 based on the AASHTO Standard Specifications (2013). A preliminary analysis showed that the critical load case would be either Group II or Group III, given in Table 4.2.

4.4.1 Case 1: The effect of number of longitudinal layers on the ultimate strength of GFRP poles

As a part of the analytical study, the effect of the number of longitudinal layers with respect to the total number of layers (Rn ratio) on the performance of the poles is examined. Two types of poles are modeled in this Section. Each type represents a different category of external dimensions. The cross sectional dimensions, the number of longitudinal and circumferential layers, and the longitudinal fiber orientations for Case 1 are presented in Tables 4.4 to 4.7.

Table 4.4: Geometric properties for 6 m poles studied in Case 1

Geometric Properties					
Total length(mm)	Bottom diameter (mm)	Top diameter (mm)	Top diameter/Bottom diameter ratio	Wall thickness (mm)	Mass (kg)
6000	210	126	0.6	2.4	14.7

Table 4.5:Fiber arrangement and numerical results for 6 m poles

Fiber Arrangement						Results			Results		
						Group load II			Group load III		
Number of circum. layers (Nc)	Number of long. layers (Nl)	Total number of layers (Nt)	Rn=Nl /Nt	Long. fiber orientation	Fiber to weight volume percentage	Maximum lateral deflection (mm)	Lateral deflection /free length (%)	Failure mode	Maximum lateral deflection (mm)	Lateral deflection/ free length (%)	Failure mode
8	0	8	0/8	+/-5°	58.10%	654	11	Tsai-Wu and Maximum stress and Maximum strain-tension side support	710	12	Tsai-Wu and Maximum stress and Maximum strain-tension side support
6	2	8	2/8			387	6	No failure	424	7	No failure
4	4	8	4/8			288	5	No failure	316	5	No failure
2	6	8	6/8			244	4	No failure	268	4	No failure
0	8	8	8/8			242	4	No failure	264	4	No failure

Table 4.6: Geometric properties for 12 m poles studied in Case 1

Geometric Properties					
Total length (mm)	Bottom diameter (mm)	Top diameter	Top diameter/Bottom diameter ratio	Wall thickness (mm)	Mass (kg)
12000	300	180	0.6	4	70

Table 4.7: Fiber arrangement and numerical results for 12 m poles studied in Case 1

Fiber Arrangement						Results			Results		
						Group load II			Group load III		
Number of circum. layers (Nc)	Number of long. layers (Nl)	Total number of layers (Nt)	Rn=Nl /Nt	Long. fiber orientation	Fiber to weight volume percentage	Maximum lateral deflection (mm)	Lateral deflection /free length (%)	Failure mode	Maximum lateral deflection (mm)	Lateral deflection/ free length (%)	Failure mode
8	0	8	0/8	+/-5°	58.10%	1703	14	Tsai-Wu and Maximum stress and Maximum strain-tension side near the support- Local Buckling near the support	1735	14	Tsai-Wu and Maximum stress and Maximum strain-tension side near the support- Local Buckling near the support
6	2	8	2/8			1354	11	Probable Local Buckling near the support	1380	12	Probable Local Buckling near the support
4	4	8	4/8			1285	11	No failure	1310	11	No failure
2	6	8	6/8			1303	11	No failure	1328	11	No failure
0	8	8	8/8			1331	11	Tsai-Wu and Maximum stress and Maximum strain-tension side near the support	1357	11	Tsai-Wu and Maximum stress and Maximum strain-tension side near the support

The composite FRP poles are designed to have a total wall thickness of 2.4 mm for 6 m poles and 4 mm for 12 m poles. These poles consist of eight layers with equal thickness. As a result 6 m and 12 m poles weigh 14.7 kg and 70 kg, respectively. To examine the effect of longitudinal layers on the structural performance of luminaires, the ratio of longitudinal layers-to-total number of layers is varied from 0/8 to 8/8. To complete Case 1, the longitudinal fiber orientation is kept constant at +/-5° with respect to the vertical axis of the structure.

Results from ten models (five for each pole length) obtained from the ANSYS finite element software are presented in this chapter. The loads used in the FEA are those calculated in Section 4.2. Failure is defined either as material failure or local buckling. Material failure criteria considered in this case are the Tsai-Wu, the Maximum Stress and the Maximum Strain criteria. Lateral tip deflections related to different Rn ratios (number of longitudinal layers/total number of layers), are shown in Figures 4.2 and 4.3 for the 6 m and 12 m poles, respectively. These results indicate that for both heights, an Rn ratio of 4/8 yields deflections smaller than the limit assigned by the AASHTO Standard Specifications, which is defined as 15% of pole length.

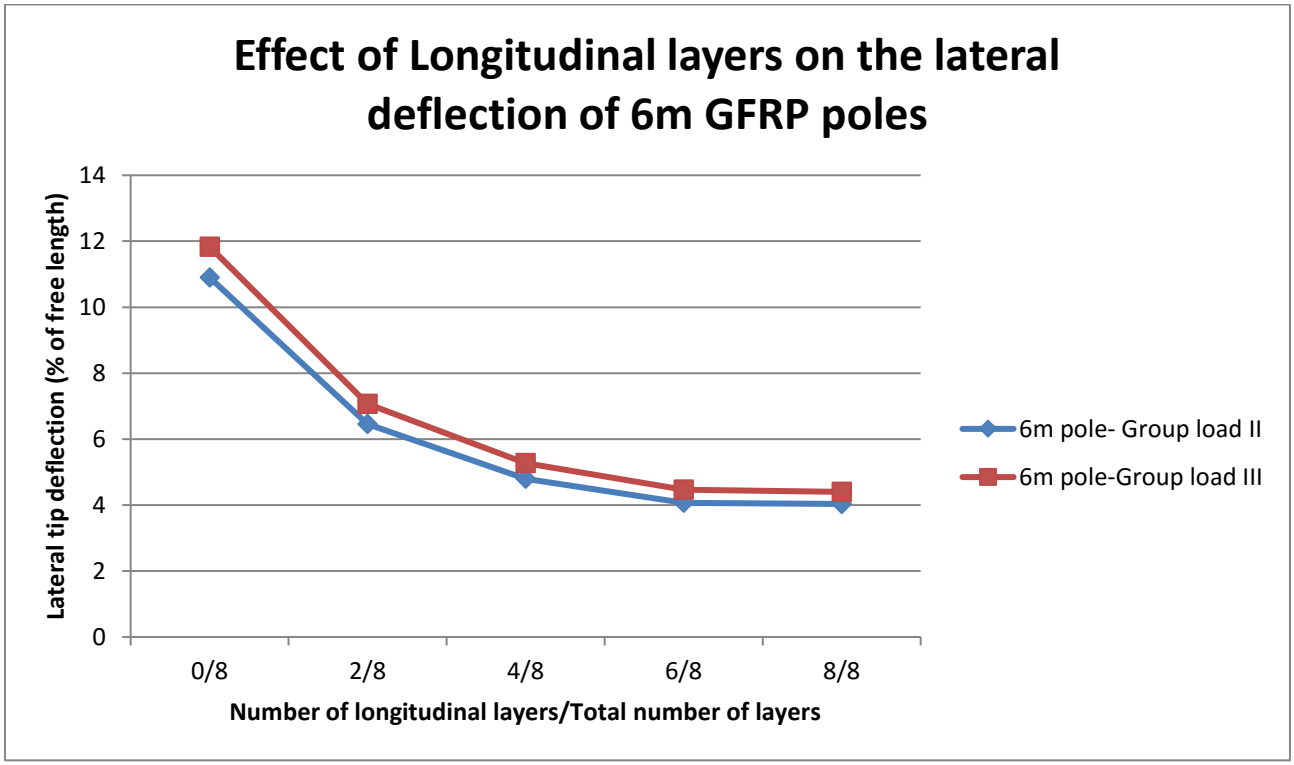

Figure 4.2: Effect of longitudinal layers on the lateral deflection of 6 m GFRP poles

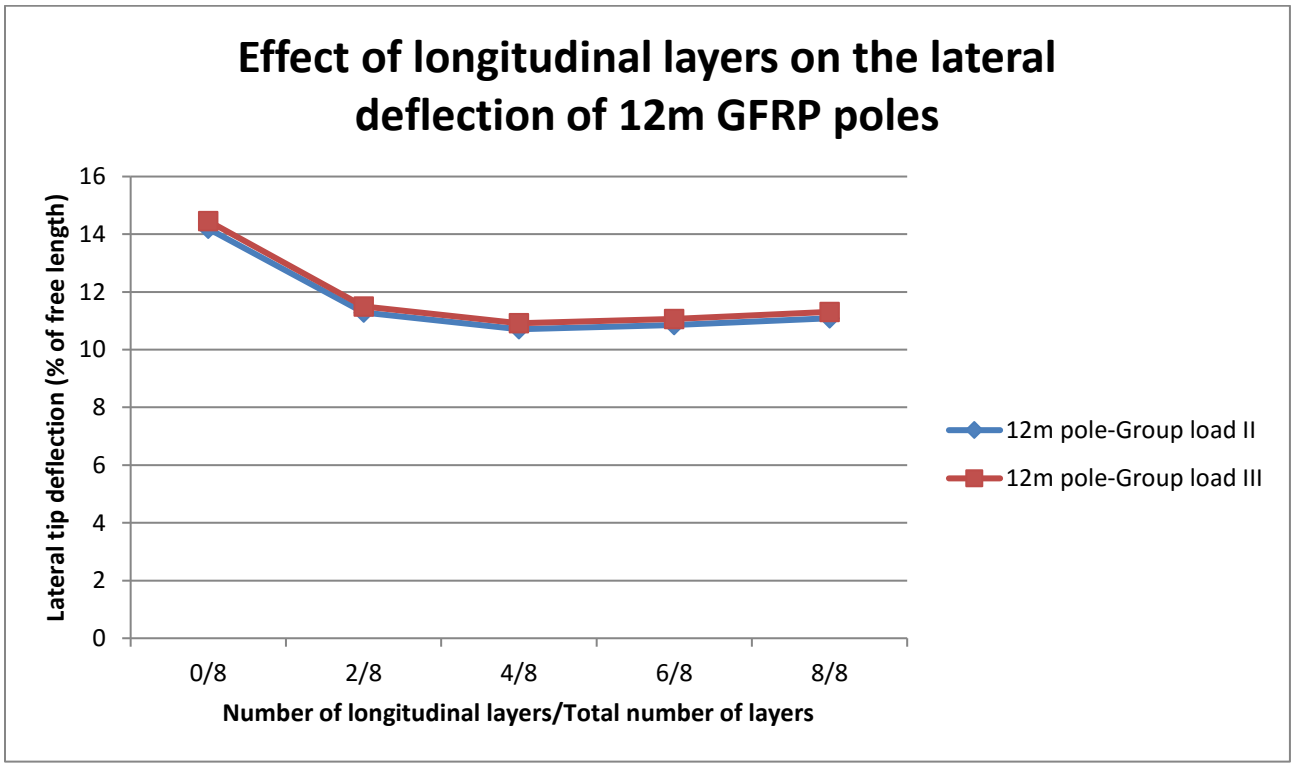

Figure 4.3: Effect of longitudinal layers on the lateral deflection of 12m GFRP poles

As shown in Figure 4.2, by increasing the number of longitudinal layers, the tip deflection decreases continuously. For both 6 m and 12 m poles, the maximum deflection is observed when no longitudinal layers are used (12% and 14% of pole height for the 6 m and 12 m poles respectively). It should be noted that axial loads, as well as lateral loads applied along the pole, are resisted by longitudinal fibers. Circumferential layers are required to resist internal shear and provide confinement to the longitudinal fibers. Without circumferential layers, longitudinal layers are more vulnerable to buckling and excessive deflection. Therefore an Rn=4/8 ratio is more practical and more effective than an Rn=8/8.

The FEA results also show that both modes of failure are present. Material failure is evident on the tension side close to support at the bottom while local buckling is the mode of failure on the compression side of poles. In the case of the 6 m poles the Tsai-Wu, the Maximum Stress and the Maximum strain criteria suggest that material failure happens when no longitudinal layers are used. In the case of the 12 m poles, material failure is observed when either no longitudinal layers (Rn=0/8) or no circumferential layers (Rn=8/8) are used. The failure criteria values for the 6 m poles (Group load III) are shown in Figures 4.4, 4.5, and 4.6, while the failure criteria values for the 12 m poles (Group load III) are shown in Figures 4.7, 4.8, and 4.9.

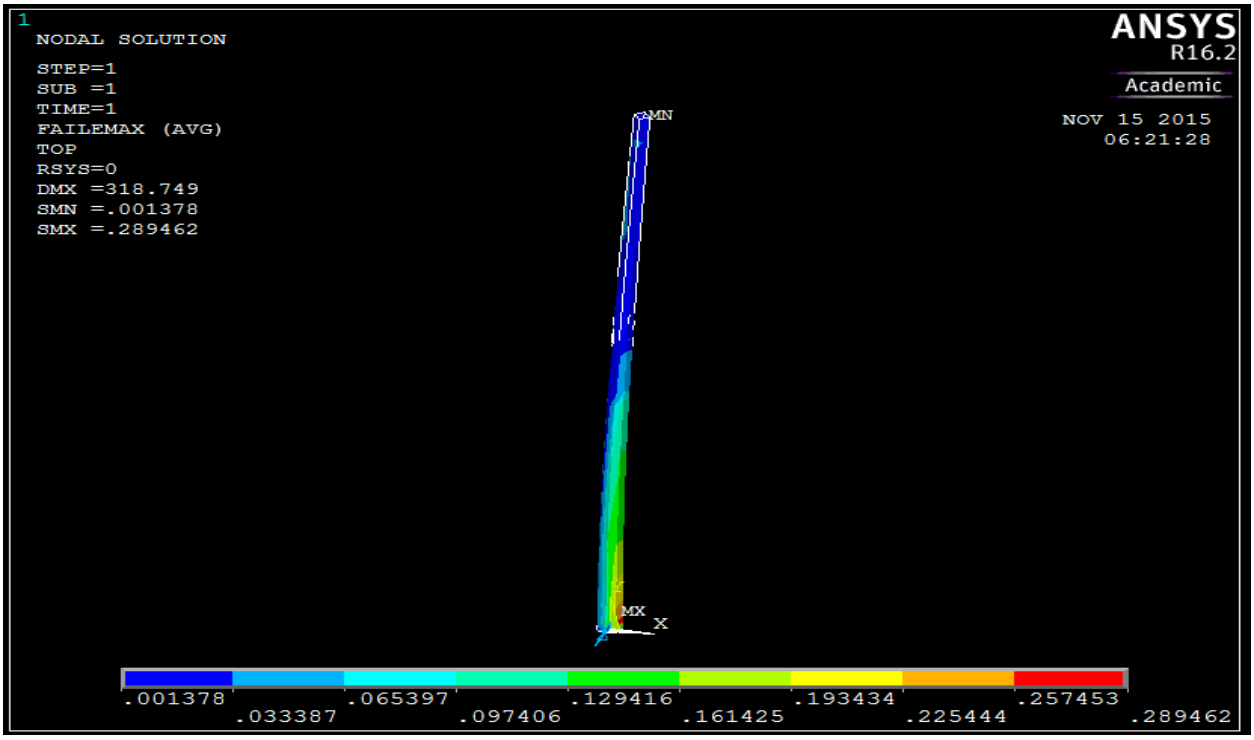

Figure 4.4: Maximum strain failure criterion for 6 m pole with Rn=4/8

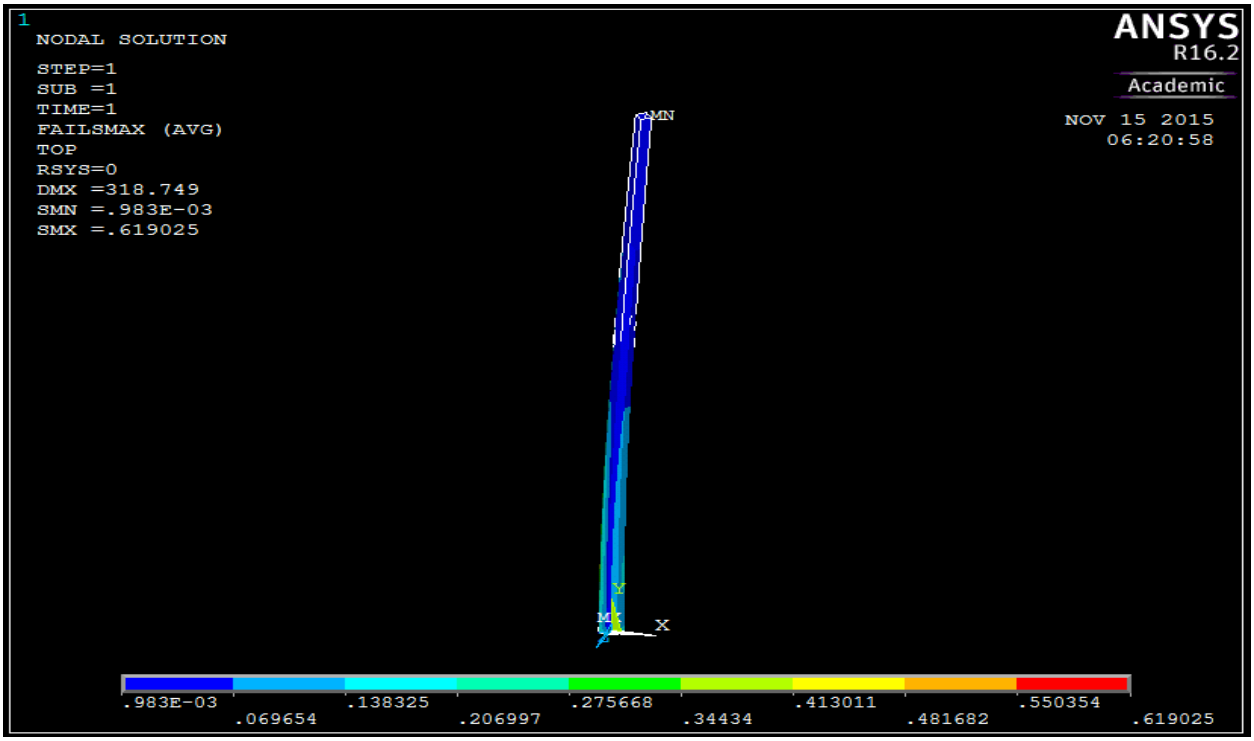

Figure 4.5: Maximum stress failure criterion for 6 m pole with Rn=4/8

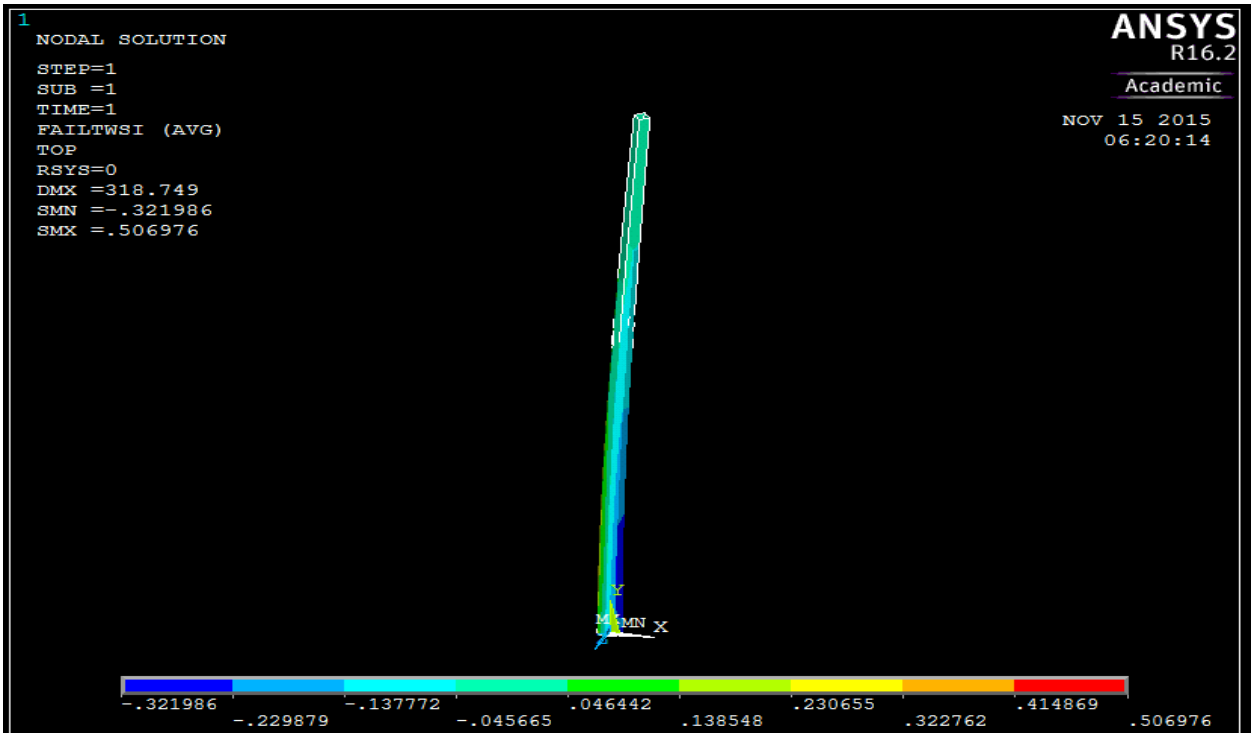

Figure 4.6: Tsai-Wu failure criterion for 6 m pole with Rn=4/8

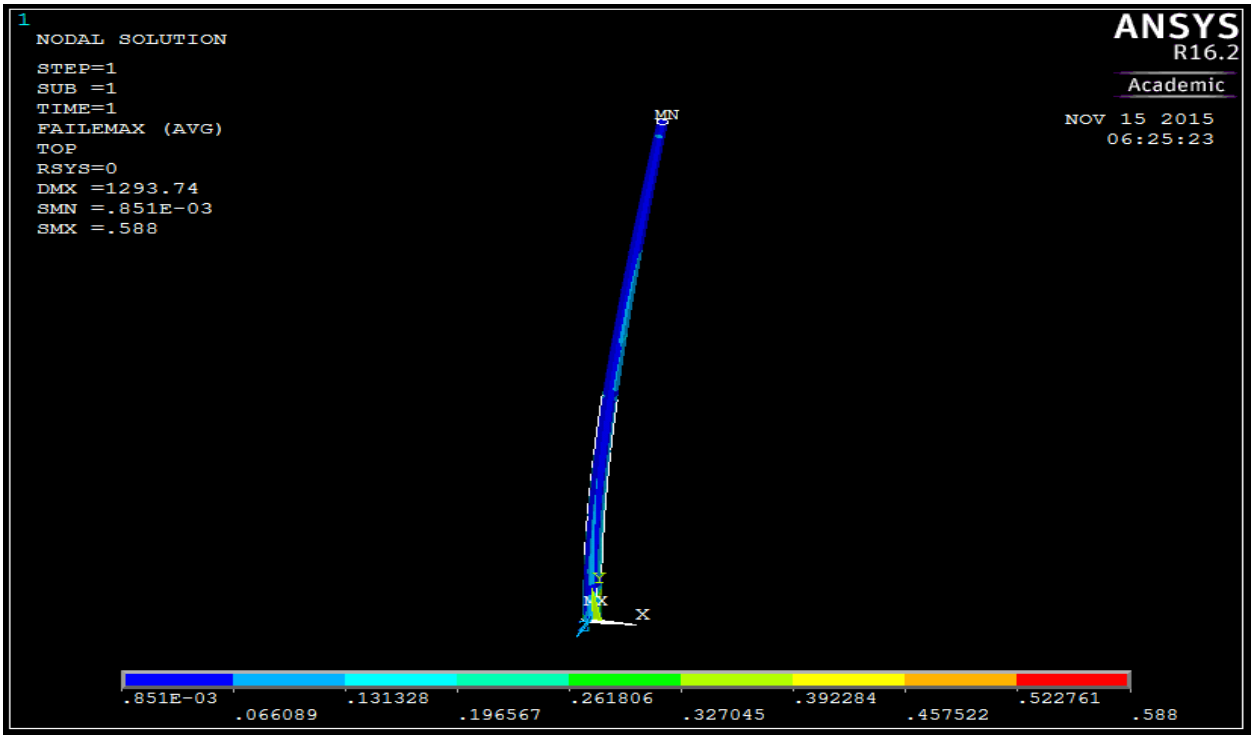

Figure 4.7: Maximum strain failure criterion for 12 m pole with Rn=4/8

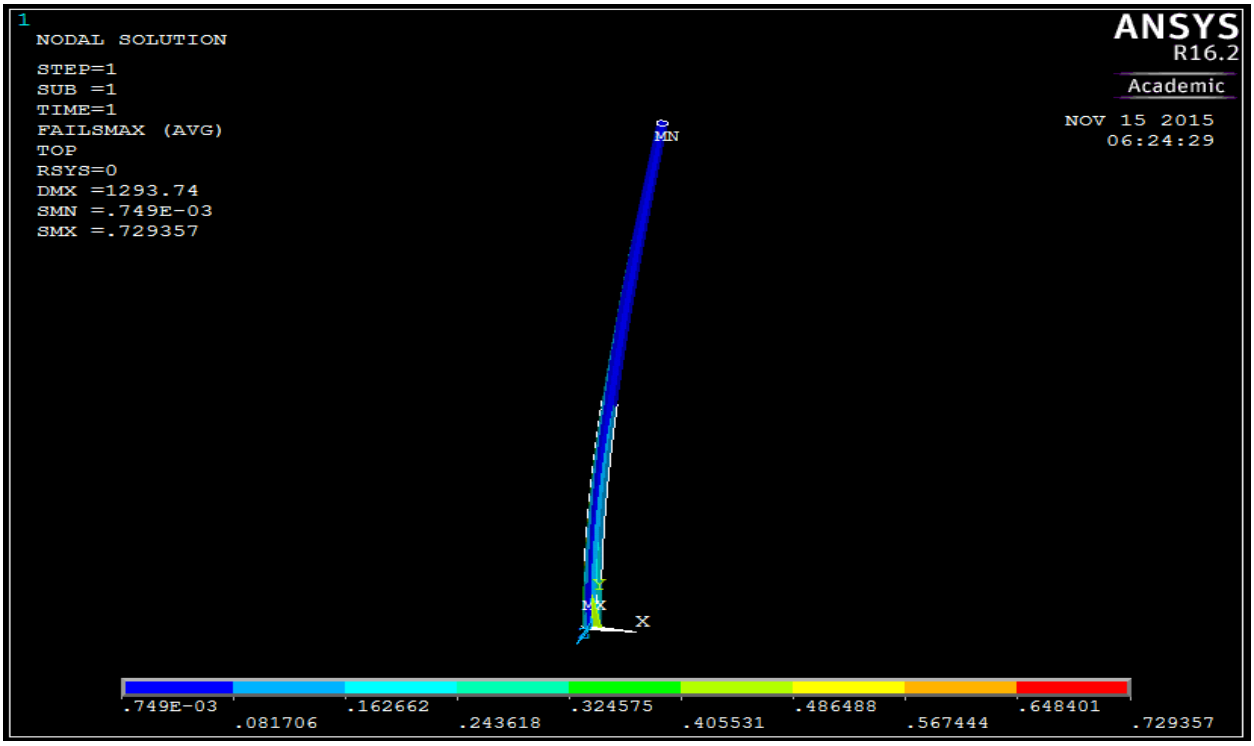

Figure 4.8: Maximum stress failure criterion for 12 m pole with Rn=4/8

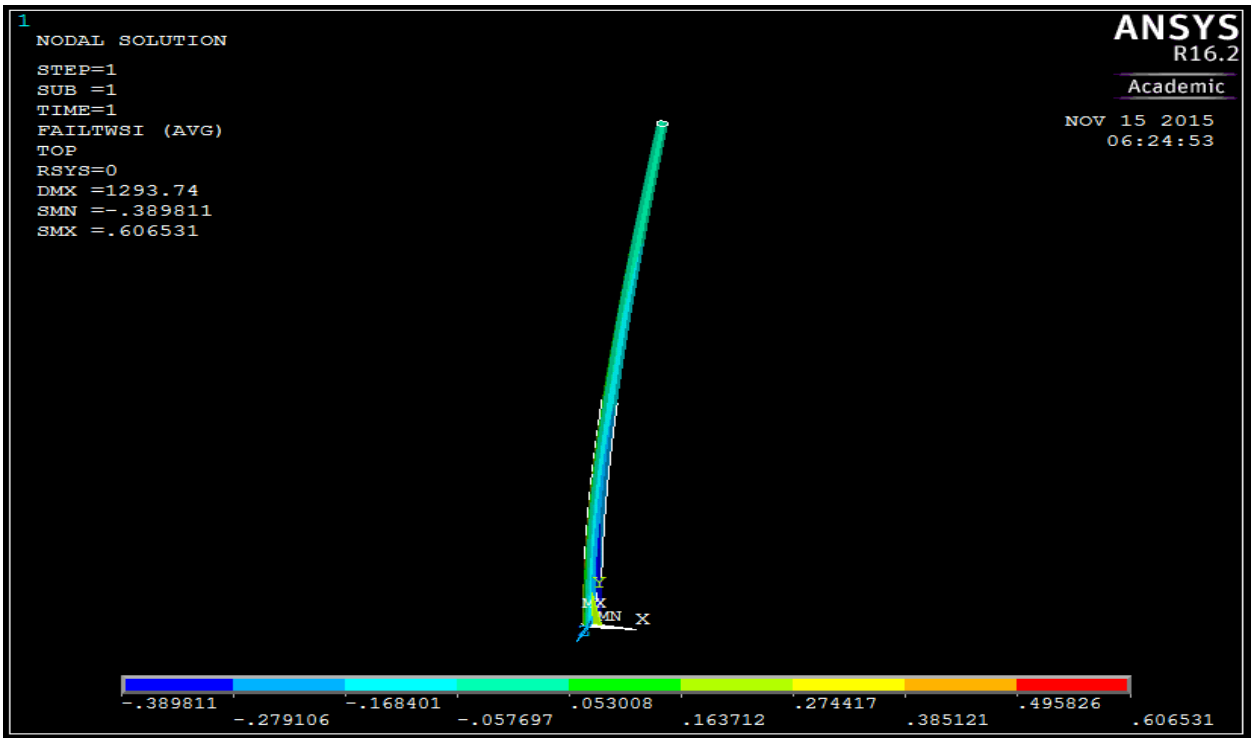

Figure 4.9: Tsai-Wu failure criterion for 12 m pole with Rn=4

4.4.2 Case 2: The effect of longitudinal fiber orientation

Five different longitudinal fiber orientations are examined, including +/-5°, +/-15°, +/-25°, +/-35°, and +/-45° using the FEM. Based on the Case 1 results, a ratio of longitudinal layers to total number of layers of 4/8 is used for both 6 m and 12 m long poles. A bottom diameter of 300 mm for the12 m poles and 210 mm for the 6 m poles is used in the analysis. As in Case 1, FRP composite poles are assumed to have a total wall thickness of 2.4 mm for the 6 m poles and 4 mm for the 12 m poles. The thickness consists of eight layers with equal thickness. The parametric variations of Case 2 are presented in Tables 4.8 to 4.11.

Table 4.8: Geometric properties for 6 m poles studied in Case 2

Geometric Properties					
Total length(mm)	Bottom diameter (mm)	Top diameter (mm)	Top diameter/Bottom diameter ratio	Wall thickness (mm)	Mass (kg)
6000	210	126	0.6	2.4	14.7

Table 4.9: Fiber arrangement and numerical results for 6 m poles studied in Case 2

Fiber arrangement						Results			Results		
						Group load II			Group load III		
Number of circum. layers (Nc)	Number of long. layers (Nl)	Total number of layers (Nt)	Rn=Nl/Nt	Long. fiber orientation	Fiber to weight volume percentage	Maximum lateral deflection (mm)	Lateral deflection/free length (%)	Failure mode	Maximum lateral deflection (mm)	Lateral deflection /free length (%)	Failure mode
4	4	8	4/8	+/-5°	58.10%	288	4.8	No failure	316	5.3	No failure
				+/-15°		287	4.8	No failure	315	5.3	No failure
				+/-25°		284	4.7	No failure	312	5.2	No failure
				+/-35°		279	4.7	No failure	306	5.1	No failure
				+/-45°		273	4.6	No failure	299	5.0	No failure

Table 4.10: Geometric properties for 12 m poles studied in Case 2

Geometric Properties					
Total length (mm)	Bottom diameter (mm)	Top diameter	Top diameter/Bottom diameter ratio	Wall thickness (mm)	Mass (kg)
12000	300	180	0.6	4	70

Table 4.11: Fiber arrangement and numerical results for 12 m poles studied in Case 2

Fiber arrangement						Results			Results		
						Group load II			Group load III		
Number of circum. layers (Nc)	Number of long. layers (Nl)	Total number of layers (Nt)	Rn=Nl/Nt	Long. fiber orientation	Fiber to weight volume percentage	Maximum lateral deflection (mm)	Lateral deflection/ free length (%)	Failure mode	Maximum lateral deflection (mm)	Lateral deflection /free length (%)	Failure mode
4	4	8	4/8	+/-5°	58.10%	1285	10.7	No failure	1310	10.9	No failure
				+/-15°		1315	11.0	No failure	1341	11.2	No failure
				+/-25°		1373	11.4	No failure	1400	11.7	No failure
				+/-35°		1448	12.1	No failure	1477	12.3	No failure
				+/-45°		1527	12.7	No failure	1557	13.0	No failure

The effect of longitudinal fiber orientation on the lateral deflection of the FRP composite poles is demonstrated in Figures 4.10 and 4.11. Figure 4.10 suggests that for 6 m poles, changing the longitudinal fiber orientation has a small effect on the poles' lateral deflection. Poles with +/-5° longitudinal fiber orientation deflected 316 mm and poles with +/-45° longitudinal fiber orientation deflected 299 mm, a reduction of 5%. Using conjugate theory and beam theory, shear deflection and bending deflections were calculated for the 6 m poles with +-5 fiber orientation. Shear deflection was calculated to be 2.5% of total deflection. Since longitudinal fibers with +/-35° and +/-45° fiber orientation provide some degrees of shear stiffness as well as bending stiffness, increasing longitudinal fiber orientation decreases the maximum tip deflection for 6 m poles.

Figure 4.11 shows that in case of the 12 m poles, decreasing the bending stiffness, due to increasing longitudinal fiber orientation, leads to higher tip deflections. The results provided in Table 4.11 suggest that 12 m poles are more sensitive to changes in longitudinal fiber orientations. Poles with +/-5° longitudinal fiber angle deflected 1310 mm whereas poles with +/-45° longitudinal fiber angle deflected 1557 mm, an increase of 16%. Since Rn=4/8 and 4 circumferential layers have been used in the composite lay-up, longitudinal fiber orientation +/-5° is used for both 6 m and 12 m poles to provide the desirable bending stiffness for these structures.

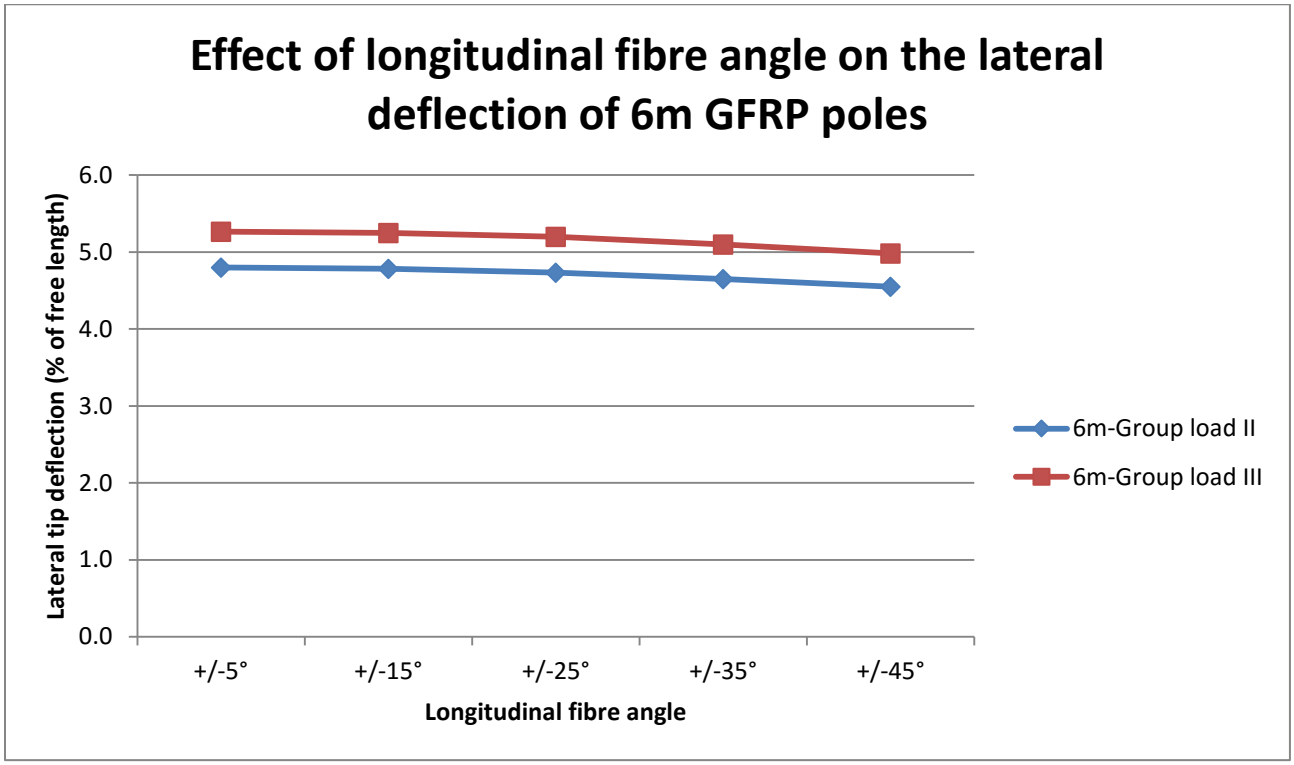

Figure 4.10: Effect of longitudinal fibre angle on the lateral deflection of 6 m GFRP poles

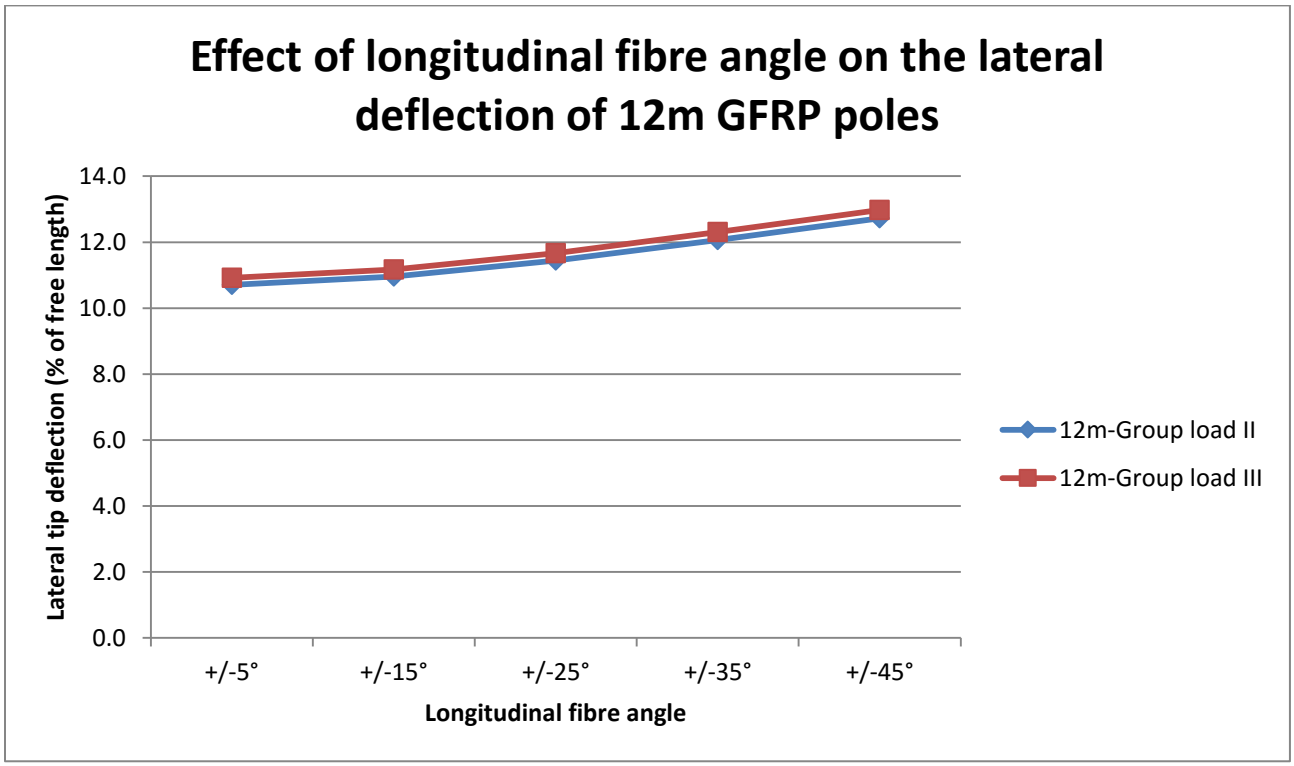

Figure 4.11: Effect of longitudinal fibre angle on the lateral deflection of 12 m GFRP poles

The finite element results indicate that none of the 6 m or the 12 m poles failed under the applied design loads calculated in Section 4.2. Figures 4.12 and 4.13 display Tsai-Wu values for the 6 m and the 12 m poles, respectively, under group load III.

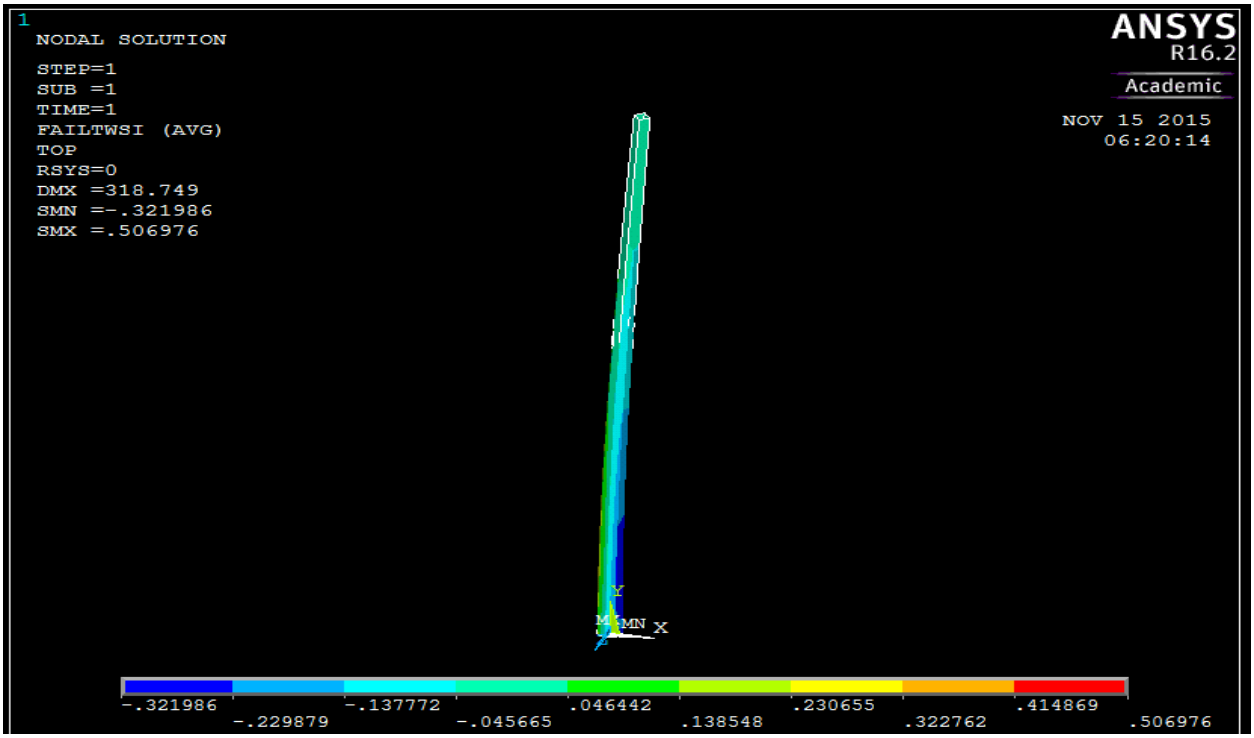

Figure 4.12: Tsai-Wu failure criterion for 6 m poles with +/-5° longitudinal fiber orientation

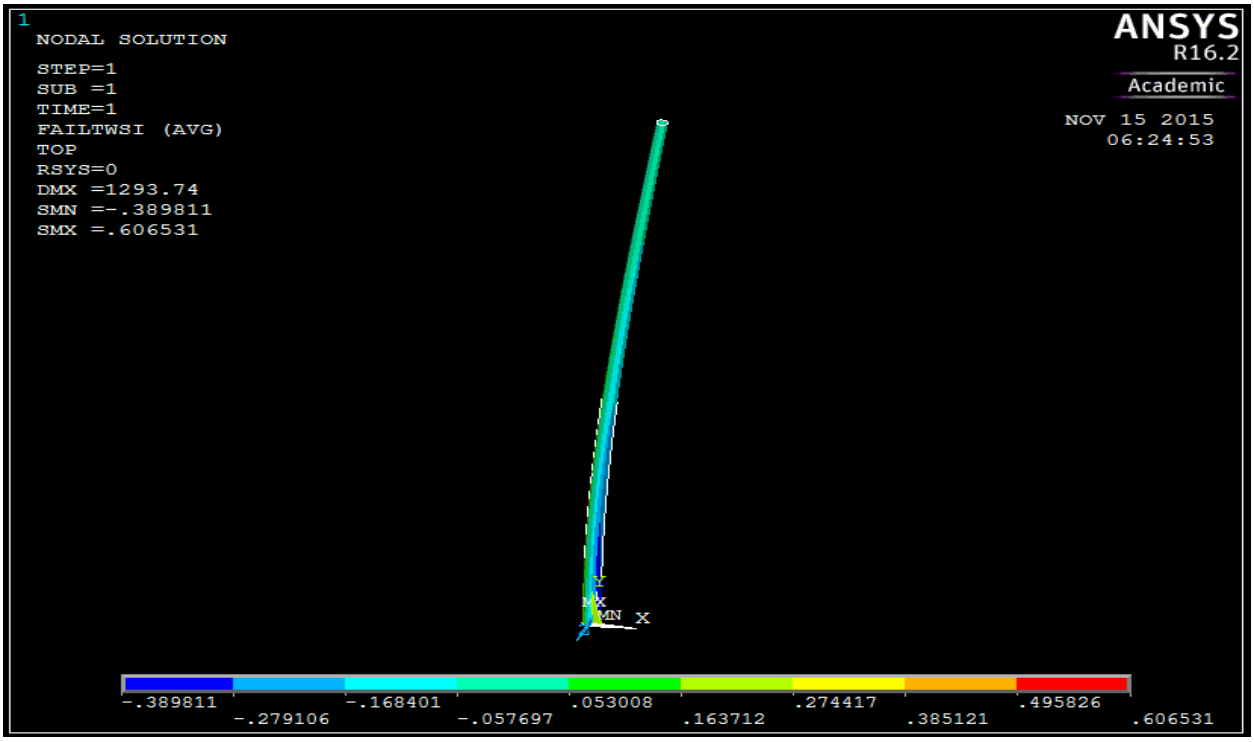

Figure 4.13: Tsai-Wu failure criterion for 12 m poles with +/-5° longitudinal fiber orientation

4.4.3 Case 3: The effect of cross section dimensions

In this Section, poles with fifteen different cross-section dimensions are examined. The bottom diameters for the 6 m FRP composite poles vary from 150 mm to 270 mm, and the bottom diameters for the 12 m composite poles vary from 230 mm to 350 mm. As suggested by Ibrahim (2000) a top-to-bottom diameter ratio of 0.6 is used. The poles are assumed to have a constant wall thickness of 2.4 mm for the 6 m poles and 4 mm for the 12 m poles.

According to Case 1 (Section 4.4.1), Rn = 4/8 is selected for both types of poles. Furthermore, as discussed in Case 2 (Section 4.4.2), a +/-5° longitudinal fiber orientation is used. The parametric variations used in Case 3 are listed in Tables 4.12 – 4.15.

Table 4.12: Geometric properties for 6 m poles studied in Case 3

Geometric Properties					
Total length(mm)	Bottom diameter (mm)	Top diameter (mm)	Top diameter/Bottom diameter ratio	Wall thickness (mm)	Mass (kg)
6000	150	90	0.6	2.4	10.5
	170	102			11.9
	190	114			13.3
	210	126			14.7
	230	138			16.2
	250	150			17.6
	270	162			19

Table 4.13: Fiber arrangement and numerical results for 6 m poles studied in Case 3

Fiber arrangement							Results Group load II			Results Group load III		
Number of circum. layers (Nc)	Number of Long. layers (Nl)	Total number of layers (Nt)	Rn=Nl/Nt	Long. fiber orientation	Fiber to weight volume percentage	Bottom diameter (mm)	Maximum lateral deflection (mm)	Lateral deflection /free length (%)	Failure mode	Maximum lateral deflection (mm)	Lateral deflection/ free length (%)	Failure mode
4	4	8	4/8	+/-5°	58.10%	150	616	10.3	Probable local buckling near the support	700	11.7	Probable local buckling near the support
						170	457	7.6	Probable local buckling near the support	518	8.6	Probable local buckling near the support
						190	358	6.0	No failure	406	6.8	No failure
						210	288	4.8	No failure	316	5.3	No failure
						230	238	4.0	No failure	270	4.5	No failure
						250	200	3.3	No failure	227	3.8	No failure
						270	169	2.8	No failure	194	3.2	No failure

Table 4.14: Geometric properties for 12 m poles studied in Case 3

Geometric Properties					
Total length(mm)	Bottom diameter (mm)	Top diameter (mm)	Top diameter/Bottom diameter ratio	Wall thickness (mm)	Mass (kg)
12000	230	138	0.6	4	53.4
	250	150			58.1
	270	162			62.9
	290	174			67.6
	300	180			70
	310	186			72.3
	330	198			77.1
	350	210			81.8

Table 4.15: Fiber arrangement and numerical results for 12 m poles studied in Case 3

Fiber arrangement							Results			Results		
							Group load II			Group load III		
Number of circum. layers (Nc)	Number of Long. layers (Nl)	Total number of layers (Nt)	Rn=Nl/Nt	Long. fiber orientation	Fiber to weight volume percentage	Bottom diameter (mm)	Maximum lateral deflection (mm)	Lateral deflection /free length (%)	Failure mode	Maximum lateral deflection (mm)	Lateral deflection/ free length (%)	Failure mode
4	4	8	4/8	+/-5°	58.10%	230	2269	18.9	TsaiWu and Maximum stress -tension side support-local buckling near the support	2317	19.3	TsaiWu and Maximum stress -tension side support-local buckling near the support
						250	1897	15.8	TsaiWu and Maximum stress -tension side support-local buckling near the support	1935	16.1	TsaiWu and Maximum stress -tension side support-local buckling near the support
						270	1607	13.4	TsaiWu and Maximum stress -tension side support-local buckling near the support	1641	13.7	TsaiWu and Maximum stress -tension side support-local buckling near the support
						290	1383	11.5	Local buckling near the support	1412	11.8	Local buckling near the support
						300	1285	10.7	No failure	1310	10.9	No failure
						310	1198	10.0	No failure	1224	10.2	No failure
						330	1049	8.7	No failure	1071	8.9	No failure
						350	925	7.7	No failure	946	7.9	No failure

In the FEA the wall thickness is kept constant for both the 6 m and 12 m poles. But, since cross-section dimensions are varied, the mass of the poles changes. Therefore, the desired design for these poles would be one that both weight and deflection are optimized. Due to the tapered shape of the poles, the magnitude of the external loads applied to the structure, such as wind load (dominant load in design) and ice load, change as well. Tables 4.16 and 4.17 and Figure 4.14 present wind load and total ice load applied to the GFRP poles using the FEA. Figure 4.15 shows the effect of cross sectional properties on the total mass of GFRP poles.

Table 4.16: Wind load applied to 6 m GFRP poles (Group load III)

Wind load applied to 6 m GFRP poles (Group load III)							
Distance from base (m)	Bottom diameters						
	150 mm	170 mm	190 mm	210 mm	230 mm	250 mm	270 mm
1	272 N	309 N	345 N	381 N	417 N	454 N	490 N
2	253 N	287 N	321 N	355 N	389 N	422 N	456 N
3	235 N	266 N	297 N	328 N	360 N	391 N	422 N
4	216 N	244 N	273 N	302 N	331 N	360 N	388 N
5	197 N	223 N	249 N	276 N	302 N	328 N	354 N
6	178 N	202 N	226 N	249 N	273 N	297 N	320 N

Table 4.17: Wind load applied to 12 m GFRP poles (Group load III)

Wind load applied to 12 m GFRP poles (Group load III)								
Distance from base (m)	Bottom diameters							
	230 mm	250 mm	270 mm	290 mm	300 mm	310 mm	330 mm	350 mm
2	836 N	909 N	982 N	1054 N	1091 N	1127 N	1200 N	1273 N
4	779 N	846 N	914 N	982 N	1015 N	1049 N	1117 N	1185 N
6	721 N	783 N	846 N	909 N	940 N	971 N	1034 N	1097 N
8	660 N	718 N	775 N	832 N	820 N	890 N	947 N	1005 N
10	602 N	655 N	707 N	759 N	789 N	812 N	864 N	917 N
12	519 N	564 N	609 N	654 N	714 N	699 N	744 N	789 N

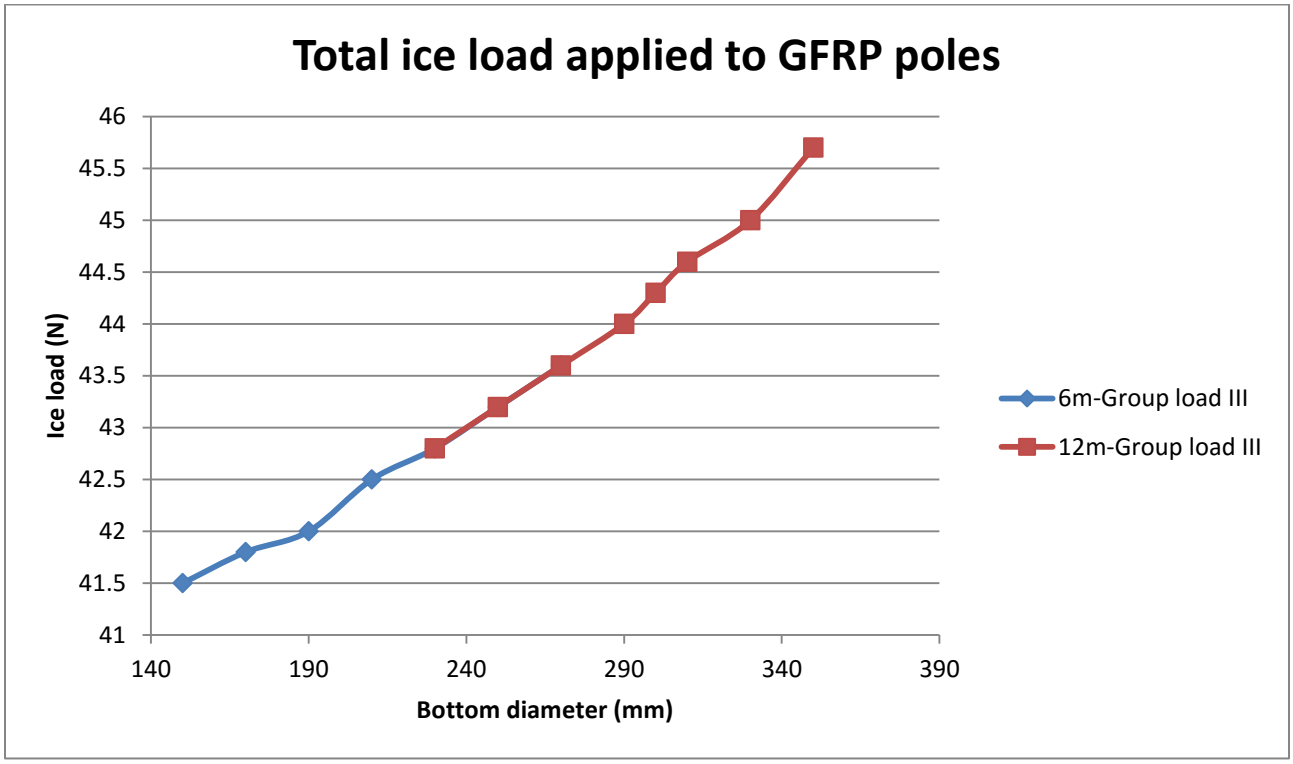

Figure 4.14: Total ice load applied to GFRP poles

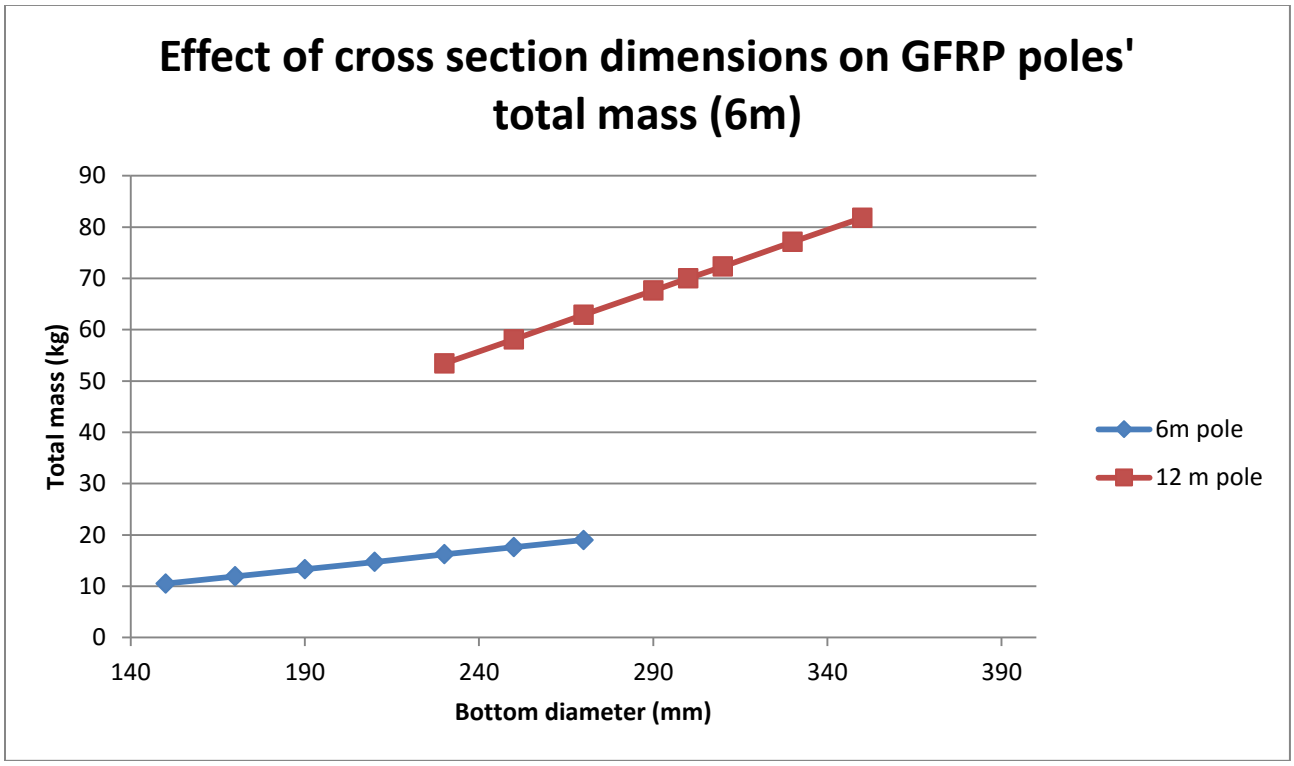

Figure 4.15: GFRP poles' total mass

The effect of cross-section dimensions on the lateral deflection of the tapered poles is demonstrated in Figures 4.16 and 4.17. The results shown in Figure 4.16 suggest that for 6 m poles, group load III is the critical load combination that results in higher deflections. Increasing the bottom diameter from 150 mm to 270 mm reduces the tip deflections from 11.7% of the pole length to approximately 3% of the pole length. The results presented in Table 4.13 suggest that 6 m poles with a 270 mm bottom diameter deflects 506 mm (8.5 % of pole length) less than poles with 150 mm bottom diameter for group III loadings. In the case of the 12 m poles, the difference between maximum and minimum lateral deflections under critical load combination (group load III) was 11.4% of the pole length. Considering the lateral deflections and failure modes given in Tables 4.13 and 4.15, a bottom diameter of 210 mm for 6 m poles and 300 mm for 12 m poles is suggested as an optimum design bottom diameter.

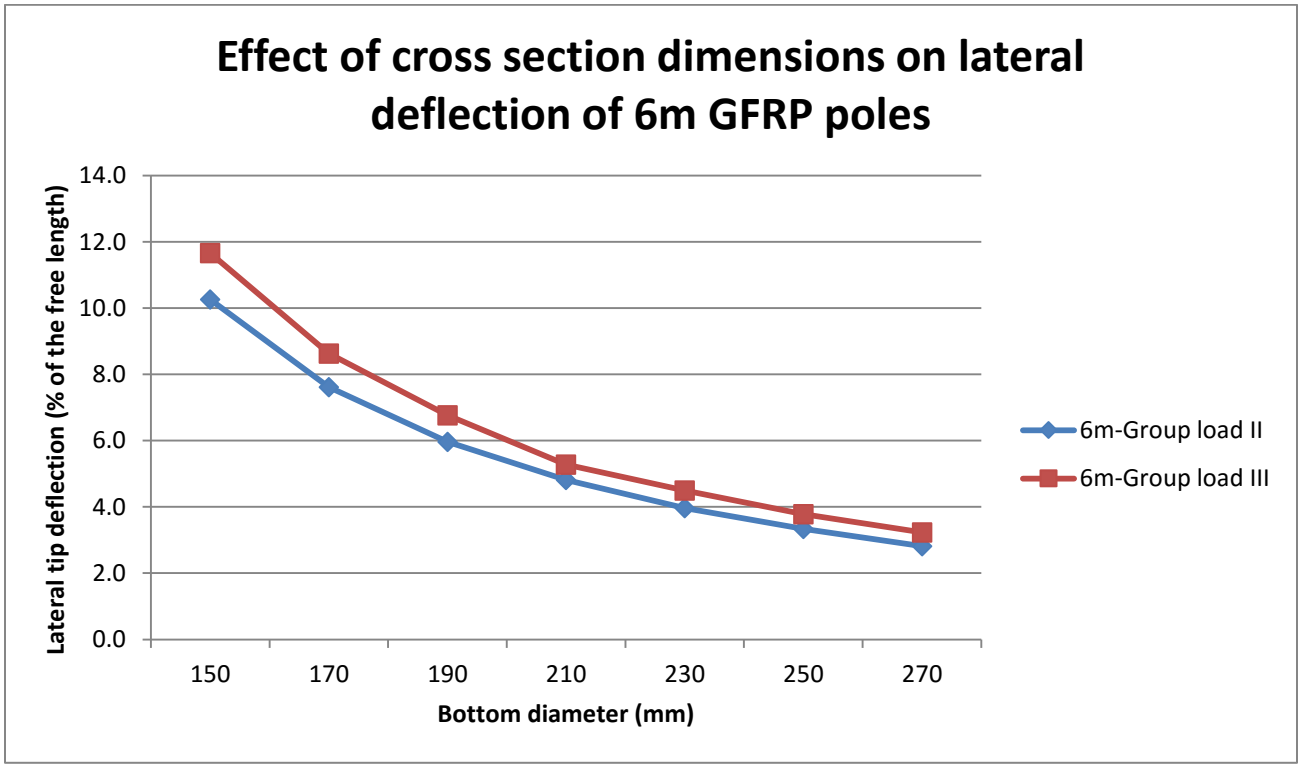

Figure 4.16: Effect of cross section dimensions on lateral deflection of 6m GFRP poles

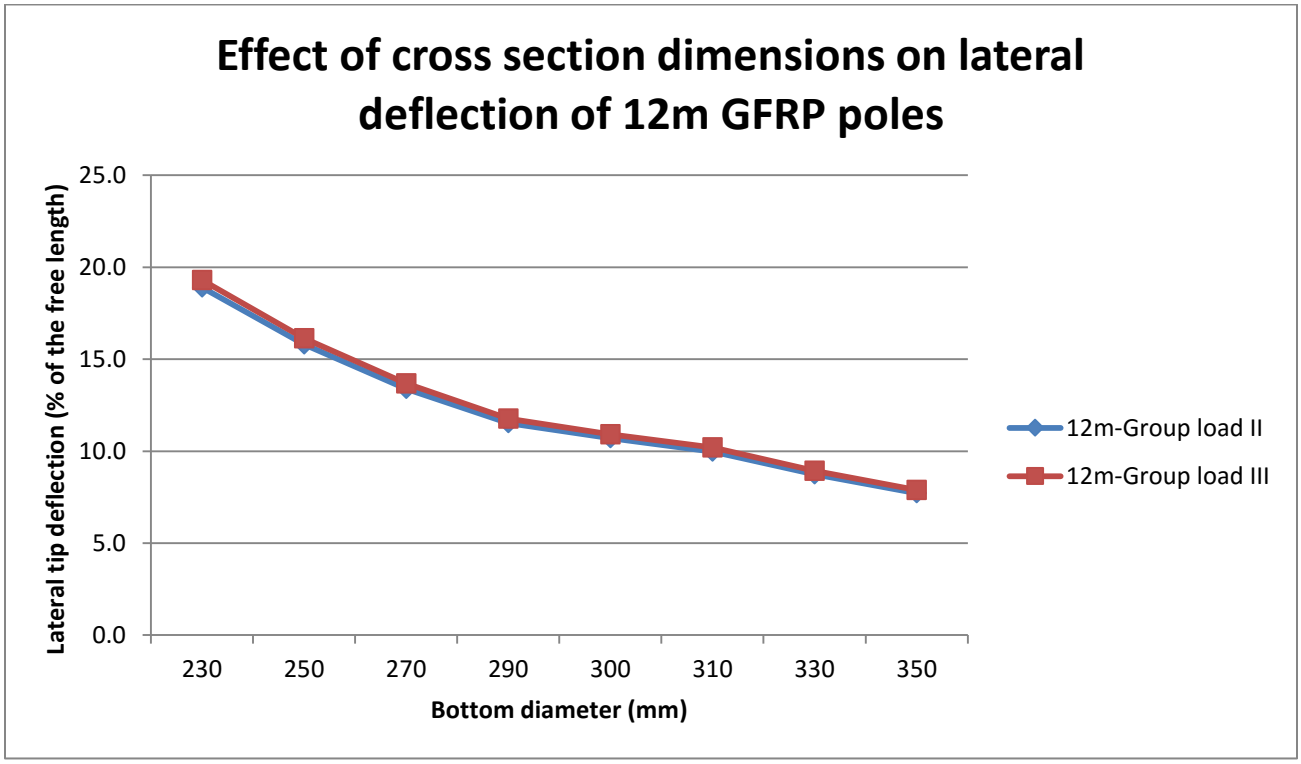

Figure 4.17: Effect of cross section dimensions on lateral deflection of 12m GFRP poles

The FEA results indicate that the 6 m poles do not experience any material failure under the design loads. Poles with 150 mm and 170 mm bottom diameters fail by local buckling near the support. In the case of the 12 m poles, both material failures of Tsai-Wu and Maximum Stress and local buckling are observed in poles with bottom diameters less than 270 mm. Table 4.15 indicates that sections with bottom diameters of more than 300 mm do not fail under the design loads. Figures 4.12 and 4.13 display the Tsai-Wu failure criteria values for the optimum cross sections suggested (210 mm for 6 m poles and 300 mm for 12 m poles).

4.5 Final designs

Two types of poles are presented and analyzed in Section 4.4 (6 m and 12 m) to find the optimum design which would reduce internal stresses in the structure, decrease deflections, and obtain the minimum overall weight. A summary of designed poles and laminate lay-up is presented in table 4.18.

Table 4.18: A summary of final designs

Summary of final designs		
Total length (mm)	**6 m**	**12 m**
Bottom diameter (mm)	210	300
Top diameter (mm)	126	180
Number of longitudinal layers (Nl)	4	4
Number of circumferential layers (Nc)	4	4
Total number of layers (Nt)	8	8
Rn=Nl/Nt	4/8	4/8
Longitudinal fiber orientation	±5˚	±5˚
Stacking sequence	90˚,90˚,+5˚,-5˚,+5˚,-5˚,90˚,90˚	90˚,90˚,+5˚,-5˚,+5˚,-5˚,90˚,90˚
Fiber to weight volume percentage	58.1%	58.1%
Wall thickness (mm)	2.4	4
Mass (kg)	14.7	70

Chapter 5: FRP wind turbine towers

5.1 Modeling FRP composite wind turbine towers

In this chapter, FRP and steel wind turbine towers are analyzed using the finite element program ANSYS. Various standards and specifications are used to compute the load requirements. These include: CAN/CSA-C61400-1:14 (Wind turbines-Part 1: Design requirements), CAN/CSA-C61400-2:08 (Wind turbines-Part 2: Design requirements for small wind turbines); ISO 4354:2009 (Wind actions on structures); the NBCC (2005); and the DNV/Risø Guidelines for design of Wind Turbines (2002). To complete FEA, it was assumed that these wind turbine towers are located in Churchill, Manitoba, Canada.

Load calculations have been divided into two parts: Loads transferred from the turbine to the tower and loads applied to the tower itself (such as wind load and snow load). Different load combinations, as specified by the CAN/CSA-C61400 Standard, are discussed in Section 5.2. Loads applied to the tower itself are calculated according to the National Building Code of Canada (2005) and are discussed in Sections 5.3.1 to 5.3.6. Table 5.1 provides technical information about the wind turbine selected for this study. The ANSYS finite element software was used to investigate the effect of the number of longitudinal layers, longitudinal fiber orientation, and cross-section dimensions of the tower on the structural performance of wind turbine towers made of FRP composite materials. These cases are discussed in Sections 5.5.1 to 5.5.3.

Table 5.1: Technical data for the selected wind turbine (NEG Micon, 2015)

Technical data: NM48/750	
Nominal output	750 KW
Nominal wind speed (m/s)	16
Cut-in (m/s)	4
Cut-out (m/s)	25
Rotor diameter (m)	48.2
Rotor swept area (m^2)	1824
Number of blades	3
Rotor revolutions (rpm)	22/15
Name plate rating	750/200 KW

5.1.1 Tower analyses

The towers are analyzed according to the CAN/CSA-C61400-1:14 Standard which is based on the ultimate limit state method. According to CSA-C61400 Clause 7.6.1.2, the following three types of analyses for a complete ultimate limit state analysis of a supporting structure must be carried out: Ultimate strength analysis; stability analysis (buckling, etc.); and critical deflection analysis. These analyses are discussed in the following Sections.

5.1.1.1 Ultimate strength analysis

To analyze the ultimate strength of wind turbine towers, CSA-C61400 Clause 7.6.2 specifies load factors, material factors and consequences of failure factors. The proper design should satisfy the following condition:

$$\gamma_f F_k \leq \frac{1}{\gamma_n} . \frac{1}{\gamma_m} f_k \qquad 5.1$$

Where

γ_f is the partial safety factor for loads

F_k is characteristic value for the load

γ_m is the partial safety factor for materials

γ_n is the partial safety factor for consequences of failure

f_k is characteristic value for the material properties

The CSA-C61400 Standard provides three different partial safety factors for loads, material properties, and consequences of failure. The partial safety factors used for ultimate strength analysis are presented in Table 5.2. Normal load cases are those that happen frequently during a wind turbine's lifetime. These load cases assume that the turbine will function in a normal state, taking into consideration that minor faults or abnormalities might happen. Abnormal load cases are less likely to occur, and they usually refer to situations that activate system protection functions.

Table 5.2: Partial safety factors for loads (CSA C61400-1)

Unfavorable loads		**Favorable loads**
Type of design situation		**All design situations**
Normal (N)	**Abnormal (A)**	
1.35	1.1	0.9

CSA-C61400 Clause 7.6.2.2 specifies the following partial safety factors for material properties and consequences of failure for ultimate strength analysis. These factors should be used for non fail-safe structural components that can cause a major failure in wind turbine system:

- γ_m=1.2 for global buckling of curved shell, such as tubular towers
- γ_m=1.3 for rupture from exceeding tensile or compression strength
- γ_n=0.9 for component Class 1 (defined in the next Section)
- γ_n=1 for component Class 2 (defined in the next Section)
- γ_n=1.3 for component Class 3 (defined in the next Section)

5.1.1.2 Stability analysis

The CSA-C61400 Standard defines three types (class) of wind turbine components:

a) Fail-safe components (Class 1): Failure of these components would not cause a severe consequence for the wind turbine. For example, replaceable shims or fuses are fail-safe components.

b) Non fail-safe *structural* components (Class 2): A failure of these structural components may result in a failure of a major part of the wind turbine.

c) Non fail-safe *mechanical* components (Class 3): These are components that connect actuators and brakes to structural support and are part of wind turbine safety systems.

According to CSA-C61400 Clause 7.6.4, buckling should not happen for non fail-safe components under design loads. In determining design loads, the partial safety factor γ_f defined in Section 5.1.1.1, is used. Other components must also be designed not to fail under characteristic loads (loads without a partial safety factor γ_f).

5.1.1.3 Critical deflection analysis

A critical deflection analysis of structural components of wind turbines is required to ensure that the structural integrity of the wind turbine is not compromised under the loads applied to the structure.

This deflection should be calculated using characteristic loads with no partial safety factors applied to loads or material properties. After completing the finite element analysis, the resulting deflections are multiplied by partial safety factors for loads, materials, and consequences of failure, as recommended by CSA-C61400 Clause 7.6.5. The maximum deflection values obtained from ultimate strength analysis and critical deflection values are then compared to

allowable deflections (distance between blades and structural support) to make sure that the structural integrity of the wind turbine would not be affected.

Load safety factors for critical deflection analysis are chosen from Table 5.2 in Section 5.1.1.1, and a value of γ_m=1.1 has been specified for material properties. The consequences of failure-safety factors used here are as follows:

- γ_n=1 for Class 1 components
- γ_n=1 for Class 2 components
- γ_n=1.3 for Class 3 components

5.1.2 Cross section dimensions

Seven bottom diameters are considered in the design of the 50 m tall FRP composite tower: 2,500 mm, 3,000 mm, 3,500 mm, 4,000 mm, 4,500 mm, 5,000 mm and 5,500 mm. The top-to-bottom diameter ratio of 0.6 is selected (Ibrahim, 2000) and constant wall thicknesses of 55.2 mm for GFRP, 60 mm for CFRP and 40 mm for steel towers are used in the FEA. The towers are assumed to have a rigid support at the base and are free at the top.

5.2 Loads transferred from the turbine to tower

The loads applied to the tower are divided into two categories: loads transferred from the turbine to tower and loads applied to the tower itself. Loads transferred from the turbine to tower are calculated according to the CSA-C61400 Standard which provides wind speed profiles for different normal or extreme conditions. These wind speed profiles are then used to calculate the wind load applied to the swept area of the turbine. Other loads, such as loads due to generator short circuit (black out), are taken from NM48/750 technical data and Ungkurapinan (2005). A summary of loads and load combinations used in the analyses are listed in Table 5.3. Figure 5.1 shows the coordination systems used in the FEA.

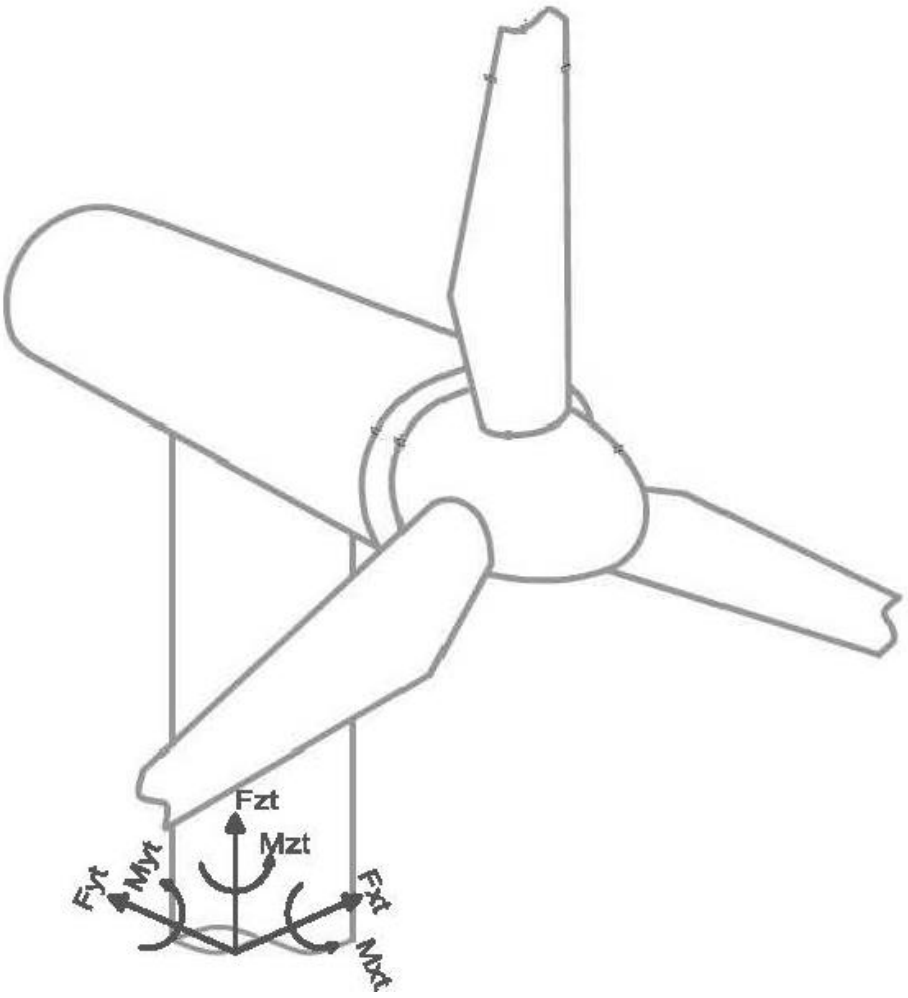

Figure 5.1: Co-ordinate systems and forces used in the FEA

Table 5.3: Wind turbine load cases (CSA-C61400)

Loads		Load Cases[1]										
		1	2	3	4	5	6	7	8	9	10	11
Loads transferred from the turbine to the tower	Loads due to wind turbine dead load	✓	✓	✓	✓	✓	✓	✓	✓	✓	✓	✓
	Extreme coherent gust with direction change (ECD)	✓										
	Extreme wind shear (EWS)		✓									
	Extreme operating gust (EOG)			✓	✓		✓					
	Extreme direction change (EDC)					✓						
	Extreme wind speed model-50 year recurrence period (EWM)							✓	✓			
	Extreme wind speed model-1 year recurrence period (EWM)									✓	✓	✓
	Generator short circuit (Black out)			✓					✓			
	Rotor blade eccentricity	✓	✓									✓
	Yaw load				✓	✓						
	Wake effects			✓	✓	✓	✓					
Loads applied to the tower itself	Tower Dead load	✓	✓	✓	✓	✓	✓	✓	✓	✓	✓	✓
	Live load	✓	✓	✓	✓	✓	✓	✓	✓	✓	✓	✓
	Snow load	✓	✓	✓	✓	✓	✓	✓	✓	✓	✓	✓
	Ice load	✓	✓	✓	✓	✓	✓	✓	✓	✓	✓	✓
	Wind load	✓	✓	✓	✓	✓	✓	✓	✓	✓	✓	✓

[1] Load cases are identified in Table 5.4

The following abbreviations are used in table 5.3:

ECD: Extreme coherent gust with direction change (CSA-C61400 Clause 6.3.2.5)

EWS: Extreme wind shear (CSA-C61400 Clause 6.3.2.6)

EOG: Extreme operating gust (CSA-C61400 Clause 6.3.2.2)

EDC: Extreme direction change (CSA-C61400 Clause 6.3.2.4)

EWM: Extreme wind speed model (CSA-C61400 Clause 6.3.2.1)

Yaw load: DNV/Risø Guidelines for design of Wind Turbines (2002) Clause 4.2.1

Wake effects: CSA-C61400 Annex D

Table 5.4: Load cases

Load cases	**Design situation**	**Wind condition**	**Partial safety factors**
1	Power production	ECD	Normal
2	Power production	EWS	Normal
3	Power production plus occurrence of fault	EOG	Abnormal
4	Start up	EOG	Normal
5	Start up	EDC	Normal
6	Normal shut down	EOG	Normal
7	Parked (Standing still or idling)	EWM with 50-year recurrence period	Normal
8	Parked (Standing still or idling) plus loss of electrical network connection	EWM with 50-year recurrence period	Abnormal
9	Parked (Standing still or idling)	EWM with 1-year recurrence period	Normal
10	Parked and fault conditions	EWM with 1-year recurrence period	Abnormal
11	Maintenance and repair	EWM with 1-year recurrence period	Abnormal

A summary of loads calculated for the 11 load cases listed in Table 5.4 is presented in Tables 5.5 to 5.15. As an example, manual calculations for load case 7, Extreme wind speed model (EWM), are provided in appendix A.

- Load case 1

Table 5.5: Loads transferred from turbine to tower, load case 1

Loads transferred from turbine to tower	**Load components**					
	Fxt (KN)	Fyt (KN)	Fzt (KN)	Mxt (KN.m)	Myt (KN.m)	Mzt (KN.m)
Loads due to wind turbine dead load	-	-	-429	680	-	-
Extreme coherent gust with direction change (ECD)	21	1063	-	-	-	4490
Rotor blade eccentricity	-	23	-	-	-	-
Σ	21	1086	-429	680	0	4490

- Load case 2

Table 5.6: Loads transferred from turbine to tower, load case 2

Loads transferred from turbine to tower	**Load components**					
	Fxt (KN)	Fyt (KN)	Fzt (KN)	Mxt (KN.m)	Myt (KN.m)	Mzt (KN.m)
Loads due to wind turbine dead load	-	-	-429	680	-	-
Extreme wind shear (EWS)	-	723	-	-	-	2904
Rotor blade eccentricity	-	23	-	-	-	-
Σ	0	746	-429	680	0	2904

- Load case 3

Table 5.7: Loads transferred from turbine to tower, load case 3

Loads transferred from turbine to tower	**Load components**					
	Fxt (KN)	Fyt (KN)	Fzt (KN)	Mxt (KN.m)	Myt (KN.m)	Mzt (KN.m)
Loads due to wind turbine dead load	-	-	-429	680	-	-
Extreme operating gust (EOG)	-	888	-	-	-	3565
Generator short circuit (Black out)	-	-	-	-	5155	-
Wake effects	Wake effects were considered					
Σ	0	888	-429	680	5155	3565

- Load case 4

Table 5.8: Loads transferred from turbine to tower, load case 4

Loads transferred from turbine to tower	**Load components**					
	Fxt (KN)	Fyt (KN)	Fzt (KN)	Mxt (KN.m)	Myt (KN.m)	Mzt (KN.m)
Loads due to wind turbine dead load	-	-	-429	680	-	-
Extreme operating gust (EOG)	-	1089	-	-	-	4375
Yaw load	-	0	-	17940	-	-
Wake effects	Wake effects were considered					
Σ	0	1089	-429	18620	0	4375

- Load case 5

Table 5.9: Loads transferred from turbine to tower, load case 5

Loads transferred from turbine to tower	**Load components**					
	Fxt (KN)	Fyt (KN)	Fzt (KN)	Mxt (KN.m)	Myt (KN.m)	Mzt (KN.m)
Loads due to wind turbine dead load	-	-	-429	680	-	-
Extreme direction change (EDC)	13	590	-	-	-	2503
Yaw load	-	0	-	17940	-	-
Wake effects	Wake effects were considered					
Σ	13	590	-429	18620	0	2503

- Load case 6

Table 5.10: Loads transferred from turbine to tower, load case 6

Loads transferred from turbine to tower	**Load components**					
	Fxt (KN)	Fyt (KN)	Fzt (KN)	Mxt (KN.m)	Myt (KN.m)	Mzt (KN.m)
Loads due to wind turbine dead load	-	-	-429	680	-	-
Extreme operating gust (EOG)	-	1089	-	-	-	4375
Wake effects	Wake effects were considered					
Σ	0	1089	-429	680	0	4375

- Load case 7

Table 5.11: Loads transferred from turbine to tower, load case 7

Loads transferred from turbine to tower	**Load components**					
	Fxt (KN)	Fyt (KN)	Fzt (KN)	Mxt (KN.m)	Myt (KN.m)	Mzt (KN.m)
Loads due to wind turbine dead load	-	-	-429	680	-	-
Extreme wind speed model-50 year recurrence period (EWM)	-	1417	-	-	-	5692
Σ	0	1417	-429	680	0	5692

- Load case 8

Table 5.12: Loads transferred from turbine to tower, load case 8

Loads transferred from turbine to tower	**Load components**					
	Fxt (KN)	Fyt (KN)	Fzt (KN)	Mxt (KN.m)	Myt (KN.m)	Mzt (KN.m)
Loads due to wind turbine dead load	-	-	-429	680	-	-
Extreme wind speed model-50 year recurrence period (EWM)	-	1155	-	-	-	4638
Generator short circuit (Black out)	-	-	-	-	5155	-
Σ	0	1155	-429	680	5155	4638

- Load case 9

Table 5.13: Loads transferred from turbine to tower, load case 9

Loads transferred from turbine to tower	**Load components**					
	Fxt (KN)	Fyt (KN)	Fzt (KN)	Mxt (KN.m)	Myt (KN.m)	Mzt (KN.m)
Loads due to wind turbine dead load	-	-	-429	680	-	-
Extreme wind speed model-1 year recurrence period (EWM)	-	907	-	-	-	3643
Σ	0	907	-429	680	0	3643

- Load case 10

Table 5.14: Loads transferred from turbine to tower, load case 10

Loads transferred from turbine to tower	**Load components**					
	Fxt (KN)	Fyt (KN)	Fzt (KN)	Mxt (KN.m)	Myt (KN.m)	Mzt (KN.m)
Loads due to wind turbine dead load	-	-	-429	680	-	-
Extreme wind speed model-1 year recurrence period (EWM)	-	739	-	-	-	2968
Σ	0	739	-429	680	0	2968

- Load case 11

Table 5.15: Loads transferred from turbine to tower, load case 11

Loads transferred from turbine to tower	**Load components**					
	Fxt (KN)	Fyt (KN)	Fzt (KN)	Mxt (KN.m)	Myt (KN.m)	Mzt (KN.m)
Loads due to wind turbine dead load	-	-	-429	680	-	-
Extreme wind speed model-1 year recurrence period (EWM)	-	739	-	-	-	2968
Rotor blade eccentricity	-	23	-	-	-	-
Σ	0	762	-429	680	0	2968

5.3 Loads applied to the tower itself

The loads applied to the tower are explained briefly in Sections 5.3.1 to 5.3.6. These loads were calculated using the National Building Code of Canada (NBCC 2005).

5.3.1 Tower dead load + turbine dead load

For the design of the wind turbine towers, the material properties obtained by Ungkurapinan (2005) are used. These properties are given in Tables 5.16 and 5.17. Cross sectional properties studied in this research are listed in tables 5.18 and 5.19. The mass values shown in Tables 5.18 and 5.19 are obtained assuming a density of 1950 kg/m^3 for GFRP, 1580 kg/m^3 for CFRP and 7600 kg/m^3 for steel.

Table 5.16: Material properties for GFRP and CFRP (Ungkurapinan table 7-5)

Material properties	**GFRP**	**CFRP**
Fiber-to-weight volume percentage	60%	60%
Density (g/cm^3)	1.95	1.58
Longitudinal modulus (E_1, GPa)	44.6	142
Transverse modulus (E_2, GPa)	12.46	10.30
In-plane shear modulus (G_{12}, GPa)	4.85	7.20
Major Poisson's Ratio (ν)	0.24	0.27
Longitudinal Tensile Strength (F_{1t}, MPa)	1300	2280
Longitudinal Compressive Strength (F_{1c}, MPa)	691	1440
Transverse Tensile Strength (F_{2t}, MPa)	47	57
Transverse Compressive Strength (F_{2c}, MPa)	130	228
In-plane shear strength (τ_u, MPa)	44	71

Table 5.17: Steel structural properties

Steel yield strength (Mpa)	Modulus of elasticity (GPA)	Density (kg/m^3)	Wall thickness (mm)
350	200	7600	30

Table 5.18: GFRP towers mass

Bottom diameter (mm)	Top diameter (mm)	Wall thickness (mm)	Mass (kg)
3500	2500	55.2	50080
4000	2400		53472
4500	2700		60273
5000	3000		67074
5500	3300		73875

Table 5.19: CFRP and steel towers mass

Bottom diameter (mm)	Top diameter (mm)	CFRP		Steel	
		Wall thickness (mm)	Mass (kg)	Wall thickness (mm)	Mass (kg)
2500	1500	60	28860	40	93500
3000	1800		34810		112580
3500	2500		43742		141230

In addition to self-weight, the towers are analyzed taking into account the weight of the moving parts such as blades and generator. The mass of these parts, along with their center of gravity, are listed in Table 5.20.

Table 5.20: Wind turbine mass distribution (Ungkurapinan Table 7-4)

Component	Mass (kg)	Center of gravity (m) with respect to Y_t axis
Blade	3•3466	7.85 (from rotor center)
Hub	2997	-
Total rotor	13395	2.237 (upwind from tower center)
Machine frame	4850	0.75 (downwind from tower center)
Gearbox	4670	-1.04
Generator	3450	-3.50
Main shaft	2015	+1.00
Cover	600	-1.50
Yaw bearing	562	0.00
Rest	2815	-
Total nacelle	19000	-1.125

5.3.2 Live load

According to DNV/Risø Guidelines for the design of Wind Turbines + NBCC table 4.1.5.3, a minimum live load of 1 kPa should be considered in the design of wind turbine towers. This live load is applied to tower roof, nacelle, and hub.

5.3.3 Snow load

The characteristic snow loads on exposed areas of the wind turbine are calculated according to NBCC Clause 4.1.6. This Code defines the snow pressure on surfaces subjected to snow accumulation as,

$$S = I_s[S_s(C_b C_w C_s C_a)] + S_r \quad 5.2$$

Where

- I_s is importance factor for snow load (NBCC table 4.1.6.2)
- S_s is 1 in 50 year ground snow load (NBCC Subsection 1.1.3)
- C_b is basic roof snow load factor (NBCC Clause 4.1.6.2)
- C_w is wind exposure factor (NBCC Clause 4.1.6.2)
- C_s is slope factor (NBCC Clause 4.1.6.2)
- C_a is shape factor (NBCC Clause 4.1.6.2)
- S_r is 1 in 50 year associated rain load (NBCC Subsection 1.1.3)

5.3.4 Ice load

Ice load is calculated using Clause 3.2.5 of the DNV/Risø Guidelines for the Design of Wind Turbines. These guidelines recommend an ice density of 700 kg/m^3 and specifies a minimum ice thickness of 30 mm on exposed surfaces.

5.3.5 Earthquake load

CSA-C61400 Clause 5.4.2.4 suggests that minimum earthquake requirements for standard wind turbine classes are not necessary.

5.3.6 Wind load

Since the natural frequency of wind turbine towers in this study (determined according to the NBCC Commentary I, Paragraph 40) is less than 1 Hz, a dynamic procedure is used to calculate the wind loads applied to the structure.

To account for the severe effects of diagonal wind, the NBCC specifies that in addition to applying 100% of wind load to each principal direction, tall structures should be designed to resist 75% of the maximum pressures for both principal directions applied simultaneously. Table 5.21 lists a summary of wind loads used in the analysis of the wind turbine towers.

Table 5.21: Summary of wind loads applied to towers

Distance above ground (m)	**100% dynamic wind load (N) on each principal direction separately**					**75% dynamic wind load (N) on each principal direction simultaneously**				
	Bottom diameter (mm)					**Bottom diameter (mm)**				
	3000	3500	4000	4500	5000	3000	3500	4000	4500	5000
5	65081	76380	86775	97622	108469	48810	57285	65081	73216	81351
10	62423	74165	83232	93635	104039	46817	55624	62424	70227	78030
15	67061	80734	89415	100592	111769	50296	60551	67062	75444	83827
20	69341	84673	92455	104012	115569	52005	63505	69341	78009	86676
25	70377	87270	93836	105566	117295	52782	65453	70377	79174	87971
30	70448	88829	93931	105673	117414	52836	66622	70449	79255	88061
35	69781	89602	93042	104673	116303	52336	67201	69782	78505	87227
40	68522	89750	91363	102784	114204	51391	67313	68522	77088	85653
45	66770	89385	89028	100156	111285	50078	67039	66771	75117	83463
50	64599	88586	86133	96899	107666	48449	66440	64599	72674	80749

5.4 FRP composite pole design

In this Section, different configurations of FRP composite tower structures are studied to determine an appropriate design that can satisfy ultimate state requirements. As in the case of poles presented in Chapter 4, a nonlinear static analysis is employed to analyze these structures and obtain deflection profiles and stress and strain distributions using the ANSYS finite element software. To find the best cross section for these 50 m tall towers, bottom diameters ranging from 2,500 mm to 5,500 mm are modeled. A top-to-bottom diameter ratio of 0.6 and a wall thickness of 55.2 mm for the GFRP towers, 60 mm for the CFRP towers and 40 mm for the steel towers is used. Furthermore, different ratios of number of longitudinal layers-to-total number of

layers and different longitudinal fiber orientations are studied to determine a lay-up that would result in low internal stresses in the structure, small deflections, and a minimum overall mass.

A set of material properties such as longitudinal and transverse modulus of elasticity, in-plane shear strength, and Poisson's ratio for GFRP and CFRP obtained by Ungkurapinan (2005) are used to model the towers discussed in Sections 5.5.1, 5.5.2, and 5.5.3. A summary of these values are given in Table 5.16. These structures are first designed according to ultimate strength criteria explained in 5.1.1.1. A stability analysis is performed in Section 5.6.1 and critical deflection analysis is presented in Section 5.6.2. These analyses are performed on this optimum section to verify whether it would pass the requirements set by the CSA-C61400 Standard. Eleven different load combinations (Table 5.3) are used for each case study presented in Sections 5.5.1, 5.5.2, and 5.5.3.

5.5 Parametric study using ultimate strength analysis

5.5.1 Case 1: The effect of longitudinal layers on ultimate strength of FRP composite towers

Towers with different Rn ratios (number of longitudinal layers/total number of layers) are modeled in this Section. Stress and strain distributions and deflection profiles obtained through the FEA are used to examine the effect of longitudinal layers on the structural performance of the wind turbine towers. Dimensions, number of longitudinal and circumferential layers, and longitudinal fiber orientations for Case 1 are presented in Tables 5.22 and 5.23.

Table 5.22: Geometric properties for towers studied in Case 1

Pole series	Geometric properties				
	Tower length (mm)	Bottom diameter (mm)	Top diameter	Wall thickness (mm)	Mass (kg)
GFRP	50000	5000	3000	55.2	67074
CFRP	50000	3500	2500	60	43742

Table 5.23: Fiber arrangement for GFRP and CFRP towers studied in Case 1

Pole series	Fiber Arrangement				
	Number of circumferential layers (Nc)	**Number of longitudinal layers (Nl)**	**Total number of layers (Nt)**	**Long. fiber orientation**	**Fiber to weight volume percentage**
GFRP and CFRP	38	10	48	+/-5°	60%
	29	19	48		
	19	29	48		
	10	38	48		
	0	48	48		

The towers in Case 1 have a wall thickness of 55.2 mm for the GFRP towers and 60 mm for the CFRP towers. These laminates consist of 48 layers with different numbers of longitudinal layers. To examine the effect of longitudinal layers on the structural performance of wind turbine towers, the Rn ratio is varied from 0.2 to 1. To complete Case 1, the longitudinal fiber orientation is kept constant at +/-5° with respect to the longitudinal axis of the tower.

Keypoints and arcs are used to create the top and bottom cross sections of the tower in the FEA. These lines are used to generate areas and form the three-dimensional geometry of the structure. After creating the geometry and boundary conditions, the models are meshed and the loads calculated in Sections 5.2 and 5.3 are applied to nodes. The lateral deflections of the GFRP

tower, with Rn=0.6, for the 11 load cases are shown in Figure 5.2. The results suggest that Load Case 7, when 100% wind load is applied in the direction of the one principal axis of FRP composite tower, causes the maximum deflection.

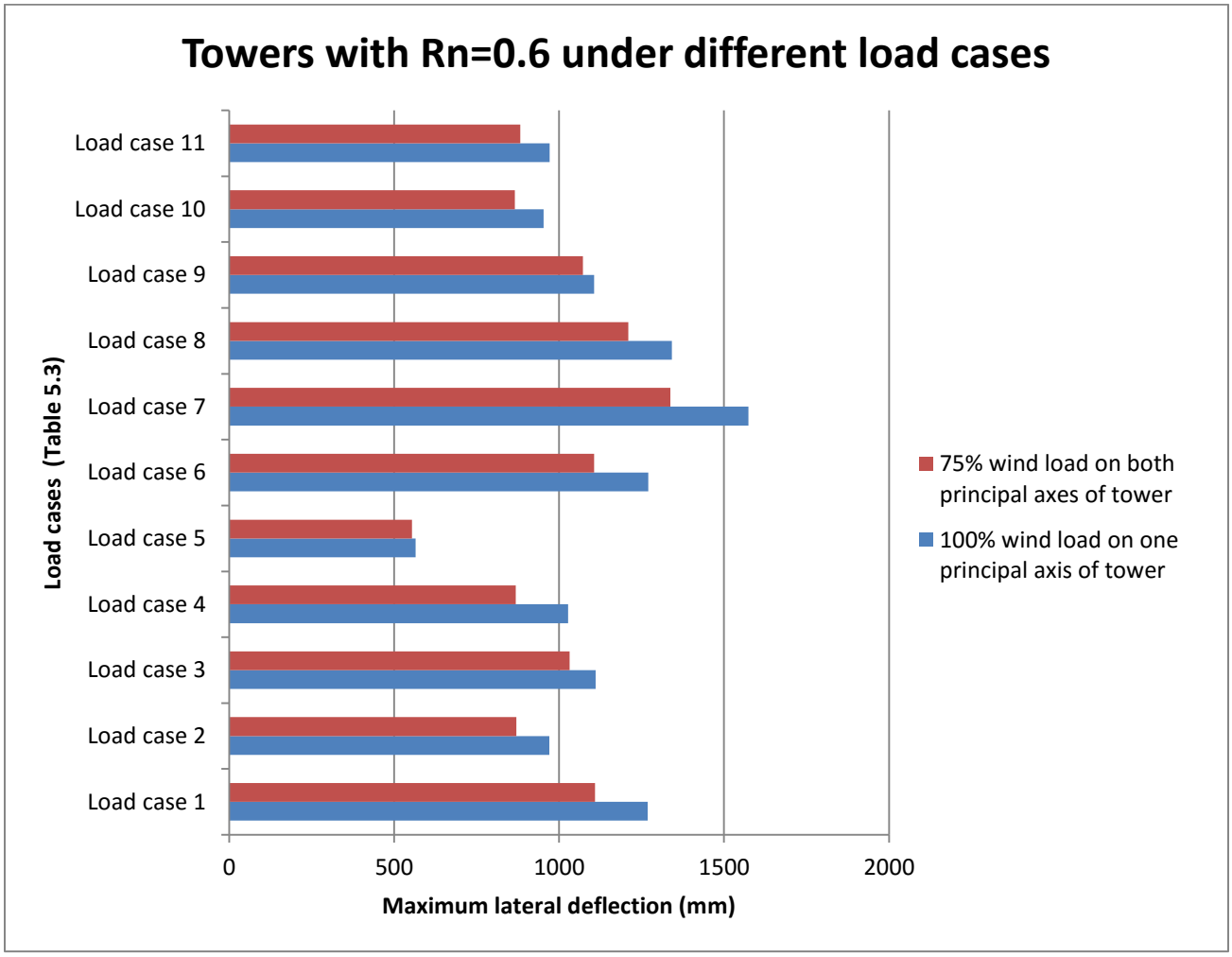

Figure 5.2: GFRP towers with Rn=0.6 under load cases presented in Table 5.3

The lateral tip deflections for the GFRP towers related to different Rn ratios studied in this Section are shown in Figures 5.3 and 5.4. These figures indicate that towers with Rn ratio of 0.8 deflect slightly less than towers with Rn ratio of 0.6. But in order to provide better confinement for longitudinal layers an Rn ratio of 0.6 is used.

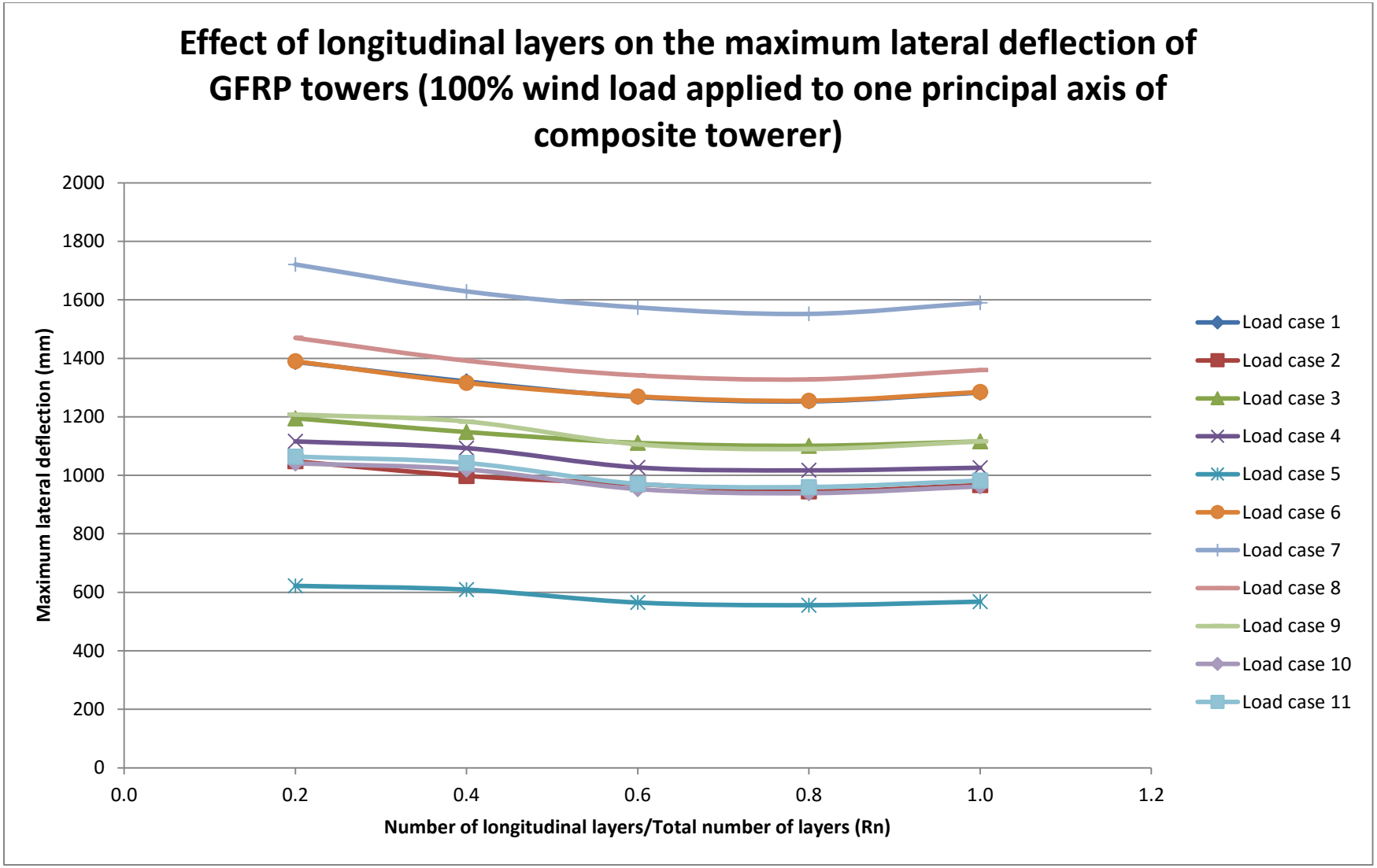

Figure 5.3: Effect of longitudinal layers on the maximum lateral deflection of GFRP towers (100% wind load applied to one principal axis of composite tower)

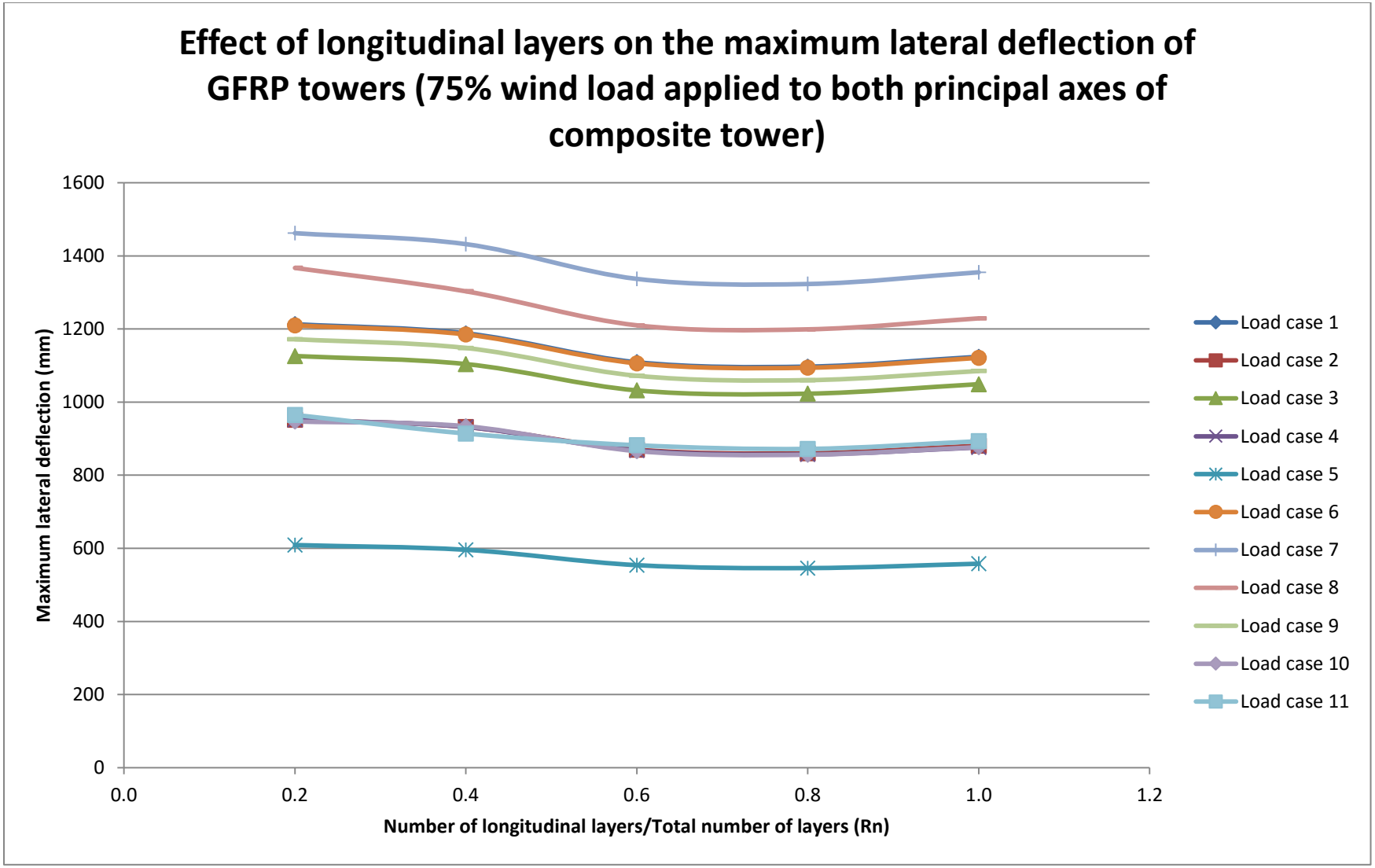

Figure 5.4: Effect of longitudinal layers on the maximum lateral deflection of GFRP towers (75% wind load applied to both principal axes of composite tower)

As shown in Figure 5.3, increasing the number of longitudinal layers up to 38 layers (Rn=0.8), the tip deflection decreases continuously. Deflections presented in Figures 5.3 and 5.4 show that there is a considerable difference when 10 longitudinal layers (Rn=0.2) are used compared to when 29 longitudinal layers (Rn=0.6) are used. For GFRP towers, under Load Case 7, the model with Rn=0.2 deflected 1721 mm whereas the tower with Rn=0.6 deflected 1574 mm, a reduction of 8.5%. In the case of CFRP structures, Rn=0.6 is selected as well. Under the Load Case 7, the lateral tip deflection is 30% (195 mm) lower compared to towers with Rn=0.2.

5.5.2 Case 2: The effect of longitudinal fiber orientation on ultimate strength of FRP composite towers

Five different longitudinal fiber orientations are examined: +/-5°, +/-15°, +/-25°, +/-35°, and +/-45°. Based on the Case 1 results (Section 5.5.1), Rn=0.6 is selected for the composite towers. As in Case 1, the bottom diameter, the top-to-bottom diameter ratio, and the wall thickness were 5,000 mm, 0.6, and 55.2 for GFRP towers respectively. For the CFRP towers these were 3500 mm, 0.6, and 60 mm respectively. The fiber arrangement used in this case are presented in Tables 5.24.

Table 5.24: Fiber arrangement for towers studied in Case 2

Pole Series	**Fiber Arrangement**					
	Number of circumferential layers (Nc)	Number of longitudinal layers (Nl)	Total number of layers (Nt)	Rn=Nl/Nt	Long. fiber orientation	Fiber to weight volume percentage
GFRP and CFRP	19	29	48	0.6	+/-5°	60%
					+/-15°	
					+/-25°	
					+/-35°	
					+/-45°	

The lateral deflections of the GFRP tower with longitudinal fiber orientation of +/-5° for the 11 load cases are shown in Figure 5.5. The results suggest that Load Case 7, where a 100% wind load is applied to one principal axis of the composite tower, yields the maximum deflection. Tip deflection of the GFRP tower under this load combination is 1,574 mm (3.1% of tower height). The effect of longitudinal fiber orientation on the lateral deflection of the composite tower is demonstrated in Figures 5.6 and 5.7. These plots indicate that towers with smaller fiber orientations provide higher degrees of stiffness. For instance, GFRP towers with +/-45° longitudinal fiber orientations deflect 15% more than towers with +/-5° longitudinal fiber orientation. In the case of CFRP structures, towers with +/-15° fiber orientation yield the smallest tip deflection. Towers with +/-15° longitudinal fiber orientation deflected 49% less than towers with a +/-45° fiber orientation. Therefore, longitudinal fiber orientations of +/-5° and +/-15° are selected for the final design of the GFRP and CFRP wind turbine towers, respectively.

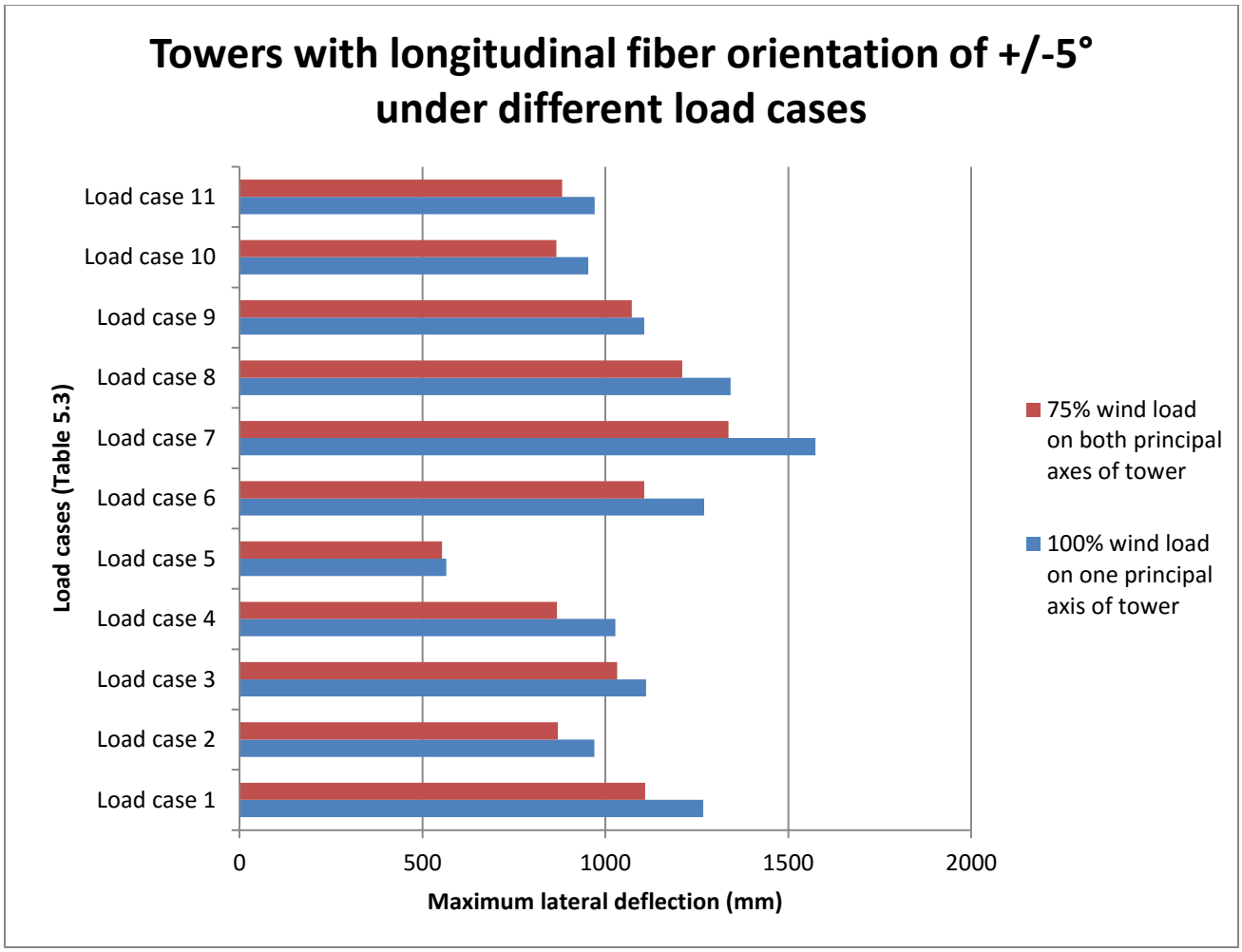

Figure 5.5: GFRP towers with +/-5° longitudinal fiber orientation under load cases presented in Table 5.3

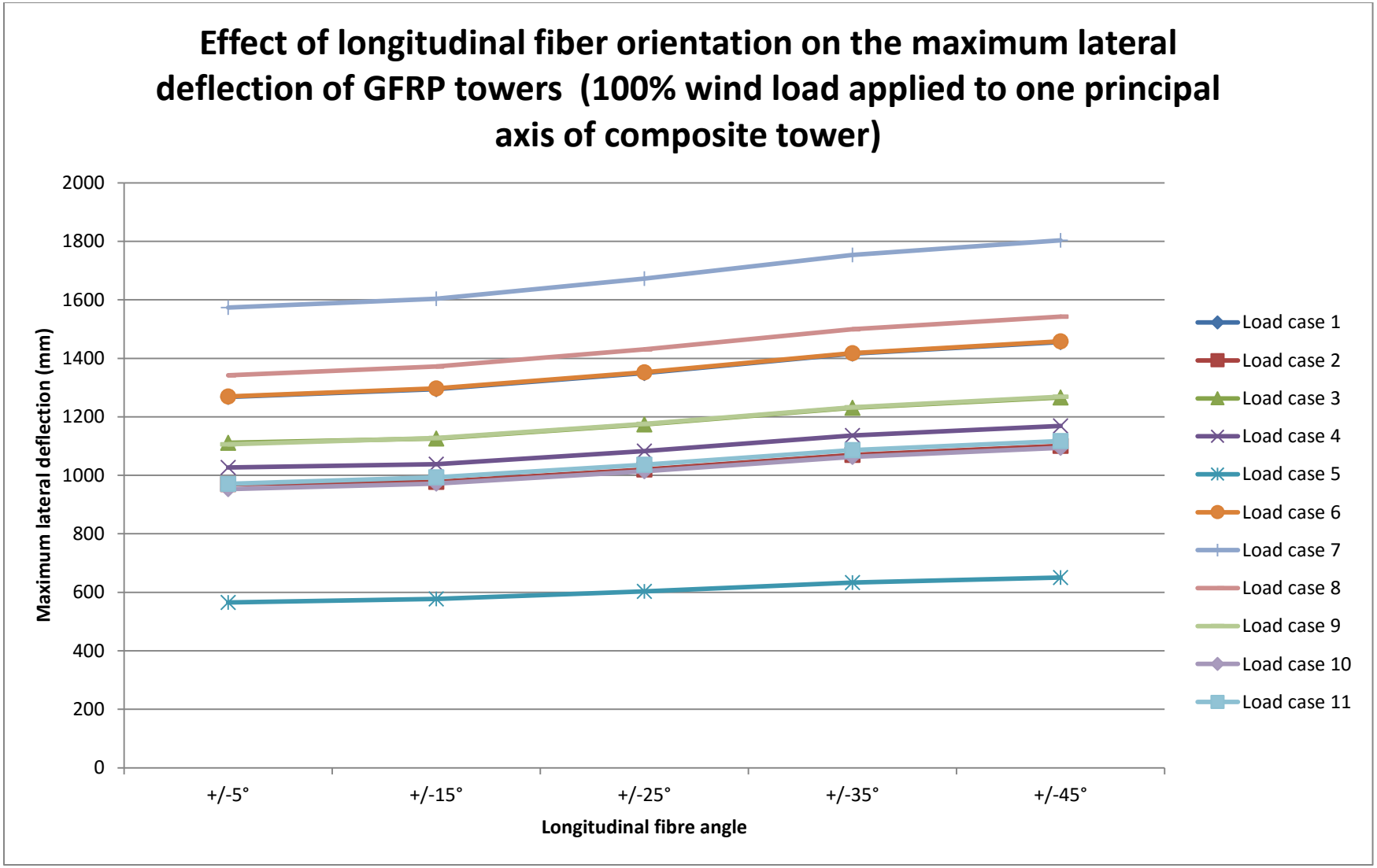

Figure 5.6: Effect of longitudinal fiber orientation on the lateral deflection of GFRP towers (100% wind load applied to one principal axis of composite tower)

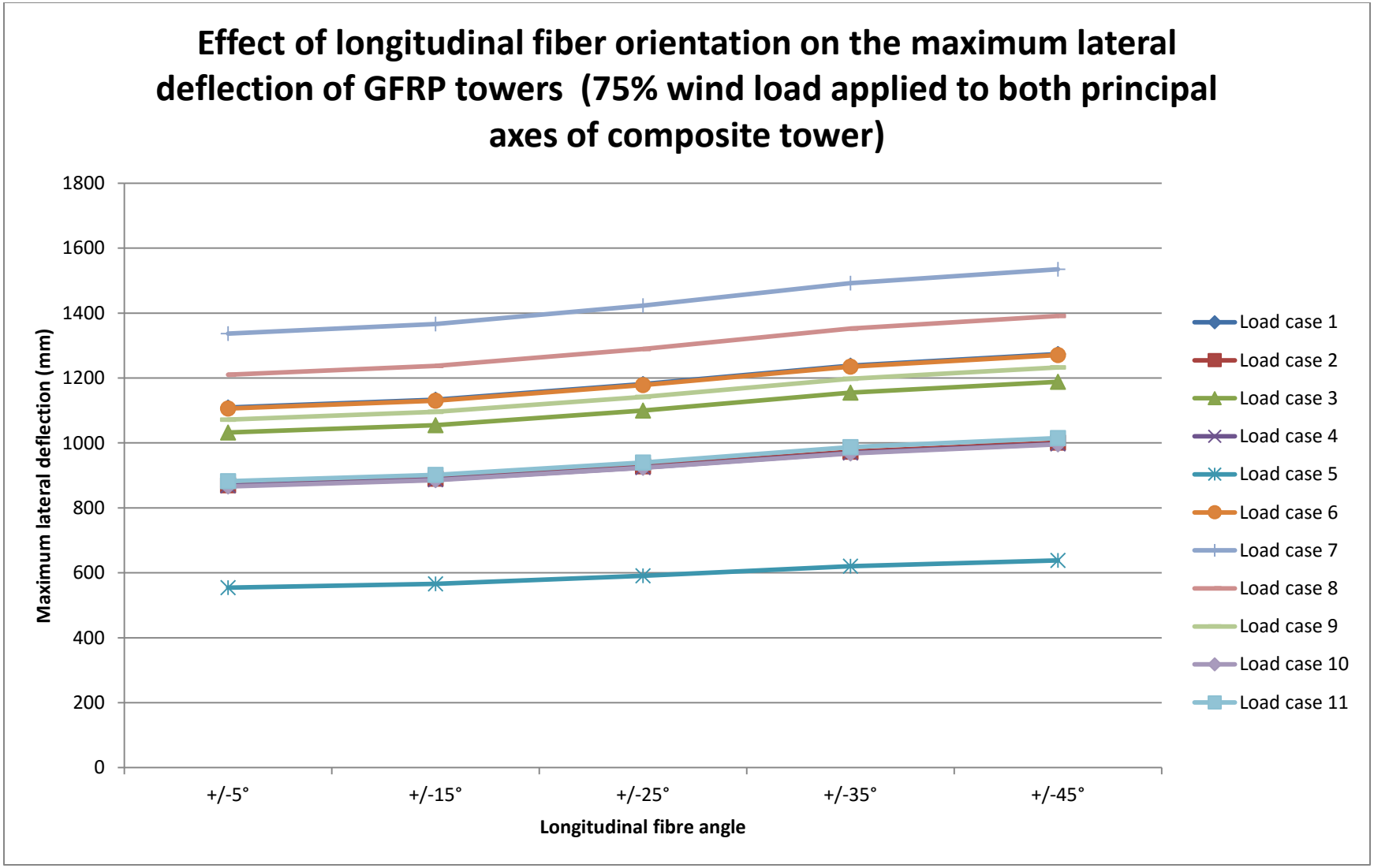

Figure 5.7: Effect of longitudinal fiber orientation on the maximum lateral deflection of GFRP towers (75% wind load applied to one principal axis of composite tower)

5.5.3 Case 3: The effect of cross section dimensions on ultimate strength of FRP composite towers

In this Section, towers with seven different bottom diameters are examined. These ranged from 2,500 mm to 5,500 mm. They are selected to examine the effect of cross-section dimensions on their structural behavior. Tables 5.25 and 5.26 provide geometric properties and fiber arrangement for these structures. As in Cases 1 and 2, a wall thicknesses of 55.2 mm for the GFRP towers, 60 mm for the CFRP towers, and 40 mm for the steel towers are used in the FEA. Therefore, the total tower masses presented in Table 5.25 are only a function of the cross-section dimensions as shown in Figure 5.8. The optimum bottom diameter for a 50 m tall composite tower is based on the total mass and tip deflection under the critical load combination. Lighter sections that can satisfy the CSA-C61400 Standard requirements may be selected as supporting structures for wind turbines.

Table 5.25: Geometric properties for towers studied in Case 3

Pole series	**Geometric properties**				
	Tower length (mm)	Bottom diameter (mm)	Top diameter (mm)	Wall thickness (mm)	Mass (kg)
GFRP	50000	3500	2500	55.2	50080
		4000	2400		53472
		4500	2700		60273
		5000	3000		67074
		5500	3300		73875
CFRP	50000	2500	1500	60	28860
		3000	1800		34810
		3500	2500		43742
Steel	50000	2500	1500	40	93500
		3000	1800		112580
		3500	2500		141230

Table 5.26: Fiber arrangement for towers studied in Case 3

Pole series	Fiber Arrangement					
	Number of circumferential layers (Nc)	Number of longitudinal layers (Nl)	Total number of layers (Nt)	Rn=Nl/Nt	Long. fiber orientation	Fiber to weight volume percentage
GFRP	19	29	48	0.6	+/-5°	60%
CFRP	19	29	48	0.6	+/-15°	60%

According to Case 1 (Section 5.5.1), the optimum ratio for number of longitudinal layers to total number of layers would be Rn=0.6 for the towers under investigation. Furthermore, as discussed in Case 2 (Section 5.5.2), +/-5° and +/-15° longitudinal fiber orientations may be used for GFRP and CFRP structures as well.

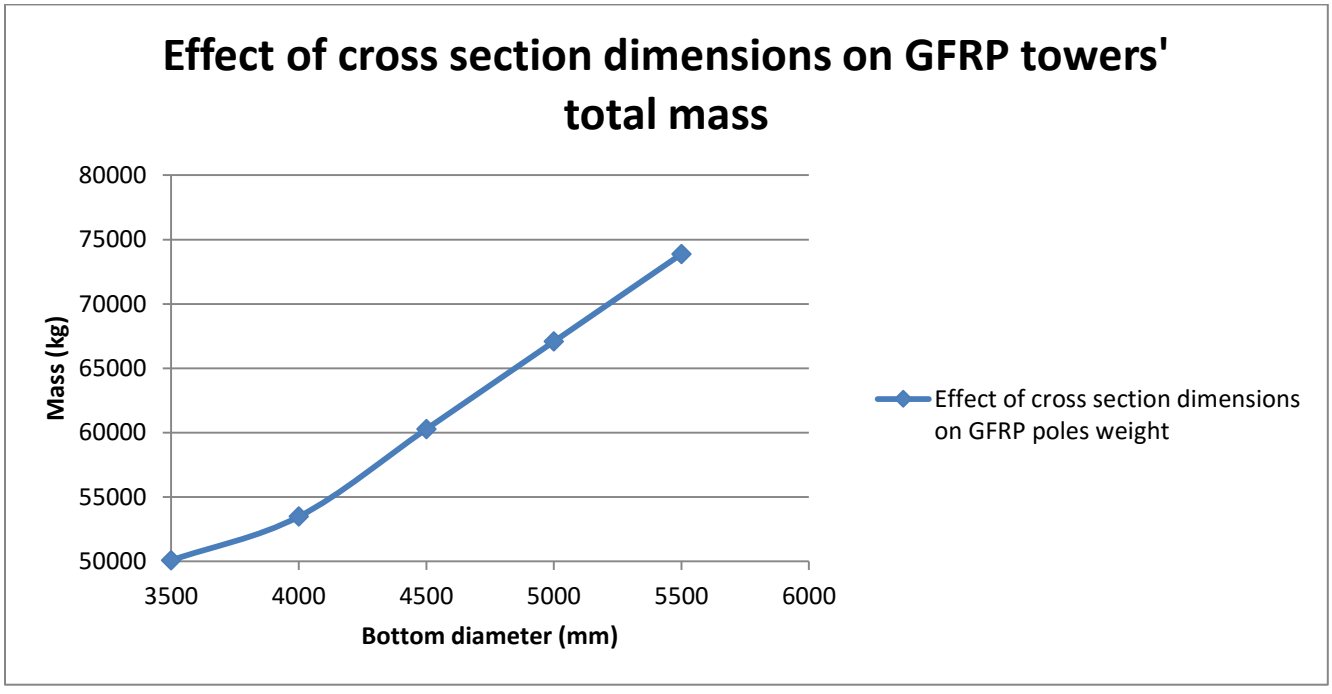

Figure 5.8: Effect of cross section dimensions on GFRP towers' total mass

The effect of cross-section dimensions on the lateral deflection of the GFRP tapered towers is demonstrated in Figures 5.10 and 5.11. As in Cases 1 and 2, the critical load combination that yields the highest deflections is Load Case 7. As expected, increasing the bottom diameter results in lower tip deflections. The results presented in Figure 5.10 suggest that GFRP towers with a 5,500 mm bottom diameter deflect 5.25% of tower height less than towers with a 3,500 mm bottom diameter. The lateral tip deflections under Load Case 7 (critical load combination) for CFRP and steel towers are presented in Tables 5.27 and 5.28. These results suggest that CFRP wind turbine towers have the smallest mass and smallest lateral deflection compared to GFRP and steel towers. The CFRP tower with bottom diameter of 3000 mm has a mass of 34810 kg and deflects 510 mm, whereas the steel tower with same bottom diameter has a mass of 112580 kg and deflects 1335 mm.

Table 5.27: CFRP towers structural performance

Pole series	**Geometric properties**			**Results for load case 7**			
				CFRP			
	Tower length (mm)	Bottom diameter (mm)	Top diameter (mm)	Wall thickness (mm)	Mass (kg)	Lateral deflection (mm)	Lateral deflection/free length (%)
1	50000	2500	1500	60	28860	713	1.4
		3000	1800	60	34810	510	1.0
		3500	2500	60	43742	252	0.5

Table 5.28: Steel towers structural performance

Pole series	Geometric properties			Results for load case 7			
				Steel			
	Tower length (mm)	Bottom diameter (mm)	Top diameter (mm)	Wall thickness (mm)	Mass (kg)	Lateral deflection (mm)	Lateral deflection/free length (%)
1	50000	2500	1500	40	93500	2268	4.5
		3000	1800	40	112580	1335	2.7
		3500	2500	40	141230	783	1.6

The CSA-C61400 Standard specifies that the deflections should not affect the structural integrity of the tower under the load conditions detailed in Table 5.4. One of the most important design considerations is to verify that no mechanical interference occurs between the blades and tower under these loads. In other words, no part of the blade should hit the supporting tower under any load combinations. Using the technical data provided for NM48/750, the distance between blades and tower is determined to be 1810 mm as shown in Figure 5.9. The maximum deflections for different cross sections are given in Figures 5.10 and 5.11. These results indicate that GFRP towers with bottom diameters less than 5,000 mm would fail to satisfy the deflection limit under the CSA-C61400 Standard load requirement. Therefore, the design of the GFRP towers is based on a minimum bottom diameter of 5,000 mm. In the case of CFRP and steel, a minimum bottom diameter of 3,000 mm satisfies the deflection limit.

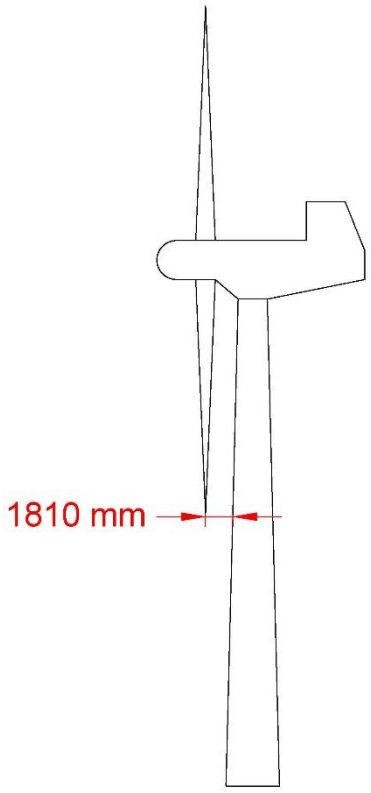

Figure 5.9: Distance between blades and tower for NM48/750 wind turbines

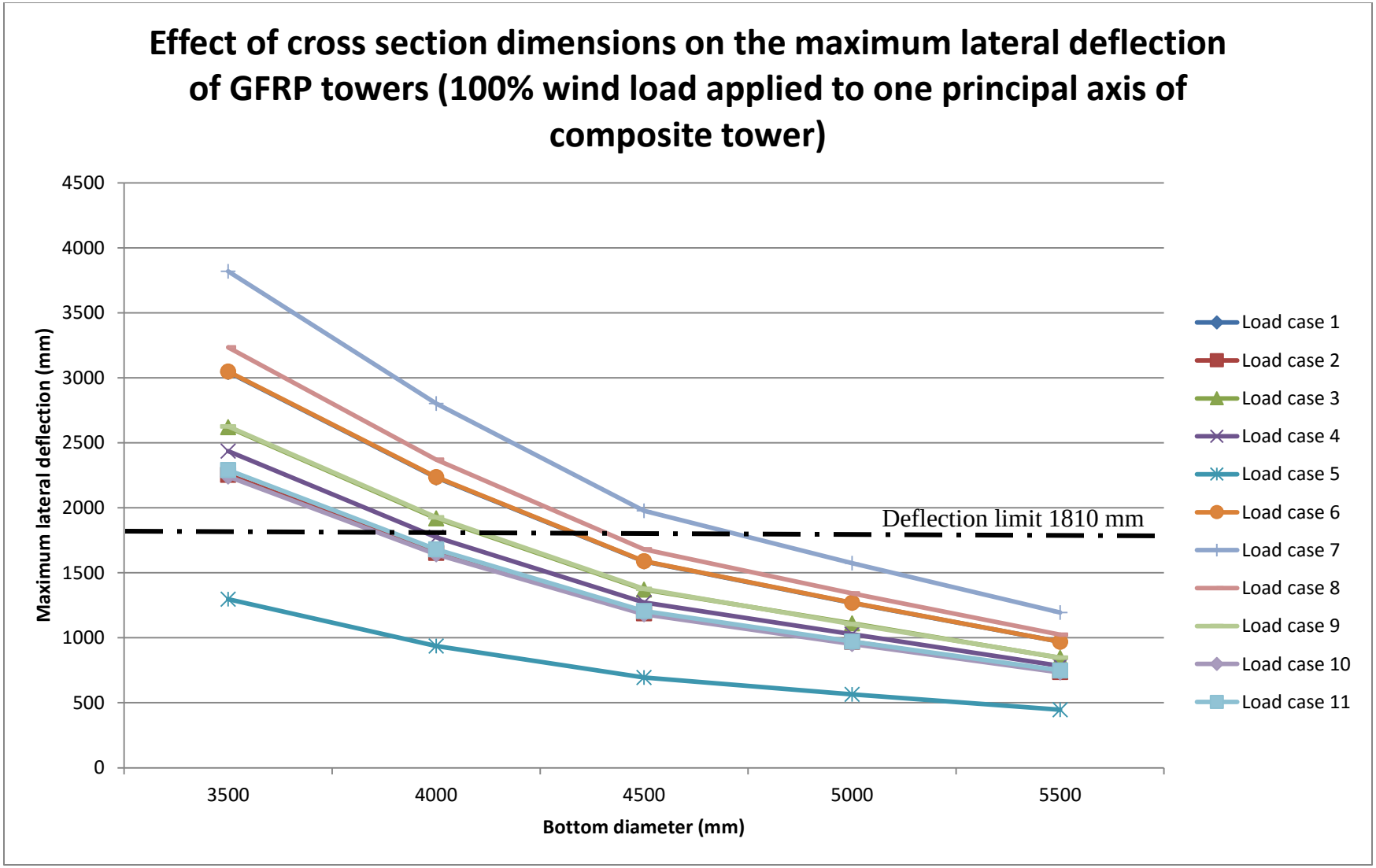

Figure 5.10: Effect of cross section dimensions on the maximum lateral deflection of GFRP towers (100% wind load applied to one principal axis of composite tower)

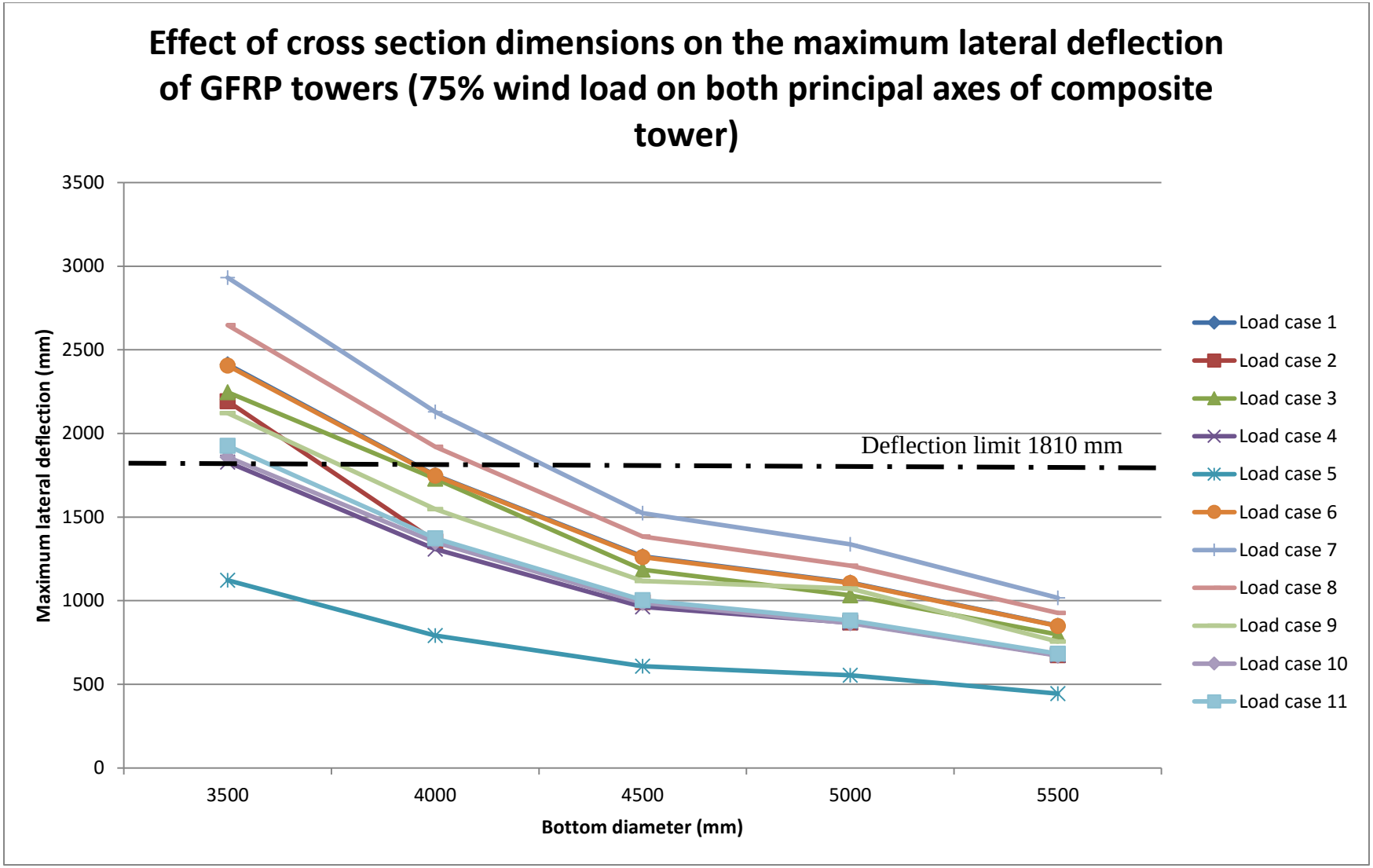

Figure 5.11: Effect of cross section dimensions on the maximum lateral deflection of GFRP towers (75% wind load on both principal axes of composite tower)

5.6 Final design

Fifty meters tall wind turbine towers are analyzed in Section 5.5 to find the optimum design which would result in low internal stresses in the structure, acceptable deflections, and low overall weight. The final configuration for GFRP composite towers consists of 29 longitudinal layers with +/-5° fiber orientation. For the CFRP towers, the same number of longitudinal layers is chosen but with +/-15° fiber orientations. In addition, both GFRP and CFRP towers are designed with 19 layers of circumferential fibers giving an Rn=0.6. For GFRP towers, the bottom diameter selected is 5,000 mm with a wall thickness of 55.2 mm. The CFRP towers are designed to have a bottom diameter of 3000 mm and a wall thickness of 60 mm. This design results in a maximum deflection of 1,574 mm for GFRP towers (3.14% of free length) and 510 mm for CFRP structures (1% of free length). These are smaller than the deflection limit of 1810 mm specified by the CSA-C61400 Standard. A summary of laminate lay-up for the two types of towers is presented in Table 5.29.

Table 5.29: Final design configurations

Geometric properties and fiber arrangement	**GFRP**	**CFRP**	**Steel**
Tower length (mm)	50000	50000	50000
Bottom diameter (mm)	5000	3000	3000
Top diameter (mm)	3000	1800	1800
Number of Long. Layers (Nl)	29	29	-
Number of Circumferential layers (Nc)	19	19	-
Total number of layers (Nt)	48	48	-
Rn=Nl/Nt	0.6	0.6	-
Long. fiber orientation	+/-5°	+/-15°	-
Stacking sequence	90,90,90,90,90,+5,90,-5,…,+5,90,-5,90,90,90,90,90	90,90,90,90,90,+15,90,-15,…,+15,90,-15,90,90,90,90,90	-
Fiber to weight volume percentage	60%	60%	-
Wall thickness (mm)	55.2	60	40
Mass (kg)	67074	34810	112580

Tsai-Wu and Maximum Stress modes of failure are observed in the numerical models. Figures 5.12 and 5.13 display the Tsai-Wu and Maximum stress values for the GFRP tower final design. These figures indicate that material failure occurs on the tension side close to the support at the bottom, and at hub height where loads are transferred from the turbine to the tower. A summary of GFRP, CFRP and steel towers' structural performance is provided in Table 5.30.

Table 5.30: GFRP, CFRP and steel towers' structural performance

Comparing structural performance of GFRP, CFRP and steel towers (Ultimate state design)				
Material		**GFRP**	**CFRP**	**Steel**
Critical loads (Load case 7)	Fxt (KN)	0	0	0
	Fyt (KN)	1417	1417	1417
	Fzt (KN)	-548.0	-548.0	-548.0
	Mxt (KN.m)	680	680	680
	Myt (KN.m)	0	0	0
	Mzt (KN.m)	5692	5692	5692
Tip deflection (mm)		1574	510	1335
Lateral deflection/free length (%)		3.148	1.02	2.67
Failure mode		Tsai Wu and Maximum stress (near the support on the tension side)	Tsai Wu and Maximum stress (near the support on the tension side)	Tsai Wu (near the support on the tension side)

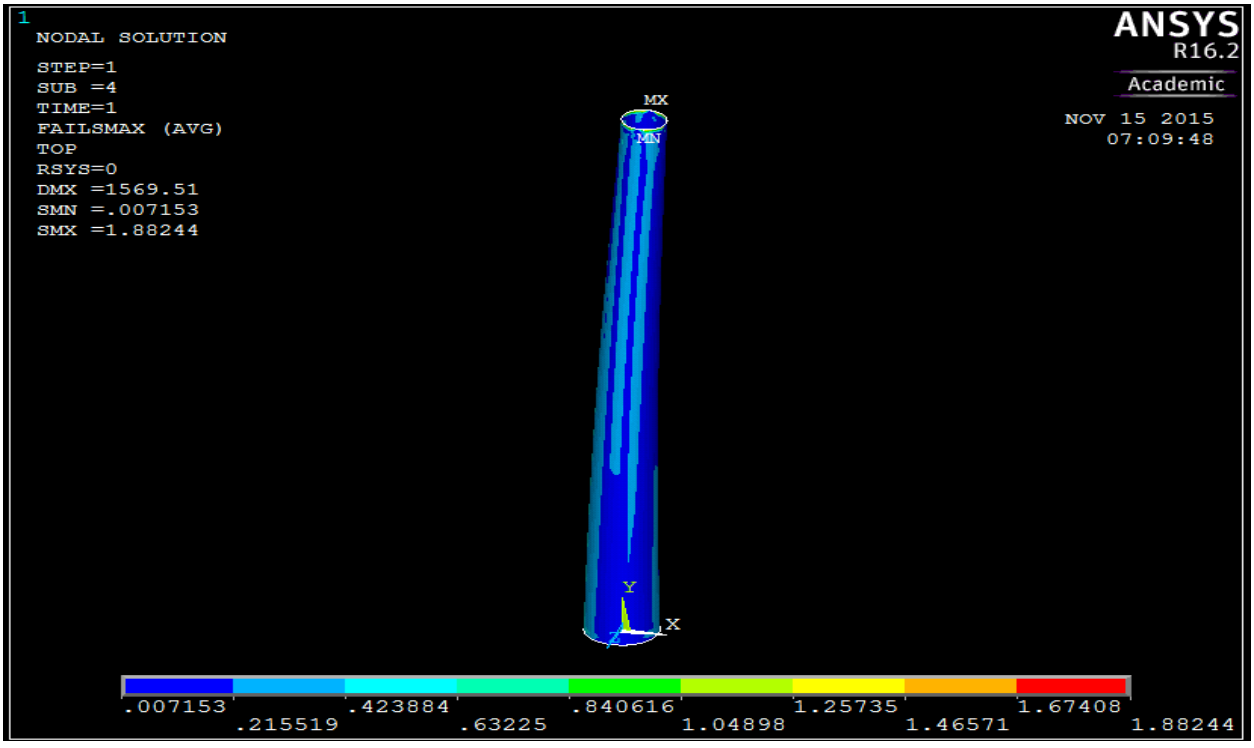

Figure 5.12: Maximum stress failure criterion for final GFRP design

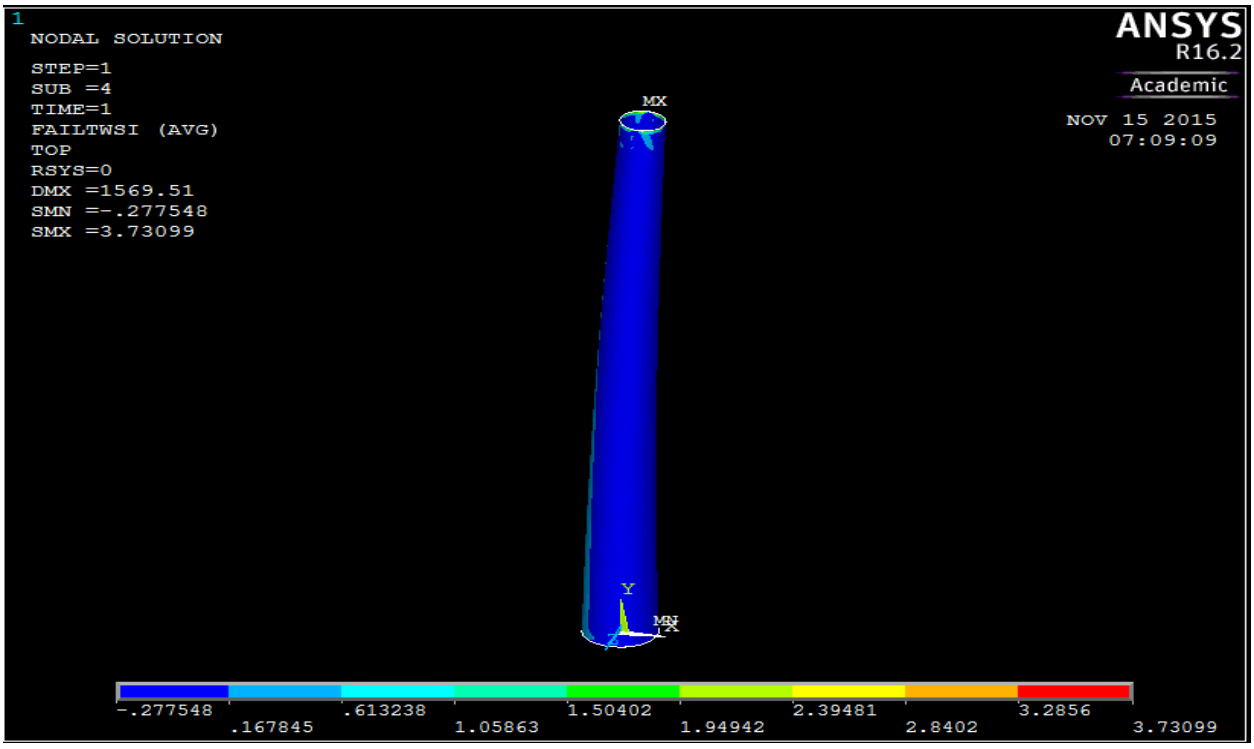

Figure 5.13: Tsai-Wu failure criterion for final GFRP design

5.6.1 Stability analysis for final design

As discussed in Section 5.1.1.2, CSA-C61400 Clause 7.6.4 requires that a stability analysis for the design of non-fail-safe components be carried out. These components should not buckle under the design loads. The results from a linear buckling analysis of the FRP composite towers, using ANSYS finite element software, are presented here. The buckling capacity of the towers is based on an elastic buckling analysis. Results obtained through the numerical analysis indicate that the ultimate axial loads that can be applied to the towers before overall buckling takes place are 42,355 KN for GFRP; 115,000 KN for CFRP; and 82,491 KN for steel towers. These ultimate axial loads are considerably higher than axial loads applied to the towers under Load Cases 1 to 11, presented in Sections 5.2 and 5.3.

5.6.2 Critical deflection analysis for final design

The results from a critical deflection analysis of the towers are presented here. The maximum deflection under the critical load combination (Load Case 7) is determined using characteristic loads or loads without the use of partial safety factors. This deflection is then multiplied by partial safety factors for loads, materials, and the consequences of failure. A summary of results for the critical deflection analysis is given in Table 5.31.

Table 5.31: Critical deflection analysis results

Comparing structural performance of GFRP, CFRP and steel towers (Critical Deflection Analysis)			
Material	**GFRP**	**CFRP**	**Steel**
Deflection without safety factors (mm)	862	315	824
Load safety factor	1.35	1.35	1.35
Material safety factor	1.1	1.1	1.1
Consequences of failure safety factor	1	1	1
Deflection multiplied by safety factors	1280	468	1224
Lateral deflection/free length (%)	2.56	0.94	2.45

The maximum deflection values obtained from the critical deflection analysis are then compared to the allowable deflection specified by the CSA-C61400 Standard, to make sure the structural integrity of wind turbine is not affected. The maximum deflection calculated by the FEA (1,280 mm for GFRP, 468 mm CFRP, and 1,224 mm for steel) are less than the allowable deflection of 1,810 mm for NM48/750 wind turbines.

Chapter 6: results and discussion

6.1 Summary and conclusions

In this research study, structural applications of FRP composite towers are investigated for use as light standards and wind turbine towers. On the basis of the experimental and numerical work presented in this thesis, the following conclusions are drawn:

Phase I: Verification of the FEA results.

- The maximum compressive stresses in the longitudinal direction obtained through the FEA were 250 MPa for Pole A and 263 MPa for Pole B. These are lower than GFRP compressive strength of 551.6 MPa obtained by Philopulos (2002). Similarly the maximum tensile stresses in the longitudinal direction obtained through the FEA were 277 MPa for Pole A and 291 MPa for Pole B which are lower than GFRP tensile strength of 620.55 MPa (Philopulos, 2002).
- The average lateral load applied by Philopulos (2002) to the poles tested is 2400 N and the resulting average tip deflection are 1120.5 mm for experimental program (Philopulos, 2002) and 1101.5 mm for numerical models.
- The dominant failure mode observed by Philopulos (2002) is local buckling for both Pole A and B.
- Shell element 281, which has eight nodes and six degrees of freedom at each node, is selected for the development of the FE models. These models can accurately predict the deflection profile for FRP composite structures. On average, the FE models have an accuracy of 98% predicting the tip deflection of poles under ultimate loads.

- The results presented in Section 3.3.2, verify the presence of local buckling in the specimen tested by Philopulos (2002).
- The strains obtained through the FEA for Specimen B in Philopulos's work correlate well with the test data. In the case of specimen A, however the numerical results are lower when compared to experimental results.

Phase II: Investigation of FRP composite poles for light standards.

- A design for FRP composite light standards is presented based on the specifications of the AASHTO Standard for structural supports for highway signs, luminaires and traffic signals (Sixth edition 2013).
- Results presented in this thesis show that the optimum design for 6 m and 12 m light standards is one with four longitudinal layers (Rn=4/8) and +/-5° longitudinal fiber orientation. A bottom diameter of 210 mm for the 6 m poles and 300 mm for the 12 poles satisfies the design criteria.
- The FEA also shows that 6 m poles deflect 316 mm (5.3 % free length) and the 12 m poles deflect 1310 mm (10.9% free length) under the critical load combination III. The recommended designs satisfy the requirements set by AASHTO Standard Specifications, which specify a tip deflection limit of 15% of the free length.

Phase III: FRP composite wind turbine towers.

- Multiple standards are used to design these structures including: CAN/CSA-C61400-1:14 (Wind turbines-Part 1: Design requirements), CAN/CSA-C61400-2:08 (Wind turbines-Part 2: Design requirements for small wind turbines), ISO 4354:2009 (Wind actions on

structures), and NBCC (2005), in addition to DNV/Risø Guidelines for Design of Wind Turbines (2002).

- A wall thickness of 55.2 mm for the GFRP and 60 mm for the CFRP are selected for analysis. Bottom diameters of 5,000 mm for the GFRP and 3000 mm for the CFRP satisfy the load criteria for a 50 m tall 750 kW wind turbine tower. These towers are designed with 29 longitudinal layers and an Rn ratio of 0.6. The optimum direction of the longitudinal fibers is +/-5° for the GFRP and +/-15° for the CFRP.
- The lateral deflections of the selected sections are 1,574 mm for GFRP towers and 510 mm for CFRP towers under the critical load combination of Load Case 7. These deflections are smaller than the limit specified by CSA C61400 which is the minimum distance between the blades and the supporting structure (1810 mm for towers under investigation).
- The Tsai-Wu and Maximum Stress failure criteria suggest that material failure might happen on the tension side near the support and at the hub height where loads are transferred from the turbine to the tower.

6.2 Recommendations for future research

The research presented in this thesis aims at developing a comprehensive numerical tool to design and analyze FRP composite tapered structures manufactured using filament winding technology. Two structural applications, including wind turbine towers and light standards, are discussed. However, more research is still required to find other potential areas where this technology can be used.

- Investigating other applications of FRP composite poles in highways, such as supporting structures for overhead and roadside signs or traffic signals.

- Designing a proper connection for composite wind turbine towers to the foundation, which can prevent material failures due to concentrated stresses.
- Investigating the fatigue behavior of the connections between segments.

References:

AASHTO. (2013). *Standard specification for structural supports for highway signs, luminaires and traffic signals.* AASHTO.

Alshurafa, S. (2012). Development of Meteorological Towers Using Advanced Composite Materials. *University of Manitoba. PhD dissertation*.

ANSYS Manual. (2015). ANSYS.

Arbon, I. (2012). The Energy Hierarchy Approach to Optimum Use of Energy Infrastructure - Sharing Ideas from the UK and Other Parts of Europe. *Proceedings of the International Symposium on Engineering.* Tokyo.

ASTM International. (2008). *Standard Test Method for Compressive Properties of Polymer Matrix Composite Materials with Unsupported Gage Section by Shear Loading.* ASTM D3410.

ASTM International. (2012). *Standard Test Method for Shear Properties of Composite Materials by the V-Notched Beam Method.* ASTM D5379.

ASTM International. (2014). *Standard Test Method for Tensile Properties of Polymer Matrix Composite Materials.* ASTM D3039.

Azzi, V., & Tsai, S. (1965). Anisotropic Strength of Composites. *Experimental Mechanics*, 283-288.

Burachynsky, V. (2002). Filament Winding of Long Tapered Tubes. *University of Manitoba, PhD dissertation*.

California Wind Energy Association, C. (2015). Retrieved from http://www.calwea.org/bigPicture.html

Chung, D. (2012). *Carbon Fiber Composites.* Butterworth-Heinemann.

Davidson, J. (2002). Composite Utility Poles & Crossarms. *ASCE*, 200-209.

Derrick, G. (1996). Fiberglass Composite Distribution and Transmission Poles. *Manufactured Distribution and Transmission Pole Structures Workshop* (pp. 55-61). Electric Power Research Institute.

Ehsani, S. (1994). seismic retrofit of existing reinforced concrete column by glass fiber composites. *Third Material Engineering Conference ASCE,* (pp. 758-763).

Energy, U. D. (2012). *Community Wind Benefits.*

Escher, G. (1982). *design and testing of an optimum fiberglass reinforced pole and market study on the demnd for utility poles in Canada.* ABCO Plastics.

Fibergrate Composite Structures. (2015). *High Performance Composite Solutions.* Fibergrate Composite Structures.

Gibson, R. (1995). *Principle of Composite Material Mechanics.* McGraw-Hill.

Global Wind Energy Council. (2014). *Market Forecast for 2014-2018.* California: GWEC.

Gould, P., & Basu, P. (1977). Geometric stiffness matrices for the finite element analysis of rotation. *Structures Mechanics*, 87-105.

Hashin, Z. (1980). Failure Criteria for Unidirectional Fiber Composites. *Applied Mechanics*, 329-334.

Hill, R. (1948). A Theory of the Yielding and Plastic Flow of Anisotropic Metals. *193* . The Royal Society. doi:10.1098

Ibrahim, S. (2000). Performance evaluation of fiber reinforced polymer poles for transmission lines . *University of Manitoba Phd dissertation*.

Ibrahim, S. M. (2000). Performance Evaluation of Fiber-Reinforced Polymer Poles for Transimission Lines. *University of Manitoba, PhD dissertation*.

Ibrahim, S., Polyzois, D., & Hassan, S. (2000). Development of glass fiber reinforced plastic poles for transmission and distribution lines. *Canadian Journal of Civil Engineering*, 850-858.

IEC 61400-1. (2005). *IEC 61400-1: Wind turbines - Part 1: Design requirements.* IEC.

Jenkins, C. (1920). *Report on Materials of Construction Used in Aircraft and Aircraft Engines.* Great Britain Aeronautical Research Committee.

Jeusette, J., & Laschet, G. (1990). Pre- and Postbuckling Finite Element Analysis of Curved Composite and Sandvich Panels. *AIAA*, 1233-1239.

Jun, S., & Hong, C. (1988). Buckling Behaviour of Laminated Composite Cylindrical panels under Axial Compression. *Computers&Structures*, 479-490.

Labossière, P., & Turkkan, N. (1992). Failure Prediction of Fibre-Reinforced Materials with Neural Networks. *Advanced Composite Materials in Bridges and Structures*, 1270-1280.

Metiche, S. (2012). Analysis and design procedures for the flexural behavior of glass fiber-reinforced polymer composite poles. *Journal of Composite Materials*, 207–229.

Miller, M. (1994). Fiberglass Distribution Poles: A Case of Study. *IEEE 13th Annual PES T&D*, (pp. 497-503).

Molded fiberglass companies. (2015). *Epoxy Resins.* MFGC.

Mufti, A., Erki, M., & Jaeger, L. (1991). *Advanced composite materials with application to bridges.* Canadian Society for Civil Engineering.

Munro, M. (1988). Review of manufacturing of fiber composite components by filament winding. *Polymer Composites*, 352 - 359.

Navaratna, D., Pian, T., & Wittmer, E. (1968). Stability analysis of shell of revolution by the finite element method. *AIAA*, 355-361.

NEG Micon. (2015). *NEG Micon 48/750.* Deutsche Windtechnik.

Noor, A., & Mathers, M. (1974). *Nonlinear Finite Element Analysis of Laminated Composite Shells.* NASA Technical Reports Server.

OTA. (1986). *New Structural Materials Technologies: Opportunities for the Use of Advanced Ceramics and Composites.* Congress of the United States: Office of Technology Assessment.

Philopulos, S. D. (2002). An investigation on the structural performance of jointed filament-wound GFRP poles for light utility applications. *University of Manitoba, Bachelor of Science Thesis*.

Polyzois, & Ungkurapinan, N. (2007). *Composite wind tower systems and methods of manufacture.* Patent publication number WO2007012201 A1.

Polyzois, D., Raftoyiannis, I., & Ochonski, A. (2013). Experimental and analytical study of latticed structures made from FRP composite materials. *Composite Strucures*, 165–175.

Polyzois, D., Raftoyiannis, I., & Ungkurapinan, N. (2009). Static and dynamic characteristics of multi-cell jointed GFRP wind turbine towers. *Composite Structures*, 34–42.

Reddy. (1981). A Finite Element Analysis of Large Deflection Bending of Laminated Anisotropic Shells. *ASME*, 249-263.

Reddy, J., & Chao, W. (1983). Nonlinear bending of bimodular-material plates. *International Journal of Solids and Structures*, 229-237.

Reichhold. (2009). *FRP material selection guide.* Reichhold.

Saigal, S., Kapania, R., & Young, T. (1986). Geometrically Nonlinear Finite Element Analysis of Imperfect Laminated Shells. *Composite Materials*, 197-214.

Standards council of Canada. (2014). *CSA-C61400-1:14- Wind turbines-Part 1: Design requirements.* CSA.

Standards council of Canada:. (2010). *CSA-C22.3 NO. 1-10 - Overhead systems.* CSA.

Tsai, S., & Wu, E. (1971). A General Theory of Strength for Anisotropic Materials. *Composite Materials*, 58-80.

U.S Department of Energy. (2015). *History of Wind Energy.* U.S. Department of Energy.

Ungkurapinan, N. (2005). Development of wind turbine towers using fiber reinforced polymers. *University of Manitoba, PhD dissertation*.

Waddoups, R. (1967). Advanced Composite Materials Mechanics for the Design and Stress Analyst. *General Dynamics, Fort Worth Division Report*.

Load case 7 - Extreme wind speed model-50 year recurrence period (EWM)

Hub height: Zhub

$z_{hub} := 50 \quad m$

Rotor diameter: D

$D := 48.2 \quad m$

Air density: p

$\rho := 1.350 \quad \frac{kg}{m^3}$ CSA-C61400-1/ clause 6.4.1-Churchill, Manitoba

$q_{site} := 0.40 \ kPA$ NBCC table C2-Churchill, Manitoba

$V_{refsite} := 33.9 \cdot \left(z_{hub}\right)^{0.11} \cdot q_{site} = 20.852 \ \frac{m}{s}$ CSA 61400-1/ clause 11.3A.2

Extreme wind speed model (EWM)

$V_{e50z} := 1.4 \cdot V_{refsite} = 29.193 \ \frac{m}{s}$ CSA 61400-1/ clause 6.3.2.1

Wind pressure

Partial safety factor for loads: CSA 61400-1/ Table 3

Load case 7 is a normal load case ----> $\gamma_f := 1.35$

Partial safety factor for materials:

$\gamma_m := 1.2$ CSA 61400-1/ clause 7.6.2.2

Partial safety factor for consequence of failure:

$\gamma_n := 1$ CSA 61400-1/ clause 7.6.2.2

$C_F := 1$ CSA-C61400-2/ clause 7.4.9

Wind pressure on the rotor area:pyt

$P_{yt} := \left(0.5 \cdot \rho \cdot V_{e50z}{}^{2}\right) \cdot C_F = 575.245 \quad PA$ ISO 4354/ clause 6

Wind load on the rotor area :Fyt

Rotor area: Ar

$A_r := \frac{\pi \cdot D^2}{4} = 1.825 \cdot 10^3 \quad m^2$

$F_{yt} := \gamma_f \cdot P_{yt} \cdot A_r = 1.417 \cdot 10^6 \ N$

Wind load on the turbine is assumed to have an eccentricity: exh

$e_{xh} := \frac{D}{12} = 4.017 \ m$ DNV 4.5.2

Moment due to eccentricities would be Mzt

$M_{ezt} := F_{yt} \cdot e_{xh} = 5.692 \cdot 10^6 \quad N.m$

Appendix B

```
!*********************
!* 6-M light standard
!*8 LAYERS
(0,0,85,95,85,95,0,0)
!*********************
/BATCH
/input,menust,tmp,'',,,,,,,,,
,,,,,,1
! /GRA,POWER
! /GST,ON
! /PLO,INFO,3
! /GRO,CURL,ON
! /CPLANE,1
! /REPLOT,RESIZE
WPSTYLE,,,,,,,,0
! /REPLOT,RESIZE
! /REPLOT,RESIZE
! /REPLOT,RESIZE
!*
/NOPR
KEYW,PR_SET,1
KEYW,PR_STRUC,1
KEYW,PR_THERM,0
KEYW,PR_FLUID,0
KEYW,PR_ELMAG,0
KEYW,MAGNOD,0
KEYW,MAGEDG,0
KEYW,MAGHFE,0
KEYW,MAGELC,0
KEYW,PR_MULTI,0
KEYW,PR_CFD,0
/GO
!*
! /COM,
! /COM,  Structural
!*
/PREP7
!*
ET,1,SHELL281
!*
KEYOPT,1,1,0
KEYOPT,1,8,1
KEYOPT,1,9,0
!*
!*
!*
MPTEMP,,,,,,,,
MPTEMP,1,0
MPDATA,DENS,1,,1.97E-
006
MPTEMP,,,,,,,,
MPTEMP,1,0
MPDE,NUXY,1
MPDE,NUYZ,1
MPDE,NUXZ,1
MPDE,PRXY,1
MPDE,PRYZ,1
MPDE,PRXZ,1
MPDATA,EX,1,,6140
MPDATA,EY,1,,19030
MPDATA,EZ,1,,6140
MPDATA,PRXY,1,,.35
MPDATA,PRYZ,1,,.35
MPDATA,PRXZ,1,,.35
MPDATA,GXY,1,,3580
MPDATA,GYZ,1,,3580
MPDATA,GXZ,1,,3580
TB,FAIL,1,,,0
TBMODIF,1,1,0
TBMODIF,1,2,1
TBMODIF,1,3,1
TBMODIF,1,4,0
TBMODIF,1,5,0
TBMODIF,1,6,0
TBMODIF,2,1,0
TBMODIF,2,2,
TBMODIF,2,3,
TBMODIF,2,4,
TBMODIF,2,5,
TBMODIF,2,6,
TBMODIF,3,1,0
```

TBMODIF,3,2,
TBMODIF,3,3,
TBMODIF,3,4,
TBMODIF,3,5,
TBMODIF,3,6,
TBMODIF,4,1,0
TBMODIF,4,2,
TBMODIF,4,3,
TBMODIF,4,4,
TBMODIF,4,5,
TBMODIF,4,6,
TBMODIF,5,1,0
TBMODIF,5,2,
TBMODIF,5,3,
TBMODIF,5,4,
TBMODIF,5,5,
TBMODIF,5,6,
TBMODIF,6,1,0
TBMODIF,6,2,
TBMODIF,6,3,
TBMODIF,6,4,
TBMODIF,6,5,
TBMODIF,6,6,
TBMODIF,7,1,0
TBMODIF,7,2,
TBMODIF,7,3,
TBMODIF,7,4,
TBMODIF,7,5,
TBMODIF,7,6,
TBMODIF,8,1,0
TBMODIF,8,2,
TBMODIF,8,3,
TBMODIF,8,4,
TBMODIF,8,5,
TBMODIF,8,6,
TBMODIF,9,1,0
TBMODIF,9,2,
TBMODIF,9,3,
TBMODIF,9,4,
TBMODIF,9,5,
TBMODIF,9,6,
TBMODIF,10,1,0
TBMODIF,10,2,
TBMODIF,10,3,
TBMODIF,10,4,
TBMODIF,10,5,
TBMODIF,10,6,
TBMODIF,11,1,0
TBMODIF,11,2,
TBMODIF,11,3,
TBMODIF,11,4,
TBMODIF,11,5,
TBMODIF,11,6,
TBMODIF,12,1,1000
TBMODIF,12,2,
TBMODIF,12,3,
TBMODIF,12,4,
TBMODIF,12,5,
TBMODIF,12,6,
TBMODIF,13,1,-1000
TBMODIF,13,2,
TBMODIF,13,3,
TBMODIF,13,4,
TBMODIF,13,5,
TBMODIF,13,6,
TBMODIF,14,1,632.62
TBMODIF,14,2,
TBMODIF,14,3,
TBMODIF,14,4,
TBMODIF,14,5,
TBMODIF,14,6,
TBMODIF,15,1,-258.7
TBMODIF,15,2,
TBMODIF,15,3,
TBMODIF,15,4,
TBMODIF,15,5,
TBMODIF,15,6,
TBMODIF,16,1,1000
TBMODIF,16,2,
TBMODIF,16,3,
TBMODIF,16,4,

TBMODIF,16,5,
TBMODIF,16,6,
TBMODIF,17,1,-1000
TBMODIF,17,2,
TBMODIF,17,3,
TBMODIF,17,4,
TBMODIF,17,5,
TBMODIF,17,6,
TBMODIF,18,1,1000
TBMODIF,18,2,
TBMODIF,18,3,
TBMODIF,18,4,
TBMODIF,18,5,
TBMODIF,18,6,
TBMODIF,19,1,1000
TBMODIF,19,2,
TBMODIF,19,3,
TBMODIF,19,4,
TBMODIF,19,5,
TBMODIF,19,6,
TBMODIF,20,1,1000
TBMODIF,20,2,
TBMODIF,20,3,
TBMODIF,20,4,
TBMODIF,20,5,
TBMODIF,20,6,
TBMODIF,21,1,-1
TBMODIF,21,2,
TBMODIF,21,3,
TBMODIF,21,4,
TBMODIF,21,5,
TBMODIF,21,6,
TBMODIF,22,1,-1
TBMODIF,22,2,
TBMODIF,22,3,
TBMODIF,22,4,
TBMODIF,22,5,
TBMODIF,22,6,
TBMODIF,23,1,-1
TBMODIF,23,2,
TBMODIF,23,3,
TBMODIF,23,4,
TBMODIF,23,5,
TBMODIF,23,6,
!*
TBDE,FAIL,1
TB,FAIL,1,,,0
TBMODIF,1,1,0
TBMODIF,1,2,1
TBMODIF,1,3,1
TBMODIF,1,4,0
TBMODIF,1,5,0
TBMODIF,1,6,0
TBMODIF,2,1,0
TBMODIF,2,2,0
TBMODIF,2,3,0
TBMODIF,2,4,0
TBMODIF,2,5,0
TBMODIF,2,6,0
TBMODIF,3,1,0
TBMODIF,3,2,0
TBMODIF,3,3,0
TBMODIF,3,4,0
TBMODIF,3,5,0
TBMODIF,3,6,0
TBMODIF,4,1,0
TBMODIF,4,2,0
TBMODIF,4,3,0
TBMODIF,4,4,0
TBMODIF,4,5,0
TBMODIF,4,6,0
TBMODIF,5,1,0
TBMODIF,5,2,0
TBMODIF,5,3,0
TBMODIF,5,4,0
TBMODIF,5,5,0
TBMODIF,5,6,0
TBMODIF,6,1,0
TBMODIF,6,2,0
TBMODIF,6,3,0
TBMODIF,6,4,0

TBMODIF,6,5,0
TBMODIF,6,6,0
TBMODIF,7,1,0
TBMODIF,7,2,0
TBMODIF,7,3,0
TBMODIF,7,4,0
TBMODIF,7,5,0
TBMODIF,7,6,0
TBMODIF,8,1,0
TBMODIF,8,2,0
TBMODIF,8,3,0
TBMODIF,8,4,0
TBMODIF,8,5,0
TBMODIF,8,6,0
TBMODIF,9,1,0
TBMODIF,9,2,0
TBMODIF,9,3,0
TBMODIF,9,4,0
TBMODIF,9,5,0
TBMODIF,9,6,0
TBMODIF,10,1,0
TBMODIF,10,2,0
TBMODIF,10,3,0
TBMODIF,10,4,0
TBMODIF,10,5,0
TBMODIF,10,6,0
TBMODIF,11,1,0
TBMODIF,11,2,0
TBMODIF,11,3,0
TBMODIF,11,4,0
TBMODIF,11,5,0
TBMODIF,11,6,0
TBMODIF,12,1,33.61
TBMODIF,12,2,0
TBMODIF,12,3,0
TBMODIF,12,4,0
TBMODIF,12,5,0
TBMODIF,12,6,0
TBMODIF,13,1,-108.94
TBMODIF,13,2,0
TBMODIF,13,3,0
TBMODIF,13,4,0
TBMODIF,13,5,0
TBMODIF,13,6,0
TBMODIF,14,1,620.55
TBMODIF,14,2,0
TBMODIF,14,3,0
TBMODIF,14,4,0
TBMODIF,14,5,0
TBMODIF,14,6,0
TBMODIF,15,1,-551.6
TBMODIF,15,2,0
TBMODIF,15,3,0
TBMODIF,15,4,0
TBMODIF,15,5,0
TBMODIF,15,6,0
TBMODIF,16,1,1000
TBMODIF,16,2,0
TBMODIF,16,3,0
TBMODIF,16,4,0
TBMODIF,16,5,0
TBMODIF,16,6,0
TBMODIF,17,1,-1000
TBMODIF,17,2,0
TBMODIF,17,3,0
TBMODIF,17,4,0
TBMODIF,17,5,0
TBMODIF,17,6,0
TBMODIF,18,1,1000
TBMODIF,18,2,0
TBMODIF,18,3,0
TBMODIF,18,4,0
TBMODIF,18,5,0
TBMODIF,18,6,0
TBMODIF,19,1,1000
TBMODIF,19,2,0
TBMODIF,19,3,0
TBMODIF,19,4,0
TBMODIF,19,5,0
TBMODIF,19,6,0
TBMODIF,20,1,1000

TBMODIF,20,2,0

TBMODIF,20,3,0

TBMODIF,20,4,0

TBMODIF,20,5,0

TBMODIF,20,6,0

TBMODIF,21,1,-1

TBMODIF,21,2,0

TBMODIF,21,3,0

TBMODIF,21,4,0

TBMODIF,21,5,0

TBMODIF,21,6,0

TBMODIF,22,1,-1

TBMODIF,22,2,0

TBMODIF,22,3,0

TBMODIF,22,4,0

TBMODIF,22,5,0

TBMODIF,22,6,0

TBMODIF,23,1,-1

TBMODIF,23,2,0

TBMODIF,23,3,0

TBMODIF,23,4,0

TBMODIF,23,5,0

TBMODIF,23,6,0

!*

FC,1,S,XTEN,33.61

FC,1,S,YTEN,620.55

FC,1,S,ZTEN,1000

FC,1,S,XCMP,-108.94

FC,1,S,YCMP,-551.6

FC,1,S,ZCMP,-1000

FC,1,S,XY,96.53

FC,1,S,YZ,96.53

FC,1,S,XZ,96.53

FC,1,S,XYCP,-1

FC,1,S,YZCP,-1

FC,1,S,XZCP,-1

!*

FC,1,EPEL,XTEN,.005474

FC,1,EPEL,YTEN,0.032609

FC,1,EPEL,ZTEN,.162866

FC,1,EPEL,XCMP,-0.0177426

FC,1,EPEL,YCMP,-0.02899

FC,1,EPEL,ZCMP,-0.1629

FC,1,EPEL,XY,0.02696

FC,1,EPEL,YZ,0.02696

FC,1,EPEL,XZ,0.02696

!*

sect,1,shell,,All pole

secdata, 0.8,1,0.0,3

secdata, 0.8,1,80,3

secdata, 0.8,1,100,3

secdata, 0.8,1,0.0,3

secoffset,MID

seccontrol,,,, , , ,

sect,2,shell,,Joint

secdata, 0.8,1,0.0,3

secdata, 0.8,1,0.0,3

secdata, 0.8,1,0.0,3

secdata, 0.8,1,0.0,3

secdata, 0.8,1,0.0,3

secdata, 0.8,1,0.0,3

secdata, 0.8,1,0.0,3

secdata, 0.8,1,0.0,3

secoffset,MID

seccontrol,,,, , , ,

sect,2,shell,,Joint

secdata, 0.8,1,0.0,3

secdata, 0.8,1,80,3

secdata, 0.8,1,100,3

secdata, 0.8,1,0.0,3

secdata, 0.8,1,0.0,3

secdata, 0.8,1,80,3

secdata, 0.8,1,100,3

secdata, 0.8,1,0.0,3

secoffset,MID

seccontrol,,,, , , ,

sect,1,shell,,Allpole

secdata, 0.8,1,0,3

secdata, 0.8,1,80,3

secdata, 0.8,1,100,3

```
secdata, 0.8,1,0,3
secoffset,MID
seccontrol,0,0,0, 0, 1, 1, 1
! /GRA,POWER
! /GST,ON
! /PLO,INFO,3
! /GRO,CURL,ON
! /CPLANE,1
! /REPLOT,RESIZE
! /REPLOT,RESIZE
WPSTYLE,,,,,,,,0
! KPLOT
ALLSEL,ALL
! KPLOT
! /GRA,POWER
! /GST,ON
! /PLO,INFO,3
! /GRO,CURL,ON
! /CPLANE,1
! /REPLOT,RESIZE
WPSTYLE,,,,,,,,0
! /REPLOT,RESIZE
/PREP7
!*
/NOPR
KEYW,PR_SET,1
KEYW,PR_STRUC,1
KEYW,PR_THERM,0
KEYW,PR_FLUID,0
KEYW,PR_ELMAG,0
KEYW,MAGNOD,0
KEYW,MAGEDG,0
KEYW,MAGHFE,0
KEYW,MAGELC,0
KEYW,PR_MULTI,0
KEYW,PR_CFD,0
/GO
!*
! /COM,
! /COM,  Structural
!*
KEYOPT,1,1,0
KEYOPT,1,8,1
KEYOPT,1,9,0
!*
MPTEMP,,,,,,,,
MPTEMP,1,0
MPDE,NUXY,1
MPDE,NUYZ,1
MPDE,NUXZ,1
MPDE,PRXY,1
MPDE,PRYZ,1
MPDE,PRXZ,1
MPDE,EX,1
MPDATA,EX,1,,6140
MPDE,EY,1
MPDATA,EY,1,,19030
MPDE,EZ,1
MPDATA,EZ,1,,6140
MPDATA,PRXY,1,,0.35
MPDATA,PRYZ,1,,0.35
MPDATA,PRXZ,1,,0.35
MPDE,GXY,1
MPDATA,GXY,1,,3580
MPDE,GYZ,1
MPDATA,GYZ,1,,3580
MPDE,GXZ,1
MPDATA,GXZ,1,,3580
!*
TBDE,FAIL,1
TB,FAIL,1,,,0
TBMODIF,1,1,0
TBMODIF,1,2,1
TBMODIF,1,3,1
TBMODIF,1,4,0
TBMODIF,1,5,0
TBMODIF,1,6,0
TBMODIF,2,1,0
TBMODIF,2,2,0
TBMODIF,2,3,0
TBMODIF,2,4,0
```

TBMODIF,2,5,0
TBMODIF,2,6,0
TBMODIF,3,1,0
TBMODIF,3,2,0
TBMODIF,3,3,0
TBMODIF,3,4,0
TBMODIF,3,5,0
TBMODIF,3,6,0
TBMODIF,4,1,0
TBMODIF,4,2,0
TBMODIF,4,3,0
TBMODIF,4,4,0
TBMODIF,4,5,0
TBMODIF,4,6,0
TBMODIF,5,1,0
TBMODIF,5,2,0
TBMODIF,5,3,0
TBMODIF,5,4,0
TBMODIF,5,5,0
TBMODIF,5,6,0
TBMODIF,6,1,0
TBMODIF,6,2,0
TBMODIF,6,3,0
TBMODIF,6,4,0
TBMODIF,6,5,0
TBMODIF,6,6,0
TBMODIF,7,1,0
TBMODIF,7,2,0
TBMODIF,7,3,0
TBMODIF,7,4,0
TBMODIF,7,5,0
TBMODIF,7,6,0
TBMODIF,8,1,0
TBMODIF,8,2,0
TBMODIF,8,3,0
TBMODIF,8,4,0
TBMODIF,8,5,0
TBMODIF,8,6,0
TBMODIF,9,1,0
TBMODIF,9,2,0
TBMODIF,9,3,0
TBMODIF,9,4,0
TBMODIF,9,5,0
TBMODIF,9,6,0
TBMODIF,10,1,0
TBMODIF,10,2,0
TBMODIF,10,3,0
TBMODIF,10,4,0
TBMODIF,10,5,0
TBMODIF,10,6,0
TBMODIF,11,1,0
TBMODIF,11,2,0
TBMODIF,11,3,0
TBMODIF,11,4,0
TBMODIF,11,5,0
TBMODIF,11,6,0
TBMODIF,12,1,33.61
TBMODIF,12,2,0
TBMODIF,12,3,0
TBMODIF,12,4,0
TBMODIF,12,5,0
TBMODIF,12,6,0
TBMODIF,13,1,-108.94
TBMODIF,13,2,0
TBMODIF,13,3,0
TBMODIF,13,4,0
TBMODIF,13,5,0
TBMODIF,13,6,0
TBMODIF,14,1,620.55
TBMODIF,14,2,0
TBMODIF,14,3,0
TBMODIF,14,4,0
TBMODIF,14,5,0
TBMODIF,14,6,0
TBMODIF,15,1,-551.6
TBMODIF,15,2,0
TBMODIF,15,3,0
TBMODIF,15,4,0
TBMODIF,15,5,0
TBMODIF,15,6,0
TBMODIF,16,1,1000

TBMODIF,16,2,0
TBMODIF,16,3,0
TBMODIF,16,4,0
TBMODIF,16,5,0
TBMODIF,16,6,0
TBMODIF,17,1,-1000
TBMODIF,17,2,0
TBMODIF,17,3,0
TBMODIF,17,4,0
TBMODIF,17,5,0
TBMODIF,17,6,0
TBMODIF,18,1,96.53
TBMODIF,18,2,0
TBMODIF,18,3,0
TBMODIF,18,4,0
TBMODIF,18,5,0
TBMODIF,18,6,0
TBMODIF,19,1,96.53
TBMODIF,19,2,0
TBMODIF,19,3,0
TBMODIF,19,4,0
TBMODIF,19,5,0
TBMODIF,19,6,0
TBMODIF,20,1,96.53
TBMODIF,20,2,0
TBMODIF,20,3,0
TBMODIF,20,4,0
TBMODIF,20,5,0
TBMODIF,20,6,0
TBMODIF,21,1,-1
TBMODIF,21,2,0
TBMODIF,21,3,0
TBMODIF,21,4,0
TBMODIF,21,5,0
TBMODIF,21,6,0
TBMODIF,22,1,-1
TBMODIF,22,2,0
TBMODIF,22,3,0
TBMODIF,22,4,0
TBMODIF,22,5,0
TBMODIF,22,6,0
TBMODIF,23,1,-1
TBMODIF,23,2,0
TBMODIF,23,3,0
TBMODIF,23,4,0
TBMODIF,23,5,0
TBMODIF,23,6,0
sect,1,shell,,Allpole
secdata, 0.5,1,0,3
secdata, 0.5,1,80,3
secdata, 0.5,1,100,3
secdata, 0.5,1,0,3
secdata, 0.5,1,0.0,3
secoffset,MID
seccontrol,0,0,0, 0, 1, 1, 1
sect,2,shell,,Joint
secdata, 0.5,1,0,3
secdata, 0.5,1,80,3
secdata, 0.5,1,100,3
secdata, 0.5,1,0,3
secdata, 0.5,1,0,3
secdata, 0.5,1,80,3
secdata, 0.5,1,100,3
secdata, 0.5,1,0,3
secdata, 0.5,1,0.0,3
secdata, 0.5,1,0.0,3
secdata, 0.5,1,0.0,3
secdata, 0.5,1,0.0,3
secdata, 0.5,1,0.0,3
secdata, 0.5,1,0.0,3
secdata, 0.5,1,0.0,3
secoffset,MID
seccontrol,0,0,0, 0, 1, 1, 1
sect,2,shell,,Joint
secdata, 0.5,1,0,3
secdata, 0.5,1,80,3
secdata, 0.5,1,100,3

secdata, 0.5,1,0,3
secdata, 0.5,1,0,3
secdata, 0.5,1,80,3
secdata, 0.5,1,100,3
secdata, 0.5,1,0,3
secdata, 0.5,1,0,3
secdata, 0.5,1,0,3
secdata, 0.5,1,0,3
secdata, 0.5,1,0,3
secdata, 0.5,1,0,3
secdata, 0.5,1,0,3
secdata, 0.5,1,0,3
secoffset,MID
seccontrol,0,0,0, 0, 1, 1, 1
sect,1,shell,,Allpole
secdata, 0.5,1,0,3
secdata, 0.5,1,85,3
secdata, 0.5,1,95,3
secdata, 0.5,1,85,3
secdata, 0.5,1,95,3
secdata, 0.5,1,85,3
secdata, 0.5,1,95,3
secdata, 0.5,1,0,3
secoffset,MID
seccontrol,0,0,0, 0, 1, 1, 1
sect,2,shell,,Joint
secdata, 0.5,1,0,3
secdata, 0.5,1,85,3
secdata, 0.5,1,95,3
secdata, 0.5,1,85,3
secdata, 0.5,1,95,3
secdata, 0.5,1,85,3
secdata, 0.5,1,95,3
secdata, 0.5,1,0,3
secdata, 0.5,1,0,3
secdata, 0.5,1,85,3
secdata, 0.5,1,95,3
secdata, 0.5,1,85,3
secdata, 0.5,1,95,3
secdata, 0.5,1,85,3
secdata, 0.5,1,95,3
secdata, 0.5,1,85,3
secdata, 0.5,1,95,3
secdata, 0.5,1,0,3
secoffset,MID
seccontrol,0,0,0, 0, 1, 1, 1
! /GRA,POWER
! /GST,ON
! /PLO,INFO,3
! /GRO,CURL,ON
! /CPLANE,1
! /REPLOT,RESIZE
! /REPLOT,RESIZE
WPSTYLE,,,,,,,,0
/PREP7
K, ,,,,
K, ,,,105,
K, ,,,-105,
K, ,-105,,,
K, ,105,,,
K, ,88.2,2400,,
K, ,-88.2,2400,,
K, ,,2400,-88.2,
K, ,,2400,88.2,
FLST,2,9,3,ORDE,2
FITEM,2,1
FITEM,2,-9
KDELE,P51X
K, ,,,,
K, ,105,,,
K, ,-105,,,

```
K, ,,,-105,
K, ,,,105,
K, ,,2700,,
K, ,86.1,2700,,
K, ,-86.1,2700,,
K, ,,2700,-86.1,
K, ,,2700,86.1,
K, ,,3300,,
K, ,81.9,3300,,
K, ,-81.9,3300,,
K, ,,3300,-81.9,
K, ,,3300,81.9,
K, ,,6000,,
K, ,63,6000,,
K, ,-63,6000,,
K, ,,6000,-63,
K, ,,6000,63,
! /VIEW,1,1,2,3
! /ANG,1
! /REP,FAST
!
/ZOOM,1,RECT,0.172303,-
0.755148
,0.539320973731 ,-
0.987753465283
!*
LARC,2,4,1,105,
!*
LARC,4,3,1,105,
!*
LARC,3,5,1,105,
!*
LARC,5,2,1,105,
! /DIST,1,1.08222638492,1
! /REP,FAST
! /DIST,1,1.08222638492,1
! /REP,FAST
! /DIST,1,1.08222638492,1
! /REP,FAST
! /DIST,1,1.08222638492,1
! /REP,FAST
! /DIST,1,1.08222638492,1
! /REP,FAST
! /DIST,1,1.08222638492,1
! /REP,FAST
! /DIST,1,1.08222638492,1
! /REP,FAST
! /DIST,1,1.08222638492,1
! /REP,FAST
! /DIST,1,1.08222638492,1
! /REP,FAST
! /DIST,1,1.08222638492,1
! /REP,FAST
! /DIST,1,1.08222638492,1
! /REP,FAST
! /DIST,1,1.08222638492,1
! /REP,FAST
! /DIST,1,1.08222638492,1
! /REP,FAST
! /DIST,1,1.08222638492,1
! /REP,FAST
! /DIST,1,1.08222638492,1
! /REP,FAST
! /DIST,1,1.08222638492,1
! /REP,FAST
! /DIST,1,1.08222638492,1
! /REP,FAST
!
/DIST,1,0.924021086472,1
! /REP,FAST
! /DIST,1,1.08222638492,1
! /REP,FAST
! /DIST,1,1.08222638492,1
! /REP,FAST
! /DIST,1,1.08222638492,1
! /REP,FAST
! /DIST,1,1.08222638492,1
! /REP,FAST
! /DIST,1,1.08222638492,1
! /REP,FAST
```

! /DIST,1,1.08222638492,1

! /REP,FAST

! /DIST,1,1.08222638492,1

! /REP,FAST

! /DIST,1,1.08222638492,1

! /REP,FAST

! /DIST,1,1.08222638492,1

! /REP,FAST

! /DIST,1,1.08222638492,1

! /REP,FAST

! /DIST,1,1.08222638492,1

! /REP,FAST

! /DIST,1,1.08222638492,1

! /REP,FAST

! /DIST,1,1.08222638492,1

! /REP,FAST

!
/ZOOM,1,RECT,0.234565,0
.610998 ,0.414796859938
,0.457020260057

!*

LARC,7,9,6,86.1,

!*

LARC,9,8,6,86.1,

!*

LARC,8,10,6,86.1,

!*

LARC,10,7,6,86.1,

! /DIST,1,1.08222638492,1

! /REP,FAST

! /DIST,1,1.08222638492,1

! /REP,FAST

! /DIST,1,1.08222638492,1

! /REP,FAST

! /DIST,1,1.08222638492,1

! /REP,FAST

! /DIST,1,1.08222638492,1

! /REP,FAST

! /DIST,1,1.08222638492,1

! /REP,FAST

! /DIST,1,1.08222638492,1

! /REP,FAST

! /DIST,1,1.08222638492,1

! /REP,FAST

! /DIST,1,1.08222638492,1

! /REP,FAST

! /DIST,1,1.08222638492,1

! /REP,FAST

! /DIST,1,1.08222638492,1

! /REP,FAST

!
/ZOOM,1,RECT,0.0871018,
0.735491 ,0.54915182482
,0.427535081988

!*

LARC,12,14,11,81.9,

!*

LARC,14,13,11,81.9,

!*

LARC,13,15,11,81.9,

!*

LARC,15,12,11,81.9,

! /DIST,1,1.08222638492,1

! /REP,FAST

! /DIST,1,1.08222638492,1

! /REP,FAST

! /DIST,1,1.08222638492,1

! /REP,FAST

! /DIST,1,1.08222638492,1

! /REP,FAST

! /DIST,1,1.08222638492,1

! /REP,FAST

! /DIST,1,1.08222638492,1

! /REP,FAST

! /DIST,1,1.08222638492,1

! /REP,FAST

```
! /DIST,1,1.08222638492,1
! /REP,FAST
! /DIST,1,1.08222638492,1
! /REP,FAST
! /DIST,1,1.08222638492,1
! /REP,FAST
! /DIST,1,1.08222638492,1
! /REP,FAST
! /DIST,1,1.08222638492,1
! /REP,FAST
! /DIST,1,1.08222638492,1
! /REP,FAST
! /DIST,1,1.08222638492,1
! /REP,FAST
! /DIST,1,1.08222638492,1
! /REP,FAST
! /DIST,1,1.08222638492,1
! /REP,FAST
! /DIST,1,1.08222638492,1
! /REP,FAST
! /DIST,1,1.08222638492,1
! /REP,FAST
! /DIST,1,1.08222638492,1
! /REP,FAST
! /DIST,1,1.08222638492,1
! /REP,FAST
! /DIST,1,1.08222638492,1
! /REP,FAST
! /DIST,1,1.08222638492,1
! /REP,FAST
! /DIST,1,1.08222638492,1
! /REP,FAST
! /DIST,1,1.08222638492,1
! /REP,FAST
! /DIST,1,1.08222638492,1
! /REP,FAST
! /DIST,1,1.08222638492,1
! /REP,FAST
! /DIST,1,1.08222638492,1
! /REP,FAST
! /DIST,1,1.08222638492,1
! /REP,FAST
! /DIST,1,1.08222638492,1
! /REP,FAST
! /DIST,1,1.08222638492,1
! /REP,FAST
! /DIST,1,1.08222638492,1
! /REP,FAST
! /DIST,1,1.08222638492,1
! /REP,FAST
! /DIST,1,1.08222638492,1
! /REP,FAST
! /DIST,1,1.08222638492,1
! /REP,FAST
! /DIST,1,1.08222638492,1
! /REP,FAST
! /DIST,1,1.08222638492,1
! /REP,FAST
!
/ZOOM,1,RECT,0.267334,0
.86326 ,0.414796859938
,0.706006208188
!*
LARC,17,19,16,63,
!*
LARC,19,18,16,63,
!*
LARC,18,20,16,63,
!*
LARC,20,17,16,63,
! /VIEW,1,,1
! /ANG,1
! /REP,FAST
LSTR,       3,       8
LSTR,       8,      13
LSTR,      13,      18
! /VIEW,1,1,2,3
! /ANG,1
! /REP,FAST
! LPLOT
! /DIST,1,1.08222638492,1
! /REP,FAST
```

```
! /DIST,1,1.08222638492,1
! /REP,FAST
! /DIST,1,1.08222638492,1
! /REP,FAST
! /DIST,1,1.08222638492,1
! /REP,FAST
! /DIST,1,1.08222638492,1
! /REP,FAST
! /DIST,1,1.08222638492,1
! /REP,FAST
! /DIST,1,1.08222638492,1
! /REP,FAST
! /DIST,1,1.08222638492,1
! /REP,FAST
! /DIST,1,1.08222638492,1
! /REP,FAST
! /DIST,1,1.08222638492,1
! /REP,FAST
! /DIST,1,1.08222638492,1
! /REP,FAST
! /DIST,1,1.08222638492,1
! /REP,FAST
! /DIST,1,1.08222638492,1
! /REP,FAST
! /DIST,1,1.08222638492,1
! /REP,FAST
! /DIST,1,1.08222638492,1
! /REP,FAST
! /DIST,1,1.08222638492,1
! /REP,FAST
! /DIST,1,1.08222638492,1
! /REP,FAST
! /DIST,1,1.08222638492,1
! /REP,FAST
! /DIST,1,1.08222638492,1
! /REP,FAST
! /DIST,1,1.08222638492,1
! /REP,FAST
! /DIST,1,1.08222638492,1
! /REP,FAST
! /DIST,1,1.08222638492,1
! /REP,FAST
! /DIST,1,1.08222638492,1
! /REP,FAST
! /DIST,1,1.08222638492,1
! /REP,FAST
! /DIST,1,1.08222638492,1
! /REP,FAST
! /DIST,1,1.08222638492,1
! /REP,FAST
! /DIST,1,1.08222638492,1
! /REP,FAST
! /DIST,1,1.08222638492,1
! /REP,FAST
! /DIST,1,1.08222638492,1
! /REP,FAST
! /DIST,1,1.08222638492,1
! /REP,FAST
! /DIST,1,1.08222638492,1
! /REP,FAST
! /DIST,1,1.08222638492,1
! /REP,FAST
! /DIST,1,1.08222638492,1
! /REP,FAST
! /DIST,1,1.08222638492,1
! /REP,FAST
! /DIST,1,1.08222638492,1
! /REP,FAST
! /DIST,1,1.08222638492,1
! /REP,FAST
! /DIST,1,1.08222638492,1
! /REP,FAST
! /DIST,1,1.08222638492,1
! /REP,FAST
! /DIST,1,1.08222638492,1
! /REP,FAST
! /DIST,1,1.08222638492,1
! /REP,FAST
! /DIST,1,1.08222638492,1
! /REP,FAST
! /VIEW,1,,1
! /ANG,1
! /REP,FAST
! KPLOT
!
/ZOOM,1,RECT,0.169026,0
.103198 ,0.375473455582
,-0.201482050132
!
/ZOOM,1,RECT,0.441012,0
.591342 ,0.991540123823
,0.0278471126199
```

```
! /ZOOM,1,RECT,0.0543323,0.74532 ,0.257503242514 ,0.362012464059
LSTR,       4,       9
LSTR,       9,      14
LSTR,      14,      19
! /DIST,1,1.08222638492,1
! /REP,FAST
! /DIST,1,1.08222638492,1
! /REP,FAST
! /DIST,1,1.08222638492,1
! /REP,FAST
! /DIST,1,1.08222638492,1
! /REP,FAST
! /DIST,1,1.08222638492,1
! /REP,FAST
! /DIST,1,1.08222638492,1
! /REP,FAST
! /DIST,1,1.08222638492,1
! /REP,FAST
! /DIST,1,1.08222638492,1
! /REP,FAST
! /DIST,1,1.08222638492,1
! /REP,FAST
! /DIST,1,1.08222638492,1
! /REP,FAST
! /DIST,1,1.08222638492,1
! /REP,FAST
! /DIST,1,1.08222638492,1
! /REP,FAST
! /DIST,1,1.08222638492,1
! /REP,FAST
! /DIST,1,1.08222638492,1
! /REP,FAST
! /DIST,1,1.08222638492,1
! /REP,FAST
! /DIST,1,1.08222638492,1
! /REP,FAST
! /ZOOM,1,RECT,0.660568,-0.473401 ,1.03086352818 ,-0.653588113844
LSTR,       2,       7
LSTR,       7,      12
LSTR,      12,      17
! /DIST,1,1.08222638492,1
! /REP,FAST
! /DIST,1,1.08222638492,1
! /REP,FAST
! /DIST,1,1.08222638492,1
! /REP,FAST
! /DIST,1,1.08222638492,1
! /REP,FAST
! /DIST,1,1.08222638492,1
! /REP,FAST
! /DIST,1,1.08222638492,1
! /REP,FAST
! /DIST,1,1.08222638492,1
! /REP,FAST
! /DIST,1,1.08222638492,1
! /REP,FAST
! /DIST,1,1.08222638492,1
! /REP,FAST
! /DIST,1,1.08222638492,1
! /REP,FAST
! /DIST,1,1.08222638492,1
! /REP,FAST
! /DIST,1,1.08222638492,1
! /REP,FAST
! /DIST,1,1.08222638492,1
! /REP,FAST
! /DIST,1,1.08222638492,1
```

```
! /REP,FAST
! /DIST,1,1.08222638492,1
! /REP,FAST
! /DIST,1,1.08222638492,1
! /REP,FAST
! /DIST,1,1.08222638492,1
! /REP,FAST
! /DIST,1,1.08222638492,1
! /REP,FAST
! /DIST,1,1.08222638492,1
! /REP,FAST
! /DIST,1,1.08222638492,1
! /REP,FAST
! /ZOOM,1,RECT,-0.528965,-0.407878 ,-0.260254914837 ,-0.93533537094
LSTR,      5,     10
LSTR,     10,     15
LSTR,     15,     20
! /AUTO,1
! /REP,FAST
! LPLOT
FLST,2,4,4
FITEM,2,14
FITEM,2,22
FITEM,2,10
FITEM,2,19
AL,P51X
FLST,2,4,4
FITEM,2,21
FITEM,2,6
FITEM,2,10
FITEM,2,18
AL,P51X
FLST,2,4,4
FITEM,2,20
FITEM,2,2
FITEM,2,6
FITEM,2,17
AL,P51X
FLST,2,4,4
FITEM,2,13
FITEM,2,22
FITEM,2,9
FITEM,2,25
AL,P51X
FLST,2,4,4
FITEM,2,5
FITEM,2,21
FITEM,2,9
FITEM,2,24
AL,P51X
FLST,2,4,4
FITEM,2,1
FITEM,2,20
FITEM,2,5
FITEM,2,23
AL,P51X
FLST,2,4,4
FITEM,2,15
FITEM,2,19
FITEM,2,11
FITEM,2,28
AL,P51X
FLST,2,4,4
FITEM,2,18
FITEM,2,11
FITEM,2,7
FITEM,2,27
AL,P51X
FLST,2,4,4
FITEM,2,26
FITEM,2,3
FITEM,2,7
FITEM,2,17
AL,P51X
FLST,2,4,4
FITEM,2,16
FITEM,2,12
```

```
FITEM,2,25
FITEM,2,28
AL,P51X
FLST,2,4,4
FITEM,2,12
FITEM,2,8
FITEM,2,24
FITEM,2,27
AL,P51X
FLST,2,4,4
FITEM,2,23
FITEM,2,8
FITEM,2,4
FITEM,2,26
AL,P51X
FLST,5,8,5,ORDE,8
FITEM,5,1
FITEM,5,3
FITEM,5,-4
FITEM,5,6
FITEM,5,-7
FITEM,5,9
FITEM,5,-10
FITEM,5,12
CM,_Y,AREA
ASEL, , , ,P51X
CM,_Y1,AREA
CMSEL,S,_Y
!*
CMSEL,S,_Y1
AATT,     1, ,   1,     0,   1
CMSEL,S,_Y
CMDELE,_Y
CMDELE,_Y1
!*
FLST,5,4,5,ORDE,4
FITEM,5,2
FITEM,5,5
FITEM,5,8
FITEM,5,11
CM,_Y,AREA
ASEL, , , ,P51X
CM,_Y1,AREA
CMSEL,S,_Y
!*
CMSEL,S,_Y1
AATT,     1, ,   1,     0,   2
CMSEL,S,_Y
CMDELE,_Y
CMDELE,_Y1
!*
AESIZE,ALL,100,
MSHKEY,0
FLST,5,12,5,ORDE,2
FITEM,5,1
FITEM,5,-12
CM,_Y,AREA
ASEL, , , ,P51X
CM,_Y1,AREA
CHKMSH,'AREA'
CMSEL,S,_Y
!*
AMESH,_Y1
!*
CMDELE,_Y
CMDELE,_Y1
CMDELE,_Y2
!*
! /VIEW,1,1,2,3
! /ANG,1
! /REP,FAST
! NPLOT
NSEL,S,LOC,Y,0
! NPLOT
NSEL,S,LOC,Y,0
NSEL,S,LOC,Y,0
! NPLOT
NSEL,S,LOC,Y,0
FLST,2,16,1,ORDE,9
FITEM,2,239
FITEM,2,295
```

FITEM,2,-298

FITEM,2,630

FITEM,2,-633

FITEM,2,950

FITEM,2,-953

FITEM,2,1214

FITEM,2,-1216

!*

/GO

D,P51X, ,0, , , ,ALL, , , , ,

! NLIST,ALL, , ,
,NODE,NODE,NODE

ALLSEL,ALL

! NLIST,ALL, , ,
,NODE,NODE,NODE

! NPLOT

NSEL,S,LOC,Y,1000

! NPLOT

NSEL,S,LOC,Y,900,1000

! NPLOT

ALLSEL,ALL

! NPLOT

NSEL,S,LOC,Y,950,1000

! NPLOT

NSEL,A,LOC,Y,1950,2000

! NPLOT

NSEL,A,LOC,Y,2950,3000

! NPLOT

NSEL,A,LOC,Y,3950,4000

! NPLOT

NSEL,A,LOC,Y,4950,5000

! NPLOT

NSEL,A,LOC,Y,6000

! NPLOT

NSEL,A,LOC,Y,6000

! /AUTO,1

! /REP,FAST

FLST,2,16,1,ORDE,16

FITEM,2,259

FITEM,2,318

FITEM,2,371

FITEM,2,416

FITEM,2,453

FITEM,2,653

FITEM,2,698

FITEM,2,735

FITEM,2,780

FITEM,2,973

FITEM,2,1026

FITEM,2,1071

FITEM,2,1108

FITEM,2,1234

FITEM,2,1279

FITEM,2,1316

!*

/GO

F,P51X,FX,167/16

FLST,2,8,1,ORDE,8

FITEM,2,280

FITEM,2,339

FITEM,2,395

FITEM,2,674

FITEM,2,756

FITEM,2,994

FITEM,2,1050

FITEM,2,1258

!*

/GO

F,P51X,FX,156/8

FLST,2,24,1,ORDE,24

FITEM,2,189

FITEM,2,-190

FITEM,2,206

FITEM,2,-207

FITEM,2,217

FITEM,2,226

FITEM,2,-227

FITEM,2,236

FITEM,2,597

FITEM,2,-598

FITEM,2,607

FITEM,2,616

FITEM,2,-617
FITEM,2,626
FITEM,2,914
FITEM,2,-915
FITEM,2,928
FITEM,2,937
FITEM,2,-938
FITEM,2,947
FITEM,2,1192
FITEM,2,1201
FITEM,2,-1202
FITEM,2,1211
!*
/GO
F,P51X,FX,144/24
FLST,2,16,1,ORDE,16
FITEM,2,18
FITEM,2,77
FITEM,2,154
FITEM,2,156
FITEM,2,178
FITEM,2,482
FITEM,2,557
FITEM,2,559
FITEM,2,582
FITEM,2,814
FITEM,2,882
FITEM,2,884
FITEM,2,902
FITEM,2,1157
FITEM,2,1159
FITEM,2,1181
FLST,2,16,1,ORDE,16
FITEM,2,18
FITEM,2,77
FITEM,2,154
FITEM,2,156
FITEM,2,178
FITEM,2,482
FITEM,2,557
FITEM,2,559
FITEM,2,582
FITEM,2,814
FITEM,2,882
FITEM,2,884
FITEM,2,902
FITEM,2,1157
FITEM,2,1159
FITEM,2,1181
!*
/GO
F,P51X,FX,133/16
FLST,2,4,1,ORDE,4
FITEM,2,39
FITEM,2,98
FITEM,2,503
FITEM,2,835
!*
/GO
F,P51X,FX,121/4
FLST,2,8,1,ORDE,7
FITEM,2,1
FITEM,2,-3
FITEM,2,463
FITEM,2,-464
FITEM,2,798
FITEM,2,-799
FITEM,2,1118
!*
/GO
F,P51X,FX,110/8
FLST,2,16,1,ORDE,16
FITEM,2,259
FITEM,2,318
FITEM,2,371
FITEM,2,416
FITEM,2,453
FITEM,2,653
FITEM,2,698
FITEM,2,735
FITEM,2,780

FITEM,2,973
FITEM,2,1026
FITEM,2,1071
FITEM,2,1108
FITEM,2,1234
FITEM,2,1279
FITEM,2,1316
FLST,2,16,1,ORDE,16
FITEM,2,259
FITEM,2,318
FITEM,2,371
FITEM,2,416
FITEM,2,453
FITEM,2,653
FITEM,2,698
FITEM,2,735
FITEM,2,780
FITEM,2,973
FITEM,2,1026
FITEM,2,1071
FITEM,2,1108
FITEM,2,1234
FITEM,2,1279
FITEM,2,1316
!*
/GO
F,P51X,FZ,34/16
FLST,2,8,1,ORDE,8
FITEM,2,280
FITEM,2,339
FITEM,2,395
FITEM,2,674
FITEM,2,756
FITEM,2,994
FITEM,2,1050
FITEM,2,1258
!*
/GO
F,P51X,FZ,32/8
FLST,2,24,1,ORDE,24
FITEM,2,189
FITEM,2,-190
FITEM,2,206
FITEM,2,-207
FITEM,2,217
FITEM,2,226
FITEM,2,-227
FITEM,2,236
FITEM,2,597
FITEM,2,-598
FITEM,2,607
FITEM,2,616
FITEM,2,-617
FITEM,2,626
FITEM,2,914
FITEM,2,-915
FITEM,2,928
FITEM,2,937
FITEM,2,-938
FITEM,2,947
FITEM,2,1192
FITEM,2,1201
FITEM,2,-1202
FITEM,2,1211
!*
/GO
F,P51X,FZ,29/24
FLST,2,16,1,ORDE,16
FITEM,2,18
FITEM,2,77
FITEM,2,154
FITEM,2,156
FITEM,2,178
FITEM,2,482
FITEM,2,557
FITEM,2,559
FITEM,2,582
FITEM,2,814
FITEM,2,882
FITEM,2,884
FITEM,2,902

```
FITEM,2,1157
FITEM,2,1159
FITEM,2,1181
!*
/GO
F,P51X,FZ,27/16
FLST,2,4,1,ORDE,4
FITEM,2,39
FITEM,2,98
FITEM,2,503
FITEM,2,835
!*
/GO
F,P51X,FZ,24/4
FLST,2,8,1,ORDE,7
FITEM,2,1
FITEM,2,-3
FITEM,2,463
FITEM,2,-464
FITEM,2,798
FITEM,2,-799
FITEM,2,1118
!*
/GO
F,P51X,FZ,22/8
ALLSEL,ALL
! NPLOT
NSEL,A,LOC,Y,5770
! NPLOT
NSEL,S,LOC,Y,5770
! NPLOT
NSEL,S,LOC,Y,5700-5770
! NPLOT
NSEL,S,LOC,Y,5700-5770
! NPLOT
ALLSEL,ALL
! NPLOT
NSEL,S,LOC,Y,5700-5770
! NPLOT
NSEL,S,LOC,Y,5770
! NPLOT
NSEL,S,LOC,Y,5770,5800
! NPLOT
ALLSEL,ALL
! NPLOT
NSEL,S,LOC,Y,5700,5770
! NPLOT
FLST,2,12,1,ORDE,12
FITEM,2,54
FITEM,2,-55
FITEM,2,113
FITEM,2,-114
FITEM,2,128
FITEM,2,518
FITEM,2,-519
FITEM,2,531
FITEM,2,850
FITEM,2,-851
FITEM,2,866
FITEM,2,1131
!*
/GO
F,P51X,FZ,73/12
FLST,2,12,1,ORDE,12
FITEM,2,54
FITEM,2,-55
FITEM,2,113
FITEM,2,-114
FITEM,2,128
FITEM,2,518
FITEM,2,-519
FITEM,2,531
FITEM,2,850
FITEM,2,-851
FITEM,2,866
FITEM,2,1131
!*
/GO
F,P51X,MY,24444/12
FLST,2,12,1,ORDE,12
FITEM,2,54
```

```
FITEM,2,-55
FITEM,2,113
FITEM,2,-114
FITEM,2,128
FITEM,2,518
FITEM,2,-519
FITEM,2,531
FITEM,2,850
FITEM,2,-851
FITEM,2,866
FITEM,2,1131
!*
/GO
F,P51X,FY,-122/12
FLST,2,12,1,ORDE,12
FITEM,2,54
FITEM,2,-55
FITEM,2,113
FITEM,2,-114
FITEM,2,128
FITEM,2,518
FITEM,2,-519
FITEM,2,531
FITEM,2,850
FITEM,2,-851
FITEM,2,866
FITEM,2,1131
! /REPLOT,RESIZE
! /REPLOT,RESIZE
!*
/GO
F,P51X,MZ,-47284/12
! /REPLOT,RESIZE
FINISH
/SOL
!*
ANTYPE,0
!*
ANTYPE,0
NLGEOM,1
!*
NLGEOM,1
NROPT,AUTO, ,
STAOPT,DEFA
LUMPM,0
EQSLV, , ,0, ,DELE
MSAVE,0
PCGOPT,0, ,AUTO, , ,AUTO
PIVCHECK,1
PSTRESS,0
TOFFST,0,
!*
! /STATUS,SOLU
SOLVE
FINISH
/POST1
! PLDISP,0
!*
! /EFACET,1
! PLNSOL, U,SUM, 0,1.0
! /EFACET,1
! PLNSOL, FAIL,TWSI, 0,1.0
ALLSEL,ALL
!*
! /EFACET,1
! PLNSOL, FAIL,TWSI, 0,1.0
! /EFACET,1
! PLNSOL, FAIL,TWSI, 0,1.0
FINISH
/PREP7
sect,1,shell,,Allpole
secdata, 0.3,1,0,3
secdata, 0.3,1,85,3
secdata, 0.3,1,95,3
secdata, 0.3,1,85,3
secdata, 0.3,1,95,3
secdata, 0.3,1,85,3
secdata, 0.3,1,95,3
secdata, 0.3,1,0,3
secoffset,MID
seccontrol,0,0,0, 0, 1, 1, 1
```

```
sect,2,shell,,Joint
secdata, 0.3,1,0,3
secdata, 0.3,1,85,3
secdata, 0.3,1,95,3
secdata, 0.3,1,85,3
secdata, 0.3,1,95,3
secdata, 0.3,1,85,3
secdata, 0.3,1,95,3
secdata, 0.3,1,0,3
secdata, 0.3,1,0,3
secdata, 0.3,1,85,3
secdata, 0.3,1,95,3
secdata, 0.3,1,85,3
secdata, 0.3,1,95,3
secdata, 0.3,1,0,3
secoffset,MID
seccontrol,0,0,0, 0, 1, 1, 1
sect,1,shell,,Allpole
secdata, 0.3,1,0,3
secdata, 0.3,1,85,3
secdata, 0.3,1,95,3
secdata, 0.3,1,85,3
secdata, 0.3,1,95,3
secdata, 0.3,1,85,3
secdata, 0.3,1,95,3
```

```
secdata, 0.3,1,0,3
secoffset,MID
seccontrol,0,0,0, 0, 1, 1, 1
FINISH
/SOL
! /STATUS,SOLU
SOLVE
FINISH
/POST1
!*
! /EFACET,1
! PLNSOL, U,SUM, 0,1.0
!*
! /EFACET,1
! PLNSOL, FAIL,TWSI, 0,1.0
! /EFACET,1
! PLNSOL, FAIL,TWSI, 0,1.0
! /GRA,POWER
! /GST,ON
! /PLO,INFO,3
! /GRO,CURL,ON
! /CPLANE,1
! /REPLOT,RESIZE
WPSTYLE,,,,,,,,0
! /REPLOT,RESIZE
GPLOT
/SOLU
```

```
FINISH
/PREP7
FLST,2,1325,1,ORDE,2
FITEM,2,1
FITEM,2,-1325
FDELE,P51X,ALL
NSEL,S,LOC,Y,950,1000
! NPLOT
NSEL,A,LOC,Y,1950,2000
! NPLOT
NSEL,A,LOC,Y,2950,3000
! NPLOT
NSEL,A,LOC,Y,3950,4000
! NPLOT
NSEL,A,LOC,Y,4950,5000
! NPLOT
NSEL,A,LOC,Y,6000
! NPLOT
NSEL,A,LOC,Y,6000
FLST,2,16,1,ORDE,16
FITEM,2,259
FITEM,2,318
FITEM,2,371
FITEM,2,416
FITEM,2,453
FITEM,2,653
FITEM,2,698
```

FITEM,2,735
FITEM,2,780
FITEM,2,973
FITEM,2,1026
FITEM,2,1071
FITEM,2,1108
FITEM,2,1234
FITEM,2,1279
FITEM,2,1316
!*
/GO
F,P51X,FX,191/16
FLST,2,8,1,ORDE,8
FITEM,2,280
FITEM,2,339
FITEM,2,395
FITEM,2,674
FITEM,2,756
FITEM,2,994
FITEM,2,1050
FITEM,2,1258
!*
/GO
F,P51X,FX,178/8
FLST,2,24,1,ORDE,24
FITEM,2,189
FITEM,2,-190
FITEM,2,206
FITEM,2,-207
FITEM,2,217
FITEM,2,226
FITEM,2,-227
FITEM,2,236
FITEM,2,597
FITEM,2,-598
FITEM,2,607
FITEM,2,616
FITEM,2,-617
FITEM,2,626
FITEM,2,914
FITEM,2,-915
FITEM,2,928
FITEM,2,937
FITEM,2,-938
FITEM,2,947
FITEM,2,1192
FITEM,2,1201
FITEM,2,-1202
FITEM,2,1211
!*
/GO
F,P51X,FX,164/24
FLST,2,16,1,ORDE,16
FITEM,2,18
FITEM,2,77
FITEM,2,154
FITEM,2,156
FITEM,2,178
FITEM,2,482
FITEM,2,557
FITEM,2,559
FITEM,2,582
FITEM,2,814
FITEM,2,882
FITEM,2,884
FITEM,2,902
FITEM,2,1157
FITEM,2,1159
FITEM,2,1181
!*
/GO
F,P51X,FX,151/16
FLST,2,4,1,ORDE,4
FITEM,2,39
FITEM,2,98
FITEM,2,503
FITEM,2,835
!*
/GO
F,P51X,FX,138/4
FLST,2,8,1,ORDE,7

FITEM,2,1
FITEM,2,-3
FITEM,2,463
FITEM,2,-464
FITEM,2,798
FITEM,2,-799
FITEM,2,1118
FLST,2,8,1,ORDE,7
FITEM,2,1
FITEM,2,-3
FITEM,2,463
FITEM,2,-464
FITEM,2,798
FITEM,2,-799
FITEM,2,1118
!*
/GO
F,P51X,FX,125/8
FLST,2,16,1,ORDE,16
FITEM,2,259
FITEM,2,318
FITEM,2,371
FITEM,2,416
FITEM,2,453
FITEM,2,653
FITEM,2,698
FITEM,2,735
FITEM,2,780
FITEM,2,973
FITEM,2,1026
FITEM,2,1071
FITEM,2,1108
FITEM,2,1234
FITEM,2,1279
FITEM,2,1316
!*
/GO
F,P51X,FX,38/16
FLST,2,16,1,ORDE,16
FITEM,2,259
FITEM,2,318
FITEM,2,371
FITEM,2,416
FITEM,2,453
FITEM,2,653
FITEM,2,698
FITEM,2,735
FITEM,2,780
FITEM,2,973
FITEM,2,1026
FITEM,2,1071
FITEM,2,1108
FITEM,2,1234
FITEM,2,1279
FITEM,2,1316
FDELE,P51X,FX
FLST,2,16,1,ORDE,16
FITEM,2,259
FITEM,2,318
FITEM,2,371
FITEM,2,416
FITEM,2,453
FITEM,2,653
FITEM,2,698
FITEM,2,735
FITEM,2,780
FITEM,2,973
FITEM,2,1026
FITEM,2,1071
FITEM,2,1108
FITEM,2,1234
FITEM,2,1279
FITEM,2,1316
!*
/GO
F,P51X,FX,191/16
FLST,2,16,1,ORDE,16
FITEM,2,259
FITEM,2,318
FITEM,2,371
FITEM,2,416

FITEM,2,453
FITEM,2,653
FITEM,2,698
FITEM,2,735
FITEM,2,780
FITEM,2,973
FITEM,2,1026
FITEM,2,1071
FITEM,2,1108
FITEM,2,1234
FITEM,2,1279
FITEM,2,1316
!*
/GO
F,P51X,FZ,38/16
FLST,2,8,1,ORDE,8
FITEM,2,280
FITEM,2,339
FITEM,2,395
FITEM,2,674
FITEM,2,756
FITEM,2,994
FITEM,2,1050
FITEM,2,1258
FLST,2,8,1,ORDE,8
FITEM,2,280
FITEM,2,339
FITEM,2,395
FITEM,2,674
FITEM,2,756
FITEM,2,994
FITEM,2,1050
FITEM,2,1258
!*
/GO
F,P51X,FZ,36/8
FLST,2,24,1,ORDE,24
FITEM,2,189
FITEM,2,-190
FITEM,2,206
FITEM,2,-207
FITEM,2,217
FITEM,2,226
FITEM,2,-227
FITEM,2,236
FITEM,2,597
FITEM,2,-598
FITEM,2,607
FITEM,2,616
FITEM,2,-617
FITEM,2,626
FITEM,2,914
FITEM,2,-915
FITEM,2,928
FITEM,2,937
FITEM,2,-938
FITEM,2,947
FITEM,2,1192
FITEM,2,1201
FITEM,2,-1202
FITEM,2,1211
!*
/GO
F,P51X,FZ,33/24
FLST,2,16,1,ORDE,16
FITEM,2,18
FITEM,2,77
FITEM,2,154
FITEM,2,156
FITEM,2,178
FITEM,2,482
FITEM,2,557

```
FITEM,2,559
FITEM,2,582
FITEM,2,814
FITEM,2,882
FITEM,2,884
FITEM,2,902
FITEM,2,1157
FITEM,2,1159
FITEM,2,1181
!*
/GO
F,P51X,FZ,30/16
FLST,2,4,1,ORDE,4
FITEM,2,39
FITEM,2,98
FITEM,2,503
FITEM,2,835
!*
/GO
F,P51X,FZ,28/4
FLST,2,8,1,ORDE,7
FITEM,2,1
FITEM,2,-3
FITEM,2,463
FITEM,2,-464
FITEM,2,798
FITEM,2,-799
FITEM,2,1118
!*
/GO
F,P51X,FZ,25/8
ALLSEL,ALL
! NPLOT
! /MREP,EPLOT
NSEL,A,LOC,Y,5700,5770
! NPLOT
NSEL,S,LOC,Y,5700,5770
! NPLOT
FLST,2,12,1,ORDE,12
FITEM,2,54
FITEM,2,-55
FITEM,2,113
FITEM,2,-114
FITEM,2,128
FITEM,2,518
FITEM,2,-519
FITEM,2,531
FITEM,2,850
FITEM,2,-851
FITEM,2,866
FITEM,2,1131
FDELE,P51X,ALL
FLST,2,12,1,ORDE,12
FITEM,2,54
FITEM,2,-55
FITEM,2,113
FITEM,2,-114
FITEM,2,128
FITEM,2,518
FITEM,2,-519
FITEM,2,531
FITEM,2,850
FITEM,2,-851
FITEM,2,866
FITEM,2,1131
!*
/GO
F,P51X,FZ,83/12
FLST,2,12,1,ORDE,12
FITEM,2,54
FITEM,2,-55
FITEM,2,113
FITEM,2,-114
FITEM,2,128
FITEM,2,518
FITEM,2,-519
FITEM,2,531
FITEM,2,850
FITEM,2,-851
FITEM,2,866
FITEM,2,1131
```

FLST,2,12,1,ORDE,12
FITEM,2,54
FITEM,2,-55
FITEM,2,113
FITEM,2,-114
FITEM,2,128
FITEM,2,518
FITEM,2,-519
FITEM,2,531
FITEM,2,850
FITEM,2,-851
FITEM,2,866
FITEM,2,1131
!*
/GO
F,P51X,MY,27908/12
FLST,2,12,1,ORDE,12
FITEM,2,54
FITEM,2,-55
FITEM,2,113
FITEM,2,-114
FITEM,2,128
FITEM,2,518
FITEM,2,-519
FITEM,2,531
FITEM,2,850
FITEM,2,-851
FITEM,2,866
FITEM,2,1131
! /REPLOT,RESIZE
! /REPLOT,RESIZE
FLST,2,12,1,ORDE,12
FITEM,2,54
FITEM,2,-55
FITEM,2,113
FITEM,2,-114
FITEM,2,128
FITEM,2,518
FITEM,2,-519
FITEM,2,531
FITEM,2,850
FITEM,2,-851
FITEM,2,866
FITEM,2,1131
!*
/GO
F,P51X,MZ,-113000/12
FLST,2,12,1,ORDE,12
FITEM,2,54
FITEM,2,-55
FITEM,2,113
FITEM,2,-114
FITEM,2,128
FITEM,2,518
FITEM,2,-519
FITEM,2,531
FITEM,2,850
FITEM,2,-851
FITEM,2,866
FITEM,2,1131
FDELE,P51X,MZ
FLST,2,12,1,ORDE,12
FITEM,2,54
FITEM,2,-55
FITEM,2,113
FITEM,2,-114
FITEM,2,128
FITEM,2,518
FITEM,2,-519
FITEM,2,531
FITEM,2,850
FITEM,2,-851
FITEM,2,866
FITEM,2,1131
!*
/GO
F,P51X,FY,-113/12
! /REPLOT,RESIZE
! /REPLOT,RESIZE
FLST,2,12,1,ORDE,12
FITEM,2,54

FITEM,2,-55
FITEM,2,113
FITEM,2,-114
FITEM,2,128
FITEM,2,518
FITEM,2,-519
FITEM,2,531
FITEM,2,850
FITEM,2,-851
FITEM,2,866
FITEM,2,1131
!*
/GO
F,P51X,MZ,-44636/12
FLST,2,12,1,ORDE,12
FITEM,2,54
FITEM,2,-55
FITEM,2,113
FITEM,2,-114
FITEM,2,128
FITEM,2,518
FITEM,2,-519
FITEM,2,531
FITEM,2,850
FITEM,2,-851
FITEM,2,866
FITEM,2,1131
!*
/GO
F,P51X,FY,-42/12
FLST,2,12,1,ORDE,12
FITEM,2,54
FITEM,2,-55
FITEM,2,113
FITEM,2,-114
FITEM,2,128
FITEM,2,518
FITEM,2,-519
FITEM,2,531
FITEM,2,850
FITEM,2,-851
FITEM,2,866
FITEM,2,1131
!*
/GO
F,P51X,MZ,-15306/12
ALLSEL,ALL
! NPLOT
FINISH
/POST1
FINISH
/SOL
!*
ANTYPE,0
! /STATUS,SOLU
SOLVE
FINISH
/POST1
!*
! /EFACET,1
! PLNSOL, U,SUM, 0,1.0
! /EFACET,1
! PLNSOL, FAIL,TWSI, 0,1.0
! /GRA,POWER
! /GST,ON
! /PLO,INFO,3
! /GRO,CURL,ON
! /CPLANE,1
! /REPLOT,RESIZE
WPSTYLE,,,,,,,,0
/PREP7
sect,1,shell,,Allpole
secdata, 0.3,1,0,3
secdata, 0.3,1,0,3
secdata, 0.3,1,95,3
secdata, 0.3,1,85,3
secdata, 0.3,1,95,3
secdata, 0.3,1,85,3
secdata, 0.3,1,0,3
secdata, 0.3,1,0,3
secoffset,MID

seccontrol,0,0,0, 0, 1, 1, 1

sect,2,shell,,Joint

secdata, 0.3,1,0,3

secdata, 0.3,1,0,3

secdata, 0.3,1,95,3

secdata, 0.3,1,85,3

secdata, 0.3,1,95,3

secdata, 0.3,1,85,3

secdata, 0.3,1,0,3

secdata, 0.3,1,0,3

secdata, 0.3,1,0,3

secdata, 0.3,1,0,3

secdata, 0.3,1,95,3

secdata, 0.3,1,85,3

secdata, 0.3,1,95,3

secdata, 0.3,1,85,3

secdata, 0.3,1,0,3

secdata, 0.3,1,0,3

secoffset,MID

seccontrol,0,0,0, 0, 1, 1, 1

sect,2,shell,,Joint

secdata, 0.3,1,0,3

secdata, 0.3,1,0,3

secdata, 0.3,1,95,3

secdata, 0.3,1,85,3

secdata, 0.3,1,95,3

secdata, 0.3,1,85,3

secdata, 0.3,1,0,3

secdata, 0.3,1,0,3

secdata, 0.3,1,0,3

secdata, 0.3,1,0,3

secdata, 0.3,1,95,3

secdata, 0.3,1,85,3

secdata, 0.3,1,95,3

secdata, 0.3,1,85,3

secdata, 0.3,1,0,3

secdata, 0.3,1,0,3

secoffset,MID

seccontrol,0,0,0, 0, 1, 1, 1

sect,1,shell,,Allpole

secdata, 0.3,1,0,3

secdata, 0.3,1,0,3

secdata, 0.3,1,95,3

secdata, 0.3,1,85,3

secdata, 0.3,1,95,3

secdata, 0.3,1,85,3

secdata, 0.3,1,0,3

secdata, 0.3,1,0,3

secoffset,MID

seccontrol,0,0,0, 0, 1, 1, 1

FINISH

/SOL

! /STATUS,SOLU

SOLVE

FINISH

/POST1

!*

! /EFACET,1

! PLNSOL, U,SUM, 0,1.0

! /EFACET,1

! PLNSOL, FAIL,SMAX, 0,1.0

! /EFACET,1

! PLNSOL, FAIL,TWSI, 0,1.0

! /EFACET,1

! PLNSOL, FAIL,EMAX,
0,1.0

!*

! PLESOL, EPTO,Y, 0,1.0

!
/ZOOM,1,RECT,0.0248398,
-0.319423
,0.601583030628 ,-
0.807566265978

! /DSCALE,ALL,60

! PLESOL, EPTO,Y, 0,1.0

! PLESOL, EPTO,Y, 0,1.0

! /FOC, 1,
313.775276634 ,
495.692869439 ,
56.8163304468

! /REPLO

! /VIEW, 1,
0.804571395739 ,
0.111106575361 ,
0.583369692450

! /ANG, 1,
12.2930889456

! /REPLO

! /VIEW, 1,
0.933875686442 ,
0.144117680051 ,
0.327270983391

! /ANG, 1,
14.7715129942

! /REPLO

!
/DIST,1,0.924021086472,1

! /REP,FAST

!
/DIST,1,0.924021086472,1

! /REP,FAST

!
/DIST,1,0.924021086472,1

! /REP,FAST

!
/DIST,1,0.924021086472,1

! /REP,FAST

!
/DIST,1,0.924021086472,1

! /REP,FAST

!
/DIST,1,0.924021086472,1

! /REP,FAST

!
/DIST,1,0.924021086472,1

! /REP,FAST

! /FOC, 1,
315.352978458 ,
458.605031732 ,
68.6463916224

! /REPLO

!
/DIST,1,0.924021086472,1

! /REP,FAST

!
/DIST,1,0.924021086472,1

! /REP,FAST

!
/DIST,1,0.924021086472,1

! /REP,FAST

!
/DIST,1,0.924021086472,1

! /REP,FAST

!
/DIST,1,0.924021086472,1

! /REP,FAST

!
/DIST,1,0.924021086472,1

! /REP,FAST

! /FOC, 1,
298.428047447 ,
306.344094749 ,
183.992011865

! /REPLO

! /VIEW, 1,
0.582794574600 ,
0.244335975793 ,
0.775016396440

! /ANG, 1,
6.77761838633

! /REPLO

FINISH

! /EXIT,MODEL

! /GRA,POWER

! /GST,ON

! /PLO,INFO,3

! /GRO,CURL,ON

! /CPLANE,1

! /REPLOT,RESIZE

WPSTYLE,,,,,,,,0

! /REPLOT,RESIZE

! /AUTO,1

! /REP,FAST

! /VIEW,1,1,2,3

! /ANG,1

! /REP,FAST

/POST1

FINISH

/PREP7

sect,1,shell,,Allpole

secdata, 0.3,1,0,3

secdata, 0.3,1,0,3

```
secdata, 0.3,1,95,3
secdata, 0.3,1,85,3
secdata, 0.3,1,95,3
secdata, 0.3,1,85,3
secdata, 0.3,1,0,3
secdata, 0.3,1,0,3
secoffset,MID
seccontrol,0,0,0, 0, 1, 1, 1
FINISH
/SOL
! /STATUS,SOLU
SOLVE
FINISH
/POST1
!*
! /EFACET,1
! PLNSOL, U,SUM, 0,1.0
```